63-2-4

ROCK ISLAND ARSENAL
RESEARCH & DEVELOPMENT DIVISION
DESIGN ENGINEERING BRANCH

TECHNICAL REPORT

THEORETICAL STUDY OF THE BLAST FIELD OF ARTILLERY WITH MUZZLE BRAKES

O. M. S. CODE NO.	5520.11.440A0.01
D. A. PROJECT NO.	5W01-01-034
REPORT NO.	62-4257
AUTHOR	George Schlenker
DATE	December 1962

Report No. 62-4257

Copy No.

THEORETICAL STUDY OF THE BLAST FIELD OF ARTILLERY WITH MUZZLE BRAKES

By

George Schlenker

Approved by

ARNOLD A. KESTER
Chief, Design Engineering Branch

December 1962

OMS Code No. 5520.11.440A0.01

Department of the Army Project No. 5W01-01-034

Rock Island Arsenal
Rock Island, Illinois

ABSTRACT

A means is described for computing the peak static and peak dynamic overpressures of the shock wave generated by an artillery piece with muzzle brake as a function of position within the crew area. Computed results are compared with recent experimental results and indicate a favorable agreement.

TABLE OF CONTENTS

LIST OF SYMBOLS

The reader is referred to RIA report Number 62-1794 for a complete list of symbols concerned with gun interior ballistics and muzzle brake parameters. A partial list is repeated here for reference.

INTERIOR BALLISTICS SYMBOLS

Symbol	Meaning	Dimension
A	area of bore plus cross sectional area of grooves	in^2
A_{cnct}	area of ammunition band in contact with tube after shear deformation	in^2
$\mathcal{V}_T$	total internal volume of gun	in^3
M_p	mass of projectile	lb_m
M_c	mass of charge	lb_m
M_{ig}	mass of igniter	lb_m
$M_T=M_c+M_{ig}$	total propellant mass	lb_m
M_r	mass of recoiling parts	lb_m
T	temperature of the propellant gases	$^\circ R$
v_o	muzzle velocity of the projectile	ft/sec
v	velocity of the propellant gases	ft/sec
V	specific volume of the propellant gases	$\frac{ft^3}{lb_m}$
p	pressure in the gas	psia
t	time	secs
t_o	time at start of gas ejection	secs
B	force on breech	lb_f
a	speed of sound in gas	ft/sec
$\gamma=C_p/C_v$	ratio of specific heats of propellant gas	
R	gas constant	$\frac{lb_f\ ft}{lb_m\ ^\circ R}$

Symbol	Meaning	Dimension
C_p	specific heat of gas at constant pressure	$\frac{Btu}{lb_m\ ^\circ R}$
C_v	specific heat of gas at constant volume	$\frac{Btu}{lb_m\ ^\circ R}$
J	Joule's constant = 777.5	$\frac{lb_f\ ft}{Btu}$
g	acceleration due to gravity = 32.17	ft/sec^2
e_c	heat of explosion of the propellant charge	$\frac{Btu}{lb_m}$
e_{ig}	heat of explosion of the igniter	$\frac{Btu}{lb_m}$
E	energy involved in a process	Btu
KEP	kinetic energy of the projectile at the start of gas ejection (t_o)	Btu
KEG	kinetic energy of the gas at t_o	Btu
KER	kinetic energy of the recoiling parts at t_o	Btu
KEB	kinetic energy spent in engraving the bore and in forcing the projectile thru, evaluated at t_o	Btu
E_g	thermal energy remaining in the gas at t_o	Btu
$\mathcal{H}$	total heat released by charge and igniter during combustion	Btu
$\mathcal{H}_c$	heat released by charge	Btu
$\mathcal{H}_{ig}$	heat released by igniter	Btu

$\beta = \frac{v_o}{a_{av\ init}}$ dimensionless velocity

$\varphi = \frac{p}{p_b}$ dimensionless pressure at t_o

$\kappa = \frac{V}{V_b}$ dimensionless specific volume at t_o

Symbol	Meaning	Dimension
$\vartheta = \frac{T}{T_b}$	dimensionless temperature at t_o; also used as an angle in the brake design	
M	cumulative mass discharged	lb_m
P	cumulative momentum discharged	lb_f secs
H	cumulative stagnation enthalpy discharged	Btu
F_z	force on brake in axial direction of gun tube	lb_f
F_y	vertical force on brake normal to axis of gun tube	lb_f
$\alpha_T = \frac{A\ g\ p_{b\ init}}{a_{b\ init}\ M_T}$	; dimensional constant used in obtaining a dimensionless time	sec^{-1}
$\tau = \alpha_T\ t$	dimensionless time	
$\mu_T = \frac{Pg}{M_T\ a_{b\ init}}$	; dimensionless cumulative momentum discharged from muzzle	
$\nu_T = \frac{M}{M_T}$	dimensionless cumulative mass discharged	
$\eta_T = \frac{H}{E_g}$	dimensionless cumulative stagnation enthalpy discharged	
$\beta = \frac{F_z}{B}$	axial momentum index, i.e., the ratio of the axial brake force to the breech force	
$\omega = \frac{F_y}{P}$	ratio of normal brake force to momentum rate of discharge	
$\lambda_r = 1.46881(1 - \beta_{eff})$	ratio of momentum propagated in axial direction thru a control surface surrounding brake to total momentum discharged from the muzzle	

SYMBOLS PERTAINING TO SHOCK ESTABLISHMENT AND DECAY

p	static pressure in gas	psia
q	dynamic pressure in gas	psia
V	specific volume of gas	$\frac{ft^3}{lb_m}$

Symbol	Meaning	Dimension
v	velocity of gas	ft/sec
$\bar{v}$	velocity of center of mass of gas mass	ft/sec
T	static temperature of gas	°R
T^o	stagnation temperature at center of shock sphere	°R
$\kappa_1 = T^o/p_y'$		°R/psia
V^o	specific volume at center of shock sphere	ft^3/lb_m
$\kappa_{2av} = \frac{V_{2av}}{V^o}$		
$\tilde{r}_2$	radius of shock being driven by mass M discharged from weapon (at $\tau = 1$)	ft
M^*	total mass of gas within sphere of radius $\tilde{r}_2$	lb_m
r	radius of a sphere of gas	ft
d_1	distance from center of muzzle brake side port to center of nearest spherical shock, at maximum shock strength	ft
ζ	path length of gas flow from center of muzzle to center of one of the side muzzle brake ports	ft
X	horizontal coordinate axis normal to gun tube axis with center at center of front port of brake	ft
Y	axis normal to axis of gun tube and X-axis, directed up, with origin at origin of X-axis	ft
Z	coordinate axis along axis of gun tube directed from the breech with origin at center of front port of muzzle brake	ft
x_o	X-distance to center of a side port of the muzzle brake	ft
y_o	Y-distance to center of a side port of the muzzle brake	ft
z_o	Z-distance to center of a side port of the muzzle brake	ft

Symbol	Meaning	Dimension
x_1	X-distance between center of a side port of m. b. and center of associated, fully developed shock sphere	ft
y_1	Y-distance between center of a side port of m. b. and center of associated, fully developed shock sphere	ft
z_1	Z-distance between center of a side port of m. b. and center of associated, fully developed shock sphere	ft
$x = x_0+x_1$	X-distance to center of shock sphere	ft
$y = y_0+y_1$	Y-distance to center of shock sphere	ft
$z = z_0+z_1$	Z-distance to center of shock sphere	ft
ξ	horizontal coordinate normal to vertical plane thru gun tube axis with origin at center of rear trunnion	ft
η	vertical coordinate measured positively upwards with origin at center of rear trunnion	ft
ν	horizontal coordinate, in plane parallel to ground, orthogonal to ξ and η measured positively toward the muzzle	ft
h	height above $\xi - \nu$ plane to reference position in blast field	ft
f	distance behind center of rear trunnion in $\xi - \nu$ plane to reference position in blast field	ft
G	distance from center of front port of muzzle brake to center of rear trunnion	ft
L	distance from center of front port of muzzle brake to reference position in blast field	ft
N	distance from center of nearest shock sphere at max static overpressure to reference position in blast field	ft
Ø	distance from center of farthest shock sphere at max static overpressure to reference position in blast field	ft
D	projection in $\xi-\nu$ plane of distance from center of front port of muzzle brake to reference position in blast field	ft

Symbol	Meaning	Dimension
QE	quadrant elevation	deg
ϑ	angle between gun tube axis and projection of D on plane of tube in plane of tube	deg
$\hat{\vartheta}$	projection of ϑ in ξ-ν plane	rad or deg
$\hat{\alpha}$	angular projection in X-Z plane that mean flow from the brake makes with Z-axis	degs
$\hat{\beta}$	angular projection in X-Y plane that mean flow makes with Y-axis	degs
$\cos A_\xi$	direction cosine of $\bar{v}_1$ vector of nearest shock sphere with respect to ξ-axis in $\xi - \eta - \nu$ system	
$\cos A_\eta$	direction cosine of $\bar{v}_1$ vector of nearest shock sphere with respect to η-axis in $\xi - \eta - \nu$ system	
$\cos A_\nu$	direction cosine of $\bar{v}_1$ vector of nearest shock sphere with respect to ν-axis in $\xi - \eta - \nu$ system	
$\cos B_\xi$	direction cosine of $\bar{v}_1$ vector of farthest shock sphere with respect to ξ-axis in $\xi - \eta - \nu$ system	
$\cos B_\eta$	as $\cos A_\eta$ above except pertains to farthest shock sphere	
$\cos B_\nu$	as $\cos A_\nu$ above except pertains to farthest shock sphere	
$p_s = p - p_\infty$	static overpressure (subscripted)	psi
$\varphi = \frac{p_s}{p_\infty}$	dimensionless static overpressure (subscripted)	psi
K	effective per unit $\bar{v}_1$ contribution to the gas velocity behind the shock front	
PF	an empirical propagation factor defined in equation 0.63	
EFF	per unit total stagnation enthalpy involved in a point source explosion at the muzzle; efficiency of energy utilization in producing shock	

Symbol	Meaning	Dimension
α	dimensional constant used in point source explosion theory	ft
$\lambda = \frac{L}{\alpha}$	non-dimensional distance from center of point source explosion	
DPP	duration of the positive static pressure phase of the shock wave	millisecs
SPLSP	impulse per unit area from the positive static pressure phase of the shock wave due to a point source explosion	psi millisecs
DPLSP	impulse per unit area from the positive dynamic pressure phase of the shock wave due to a point source explosion	psi millisecs

SUBSCRIPTS

o	refers to conditions at the muzzle
∞	refers to ambient (free field) conditions
g	pertains to the combustion products
b	refers to value of variable at the breech
eff	refers to an effective value
av	refers to an average (or weighted average) value over a volume
init	refers to initial conditions for gas ejection
T	refers to a cumulative or integrated value
x	refers to conditions upstream of a normal shock
y	refers to conditions downstream of (or behind) a normal shock
x y z	pertains to components along X-, Y-, and Z-, coordinate axes
0	refers to location of muzzle brake ports in X-Y-Z system
1	pertains to each of the two spherical shocks created by the muzzle brake, at max peak overpressure
2	pertains to conditions in a shell of compressed ambient air in the single shock sphere model as observed in a frame stationary with respect to the center of mass of this system
3	refers to conditions at reference position in blast field

SUPERSCRIPTS

^{o}	refers to a stagnation value
$\hat{}$	distinguishes angular projections, as noted
$\sim$	refers to conditions predicted by the point source explosion model
$\bar{}$	pertains to motion of center of mass of gas discharged
$'$	refers to normal shock conditions as viewed by an observer with respect to whom the shock is moving in still air

INTRODUCTION

It has appeared to be desirable to have an analytical means for predicting the severity of the artillery blast within the crew area. The practice of designing muzzle brakes from only the point-of-view of reducing rod pull and without regard to the effect of the brake design upon the blast field has been perpetuated because a good analytical tool for predicting the performance of a brake-weapon system in terms of operator comfort has been lacking. The purpose of this report is to fill that need insofar as engineering results are concerned. There is much more that one could say that would give a better understanding of the physical mechanisms involved in the creation of atmospheric shock from artillery.

It is recognized that the mathematical model presented here has oversimplified the phenomenon. At the outset of this study there was the hope that the assumptions involved in the model were not so unrealistic that quantitative agreement with experiment was precluded. As a working goal, it was decided that an agreement in the peak static overpressure of better than 20% of max value for all points within the crew area was necessary. To achieve this goal, a minimum number of empirical constants were to be introduced and ad hoc assumptions were to be eliminated, if possible.

Since there seems to be a positive correlation between the discomfort that a human operator experiences and the peak static overpressure in the incident shock wave, and since the latter parameter has been accepted for some time as a critical parameter in the man-weapon system, this theory was constructed to predict the peak static overpressure for any position within the crew area. Additionally, the peak dynamic pressure component is given.

For reference and comparison purposes the following parameters predicted by a competitive theory are given: the peak static and dynamic pressures, the total positive impulse, and the duration of the positive pressure phase in the shock wave. These computations were made by assuming a point source explosion at the muzzle with a total energy release equal to the total stagnation enthalpy discharged times an efficiency factor. The latter values indicate what is expected for a spherically symmetric burst and, by comparison with the results of the present theory, indicate the directional effects of the brake-weapon system.

In predicting the peak static overpressure, it was desirable to take into account specific geometric details of the muzzle brake such as the size and shape of the brake and to take into account such physical factors as the momentum indices in the axial and transverse vertical directions (for vertically asymmetric brakes). This was done in sufficient generality to include the majority of the presently used brake designs. Also, the interior ballistic factors were considered as well as the relevant weapon dimensions.

Computations were made from the theory using a digital computer. The computed results have been compared (insofar as is possible) with recent experimental results obtained by the Artillery Weapons Branch, Artillery Division, Development and Proof Services for the Human Engineering Laboratories, Aberdeen Proving Ground, Md. (Reference 12.)

Since hand calculation from the theory is extremely laborious, the author has included the logic diagram and the FORTRAN program for making these computations with a digital computer.

THE MATHEMATICAL MODEL

It is recognized that gaseous discharge from the muzzle of an artillery piece does not admit the same simplifications in the mathematical model as, say, the explosion at a point, in which case an instantaneous release of energy is validly assumed. The discharge from a gun tube is neither a pure energy- nor a pure mass-source as far as the shock field near the muzzle is concerned.

In the case of gas discharged from a gun tube without a muzzle brake, the events occurring prior to the establishment of maximum shock strength have been described in some detail qualitatively in reference 7. The essential feature of that description which I wish to use is the idea of a "shock bottle." As the combustion products are discharged, they push back the ambient air replacing a volume formerly occupied by air. This process may be thought of as a three dimensional fluid piston expanding in air. During this discharge, which occurs transonically in the combustion products but supersonically relative to the air, a shock wave is established in the air. This shock grows in strength as more gas is fed into the bottle-shaped volume of combustion products at the muzzle.

FIGURE 1.A

SINGLE SPHERE SHOCK MODEL

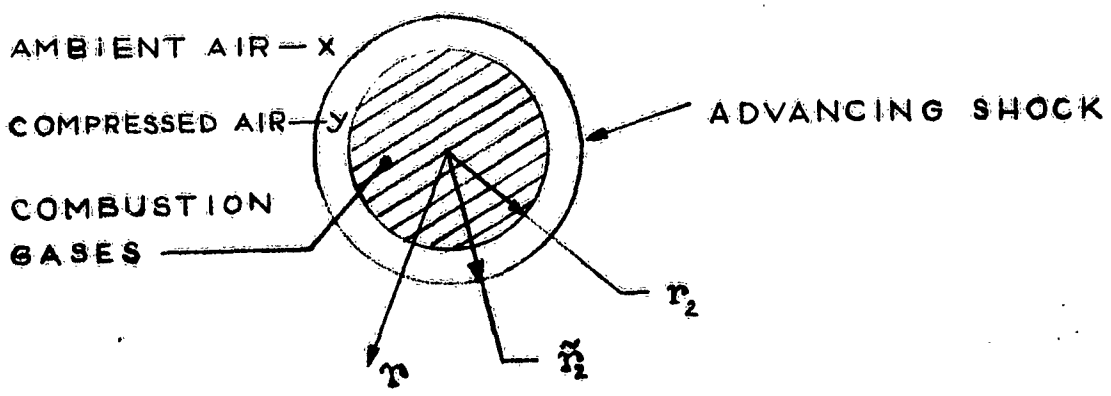

1.B

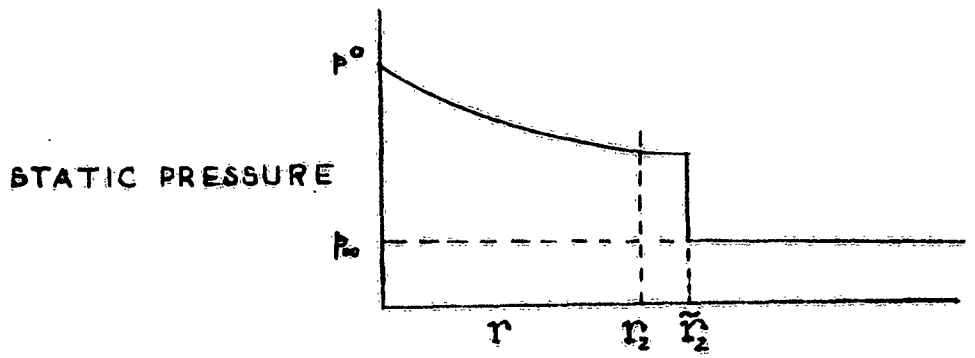

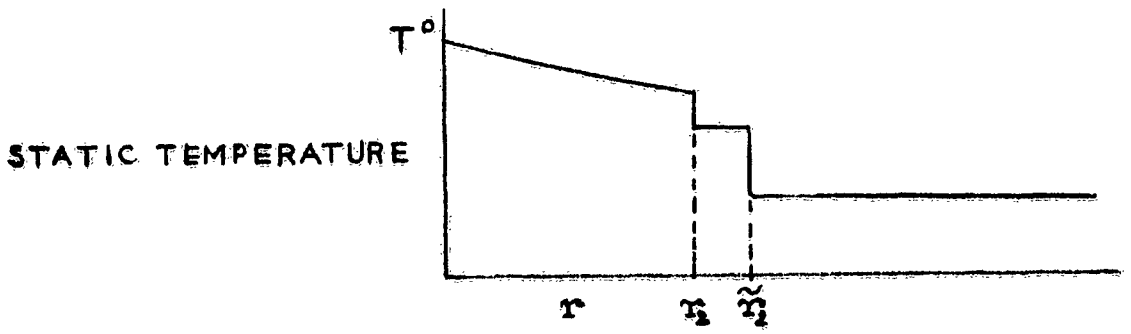

1 . B

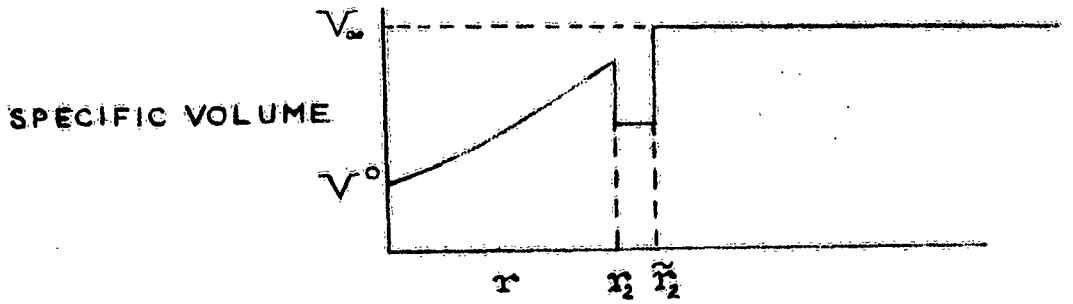
SPECIFIC VOLUME
V_∞
V°
r
r_2
$\tilde{r}_2$

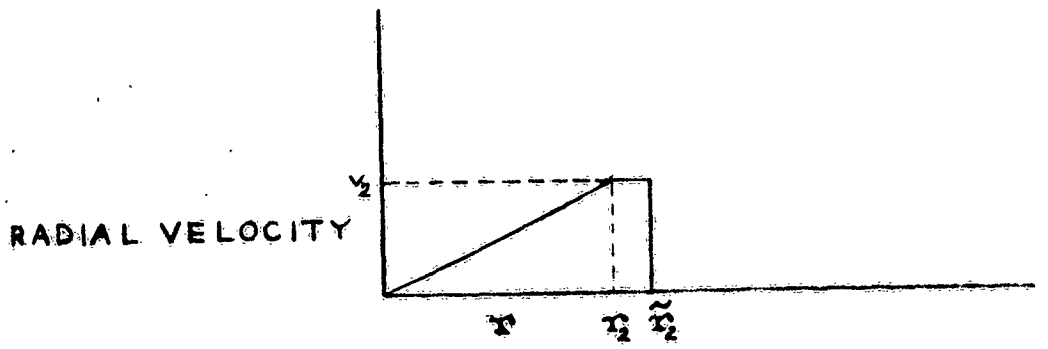
RADIAL VELOCITY
v_2
r
r_2
$\tilde{r}_2$

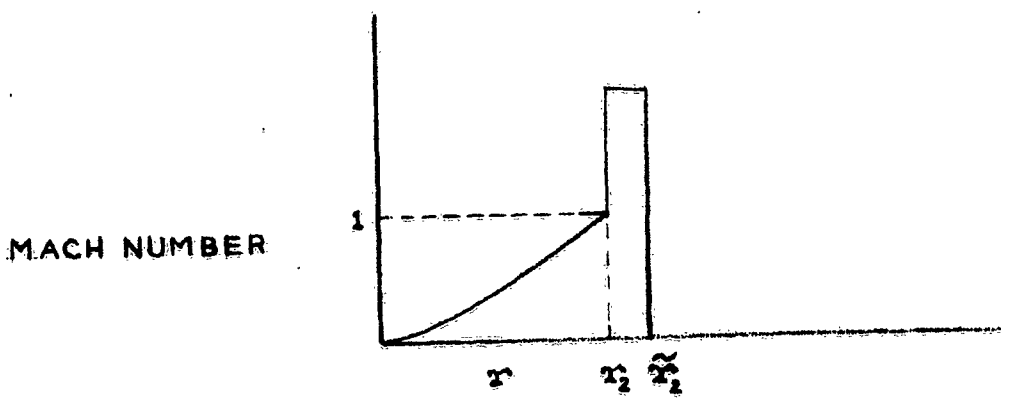
MACH NUMBER
1
r
r_2
$\tilde{r}_2$

Since the mass-, momentum- and enthalphy-rates of discharge are rapidly decreasing, a point is reached where the bottle of driving gases cannot affect an increase in shock strength, i.e., cannot accelerate the shell of compressed air advancing before it. At this moment in time the shock is said to be fully developed. Subsequent propagation of the shock wave in the air away from the driving gases only serves to attenuate the peak overpressure, baring coalescence of two shock waves upon shock reflection.

At maximum shock strength the dimensions of the shock bottle are such that the max streamwise dimension from the muzzle is approximately equal to the max transverse dimension (reference 7).

For weapons such as the standard 105mm howitzer, this has been found to occur at a non-dimensional time of $\mathcal{T} = 1$. Certainly, one would suspect that this time would vary from weapon to weapon and from one zone charge to another, for a given weapon. However, slight variations in the predicted time of max shock strength should not alter appreciably the predicted max overpressure, since the latter value changes slowly in time near its maximum, where time derivatives are zero.

Thus, in the mathematical model, max peak overpressure occurs at $\mathcal{T} = 1$. Further simplification in the model was obtained by assuming the shock bottle is spherical. The geometry of the shock model is illustrated in figure 1a.

Variables within the driving gas at the interface with the shell of compressed air are subscripted with the number 2. Conditions within the thin shell of compressed air are assumed to be uniform and are subscripted with the letter y. Conditions upstream of the moving shock -- ambient conditions, in this case -- are subscripted with the letter x or the symbol ∞.

Since the combustion gases are also transporting momentum along the tube axis, the shock sphere must be moving in an axial direction with a mean velocity $\overline{v}_2$. In a frame of reference moving with the center of mass, the state variables are assumed to have the distributions shown in figure 1b.

Note $p_y = p_2$, i.e., that at max shock strength the pressure gradient at the driving interface has vanished. Also note that turbulent mixing has not been such as to raise the temperature of the compressed air shell to the value T_2. This assumption is based upon the fact that maximum shock strength is developed in a very brief

interval and that heat transfer mechanisms in a dilute gas require a longer active period to be effective. A third significant aspect of this model is the requirement that the mach number of the driving gas at the interface equal unity. If the mach number were lower, expansion would quickly raise its value; however, if the mach number here were higher than unity, shock reflection at the interface would bring its value down.

The value of the stagnation pressure and of the stagnation temperature of the combustion gases within the driving sphere and, in fact, the size of the sphere itself is a function of the cumulative -mass, -momentum, and -stagnation enthalpy discharged up to $\sigma = 1$. Further the Rankine-Hugoniot conditions (Appendix I) require that definite relationships exist between variables on either side of the shock -- assumed here to be a one-dimensional normal shock -- e.g., between p_y and p_x. Conditions in front of the shock are known. Therefore, one can write a set of equations which determine the peak overpressure, $p_y - p_x = p_s$, at maximum shock strength. The derivation of these equations is found in Appendix II. It is also shown in this appendix that the presence of a muzzle brake, which alters the distribution of mass from the muzzle, does not change the maximum peak overpressure in the stationary shock frame of reference. It is assumed that the muzzle brake causes two initially distinct shock spheres to be developed, each of which propagates with an independent decay rate until coalescence. Constructive interference within the crew area is assumed. (See Appendix III.) The effect of shock reflection from the ground is not considered, altho at low quadrant elevations this phenomenon undoubtedly plays a role in determining peak overpressure in the crew area.

The directional effects of the shock wave are obtained by considering the maximum peak overpressure in a frame of reference that is fixed with respect to the ground. Reference 3 suggests that, for the simplified model considered there, strong directional effects are absent in the blast field of a moving fluid source whenever the mach number of the source in the medium is less than unity. However, even for a subsonic source, there are directional effects. These result in a strengthening of the shock in the direction of motion of the source and a weakening of the shock in the opposite direction. To account for the directional effects due to the motion of the shock sphere relative to the ground, the center-of-mass velocity component in the direction of the reference position was multiplied by an empirical propagation factor and added to the max radial velocity of the shock wave in the center-of-mass system to obtain a maximum

effective shock wave velocity in a ground fixed frame. By the Rankine-Hugoniot relations, the peak overpressure is dependent upon the shock velocity. Thus, the maximum peak overpressure in the ground frame of reference can be obtained.

Having obtained the max peak overpressure, one must consider the rate of decay of a shock wave with distance to be able to predict the peak overpressure at the reference position. Reference 3 indicates that overpressure varies approximately as r^{-1} as the overpressure approaches zero. Reference 1, considering point source explosions in air, indicates a much more rapid decay for very strong shocks with an approximately $r^{-3/2}$ dependence for shocks having a strength within the range commonly encountered in muzzle blast (7 - .1 atm overpressure), the dependence gradually approaching r^{-1} for shocks of infinitesimal strength.

It seems appropriate to choose an $r^{-3/2}$ overpressure decay for the present mathematical model. Then, knowing the max peak overpressure and the shock radius at this time and knowing the distance between the center of the shock and the reference position, one can compute the peak overpressure at the reference position. Details of the derivation of the equations concerning the overpressure at the reference position are found in Appendix III.

For the derivation of the equations concerning the gun internal ballistics, the reader is referred to the appendicies of reference 10.

The equations referring to conditions in the blast field due to a point source explosion were obtained from references 1 and 2. It was found that quadratic best fits on log-log paper to the data given in these references provided convenient computational formulae, of sufficient accuracy, for obtaining the desired parameters.

EQUATIONS

The following equations, used in the computer program, (listed in order used) are derived in Appendices I, II, and III of this report and in Appendices I, II, and III of reference 10.

0.1 $\mathcal{H}_{ig} = e_{ig} M_{ig}$

0.2 $\mathcal{H}_c = e_c M_c$

0.3 $\mathcal{H} = \mathcal{H}_{ig} + \mathcal{H}_c$

0.4 $M_T = M_c + M_{ig}$

0.5 $KEP = \frac{M_p v_o^2}{2gJ}$

0.6 $\frac{v_r}{v_o} = \frac{\frac{M_T}{2} + M_p}{\frac{M_T}{2} + M_r}$

0.7 $CONST\ 1 = (1/3)\left[1+\frac{v_r}{v_o}\right]^2 + \left(\frac{v_r}{v_o}\right)^2 - \left(\frac{v_r}{v_o}\right)\left(1+\frac{v_r}{v_o}\right)$

0.8 $KEG = \frac{M_T v_o^2}{2gJ}\ CONST\ 1$

0.9 $KER = \frac{M_r v_o^2}{2gJ}\left(\frac{v_r}{v_o}\right)^2$

0.10 $KEB = \frac{0.18\ A_{cnct}}{A}\ KEP$

0.11 $E_g = \mathcal{H} - \Sigma\ KE's$

0.12 $T_{av\ init} \equiv T_g = \frac{E_g(\gamma_2 - 1)J}{R_2 M_T}$

0.13 $p_{av\ init} \equiv p_g = \frac{12\ E_g(\gamma_2 - 1)J}{\mathcal{V}_T}$

0.14 $a_{av\ init} = (\gamma_2 g R_2 T_{av\ init})^{1/2}$

0.15 $$\beta = \frac{v_o}{a_{av\ init}}$$

0.16 $$\varphi_{av} = 1.04952 - 0.25021815\,\beta - 0.061082024\,\beta^2$$

0.17 $$\kappa_{av} = 0.97960297 + 0.10274869\,\beta + 0.19109947\,\beta^2$$

0.18 $$\psi_{av} = \varphi_{av}\ \kappa_{av}$$

0.19 $$p_{b\ init} = \frac{p_{av\ init}}{\varphi_{av}}$$

0.20 $$a_{b\ init} = \frac{a_{av\ init}}{(\varphi_{av})^{1/2}}$$

0.21 $$\alpha_T = \frac{A\ g\ p_{b\ init}}{a_{b\ init}\ M_T}$$

0.22a $$M(\mathcal{T}) = \nu_T\ M_T$$

b $$M(1) = 0.50688 M_T$$

0.23a $$P(\mathcal{T}) = \mu_T\ \frac{a_{b\ init}\ M_T}{g}$$

b $$P(1) = 0.44775\ \frac{a_{b\ init}\ M_T}{g}$$

0.24a $$H(\mathcal{T}) = \eta_T\ E_g$$

b $$H(1) = 0.58948\ E_g$$

0.25a $$\lambda_r = \frac{B}{\dot{p}}\ (1 - \nu_{eff})$$

b $$\lambda_r = 1.46881(1 - \nu_{eff})$$

Values of constants in equations 0.22 -- 0.25 were obtained for $\gamma = 1.26$.

0.26 $$\chi_1 = \chi_1(T^o)$$ See table.

0.27 $$\frac{V_y}{V_x} \equiv \frac{V_y}{V_\infty} = \frac{V_y}{V_\infty}\ (T^o)$$ See table.

0.28a $$\frac{4\pi r_2^3}{3} = \frac{M(1)\ \kappa_{2\ av}\ R_2\ \kappa_1}{144\left(\frac{\gamma_2+1}{2}\right)^{\left[\gamma_2/(\gamma_2-1)\right]}}$$

b $$\kappa_{2\ av} = 1.309 \text{ for } \gamma_2 = 1.26$$

0.29 $$M^*(1) = M(1) + \frac{4\pi r_2^3}{3V_\infty}$$

0.30 $$\bar{v}_1 = \frac{1.46881\ g\ P(1)}{M^*(1)}$$

0.31 $$J\,H(1) = \frac{M^*\bar{v}_1^2}{2g} + \frac{\gamma_2\ R_2}{\gamma_2 - 1}\ M(1)T^\circ + 144\ p_\infty\left(\frac{4\pi r_2^3}{3}\right)\left(1 + \frac{V_y}{V_\infty}\right)$$

Equations 0.26 -- 0.31 are solved iteratively for T° .

0.32 $$p_{s2} = p_s(T^\circ)$$

0.33 $$\tilde{r}_2^3 = r_2^3\left(1 + V_y/V_\infty\right)$$

0.34 $$r_1 = \left(\frac{\tilde{r}_2^3}{2}\right)^{1/3}$$

0.35 $$v_2 = v_s(T^\circ) \cong a\left(\frac{6}{7}\frac{p_{s2}}{p_\infty} + 1\right)^{1/2}$$

0.36 $$d_1 = 0.523\ \frac{a_{b\ init}}{\alpha_T} - \zeta$$

0.37 $$z_1 = d_1\ \frac{\lambda_r}{1.46881}$$

0.38 $$y_1 = d_1\ \frac{\omega}{1.46881}$$

0.39 $$x_1 = (d_1^2 - z_1^2 - y_1^2)^{1/2}$$

0.40a $$\frac{\bar{v}_{z1}}{\bar{v}_1} = \frac{F_z}{B} = 1 - \nu_{eff}$$

b $$\bar{v}_{z1} = \frac{\lambda_r}{1.46881} \bar{v}_1$$

0.41a $$\frac{\bar{v}_{y1}}{\bar{v}_1} = \frac{F_y}{B} = \frac{\omega}{1.46881}$$

b $$\bar{v}_{y1} = \frac{\omega}{1.46881} \bar{v}_1$$

0.42 $$\bar{v}_{x1} = (\bar{v}_1^2 - \bar{v}_{y1}^2 - \bar{v}_{z1}^2)^{1/2}$$

0.43a $$\hat{\alpha} = \tan^{-1}\left(\frac{\bar{v}_{x1}}{\bar{v}_{z1}}\right), \text{ for } v_{z1} > 0 .$$

b $$\hat{\alpha} = \frac{\pi}{2}, \text{ for } \bar{v}_{z1} = 0$$

c $$\hat{\alpha} = \pi + \tan^{-1}\left(\frac{\bar{v}_{x1}}{\bar{v}_{z1}}\right), \text{ for } \bar{v}_{z1} < 0 .$$

0.44a $$\hat{\beta} = \tan^{-1}\left(\frac{\bar{v}_{x1}}{\bar{v}_{y1}}\right), \text{ for } \bar{v}_{y1} \neq 0$$

b $$\hat{\beta} = \frac{\pi}{2}, \text{ for } \bar{v}_{y1} = 0$$

0.45 $$\cos\hat{\vartheta} = \frac{\cos\vartheta \cos(QE)}{\left|\sin^2\vartheta + \cos^2\vartheta \cos^2(QE)\right|^{1/2}}$$

0.46 $$\sin\hat{\vartheta} = (1 - \cos^2\hat{\vartheta})^{1/2}$$

0.47 $$D = \frac{G \cos(QE) + f}{\cos\hat{\vartheta}}$$

0.48 $$x = x_0 + x_1$$

0.49 $$y = y_0 + y_1$$

0.50 $$z = z_0 + z_1$$

0.51 $N^2 = (D \sin\hat{\vartheta} - x)^2$

$+((G + z) \sin(QE) + y \cos(QE) - h)^2$

$+ (D \cos\hat{\vartheta} + z \cos(QE) - y \sin(QE))^2$

0.52 $\emptyset^2 = (D \sin\hat{\vartheta} + x)^2$

$+ ((G + z) \sin(QE) + y \cos(QE) - h)^2$

$+ (D \cos\hat{\vartheta} + z \cos(QE) - y \sin(QE))^2$

0.53 $L^2 = D^2 + (G \sin(QE) - h)^2$

0.54 $\cos A_\xi = \frac{D \sin\hat{\vartheta} - x}{N}$

0.55 $\cos A_\eta = \frac{(G + z) \sin(QE) + y \cos(QE) - h}{N}$

0.56 $\cos A_\nu = \frac{D \cos\hat{\vartheta} + z \cos(QE) - y \sin(QE)}{N}$

0.57 $\cos B_\xi = \frac{D \sin\hat{\vartheta} + x}{\emptyset}$

0.58 $\cos B_\eta = \frac{(G + z) \sin(QE) + y \cos(QE) - h}{\emptyset}$

0.59 $\cos B_\nu = \frac{D \cos\hat{\vartheta} + z \cos(QE) - y \sin(QE)}{\emptyset}$

0.60 $\bar{v}_\xi = \bar{v}_{x1}$

0.61 $\bar{v}_\eta = \bar{v}_{y1} \cos(QE) + \bar{v}_{z1} \sin(QE)$

0.62 $\bar{v}_\nu = \bar{v}_{z1} \cos(QE) - \bar{v}_{y1} \sin(QE)$

0.63 $K = PF/1.46881$

0.64 $v_1 = v_2 + K(\bar{v}_\xi \cos A_\xi - \bar{v}_\eta \cos A_\eta - \bar{v}_\nu \cos A_\nu)$

0.65 $v_1' = v_2 - K(\bar{v}_\xi \cos B_\xi + \bar{v}_\eta \cos B_\eta + \bar{v}_\nu \cos B_\nu)$

0.66 $\varphi_{11} = \frac{7}{6}\left[\left(\frac{v_1}{a}\right)^2 - 1\right]$

0.67 $$\varphi_{12} = \frac{7}{6}\left[\left(\frac{v_1'}{a}\right)^2 - 1\right]$$

0.68 $$\varphi_{31} = \varphi_{11}\left(\frac{r_1}{N}\right)^{3/2}$$

0.69 $$\varphi_{32} = \varphi_{12}\left(\frac{r_1}{\emptyset}\right)^{3/2}$$

0.70 $$\varphi_3 = (\varphi_{31}^2 + \varphi_{32}^2)^{1/2}$$

0.71 $$p_{s31} = \varphi_{31}\, p_\infty$$

0.72 $$p_{s3} = \varphi_3\, p_\infty$$

0.73 $$q = p_\infty\left[5\varphi_3^2/2(7 + \varphi_3)\right]$$

0.74 $$\alpha = \left[\frac{(EFF)(E_g)(777.5)}{144\, p_\infty}\right]^{1/3}$$

0.75 $$\lambda = \frac{L}{\alpha}$$

0.76 $$\tilde{\varphi}_3 = \exp\left[-0.77394019 - 1.8989116(\ln\lambda) + 0.30859282(\ln\lambda)^2\right]$$

0.77 $$\tilde{p}_{s3} = \tilde{\varphi}_3\, p_\infty$$

0.78 $$\tilde{q} = p_\infty \cdot \exp\left[-2.7823354 - 3.2585905(\ln\lambda) + 0.30799213(\ln\lambda)^2\right]$$

0.79 $$DPP = 10^3\,\frac{\alpha}{a}\,\exp\left[-1.7935746 - 0.32274651(\ln\tilde{\varphi}_3) - 0.021788577(\ln\tilde{\varphi}_3)^2\right]$$

0.80 $$SPLSP = \frac{32.2\, p_\infty\, \alpha}{a\,\lambda}$$

0.81 $$DPLSP = \frac{10^3\, p_\infty\, \alpha}{a}\left[\frac{0.004}{\sqrt{\lambda}\,(0.089 + \lambda^2)} + \frac{0.0000314\,\lambda}{0.00231 + \lambda^5}\right]$$

THE DIGITAL COMPUTER PROGRAM

The computer program, designed to evaluate the equations, permits one to choose the parameter space for which the computations of pressure, etc. are made. One must enter the relevant gun constants and internal ballistic parameters (listed later in this section) along with the desired initial values and increments of the following variables: ω , ψ , QE, h, f, ϑ . Provision has been made for specifying the number of values of each of the above variables. The number of values (levels) for each variable is given a code word in the FORTRAN program. The values are called in order into computer memory under the following code words:

Variable	Code Word for Counter	Code Word for Number of Levels
ω	KATE	KENDAL
ψ	KAY	KEN
QE	NIEL	NORMA
h	MAC	MAGE
f	LENNY	LAURA
ϑ	IRENE	IVAN

Thus, if one required answers for two levels of ω , he would enter 2 for the code word KENDAL. Operationally, the computer would establish a counter labeled KATE which would take on integral values from 1 thru KENDAL, or 2, in this case.

The computer performs a complete factorial among the variables. Variables are listed in the above table in order of progressive nesting, ϑ being most deeply nested.

Using the notation Δx as the finite increment of the variable x, one must prepare data cards, in the following order, having the values of: ζ , h, f, ϑ , QE, ψ , Δh, Δf, $\Delta\vartheta$, ΔQE, $\Delta\psi$, a, G, x_o, y_o, z_o, ω , p_∞ , PWR, $\Delta\omega$, PF, EFF, where PWR represents the abs value of the power of distance in the peak overpressure-distance relationship -- taken here as 3/2. The tables of $\bar{x}_1(T^o)$, $V_y/V_x(T^o)$, $p_s(T^o)$, $v_x(T^o)$ follow the above data. Finally, the gun constants and internal ballistic parameters are entered as follows: γ_2, R_2, e_c, e_{ig}, A, A_{cnct}, $\mathcal{V}_T$, M_c, M_{ig}, M_p, M_R, v_o .

A logic diagram of the program and the source program, written in full FORTRAN, follow.

LOGIC DIAGRAM

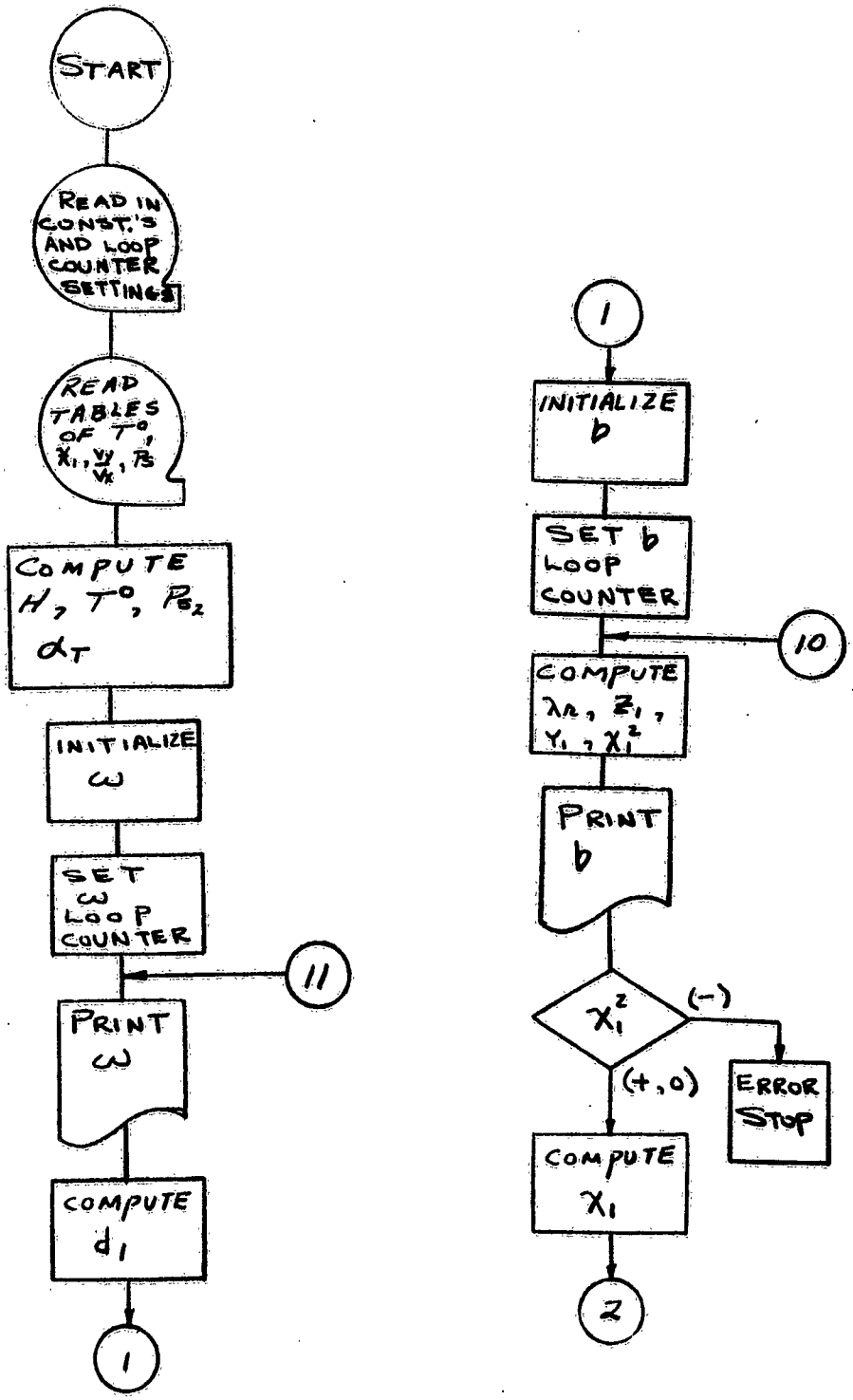

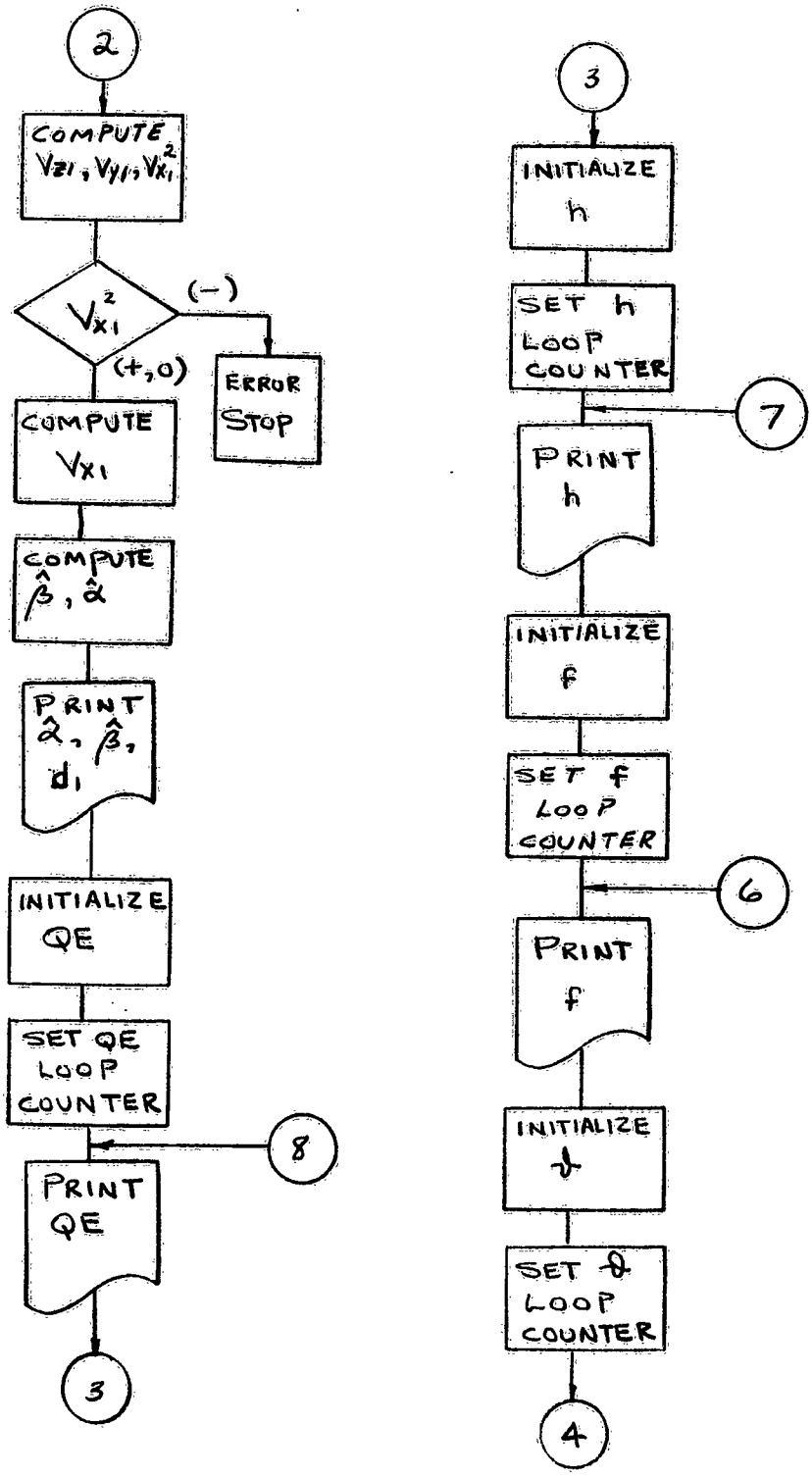
2
COMPUTE V_{zi}, V_{yi}, V_{xi}^2
V_{xi}^2
(−)
(+,0)
ERROR STOP
COMPUTE V_{xi}
COMPUTE $\hat{\beta}, \hat{\alpha}$
PRINT $\hat{\alpha}, \hat{\beta}, d_i$
INITIALIZE QE
SET QE LOOP COUNTER
8
PRINT QE
3
3
INITIALIZE h
SET h LOOP COUNTER
7
PRINT h
INITIALIZE f
SET f LOOP COUNTER
6
PRINT f
INITIALIZE ϕ
SET ϕ LOOP COUNTER
4

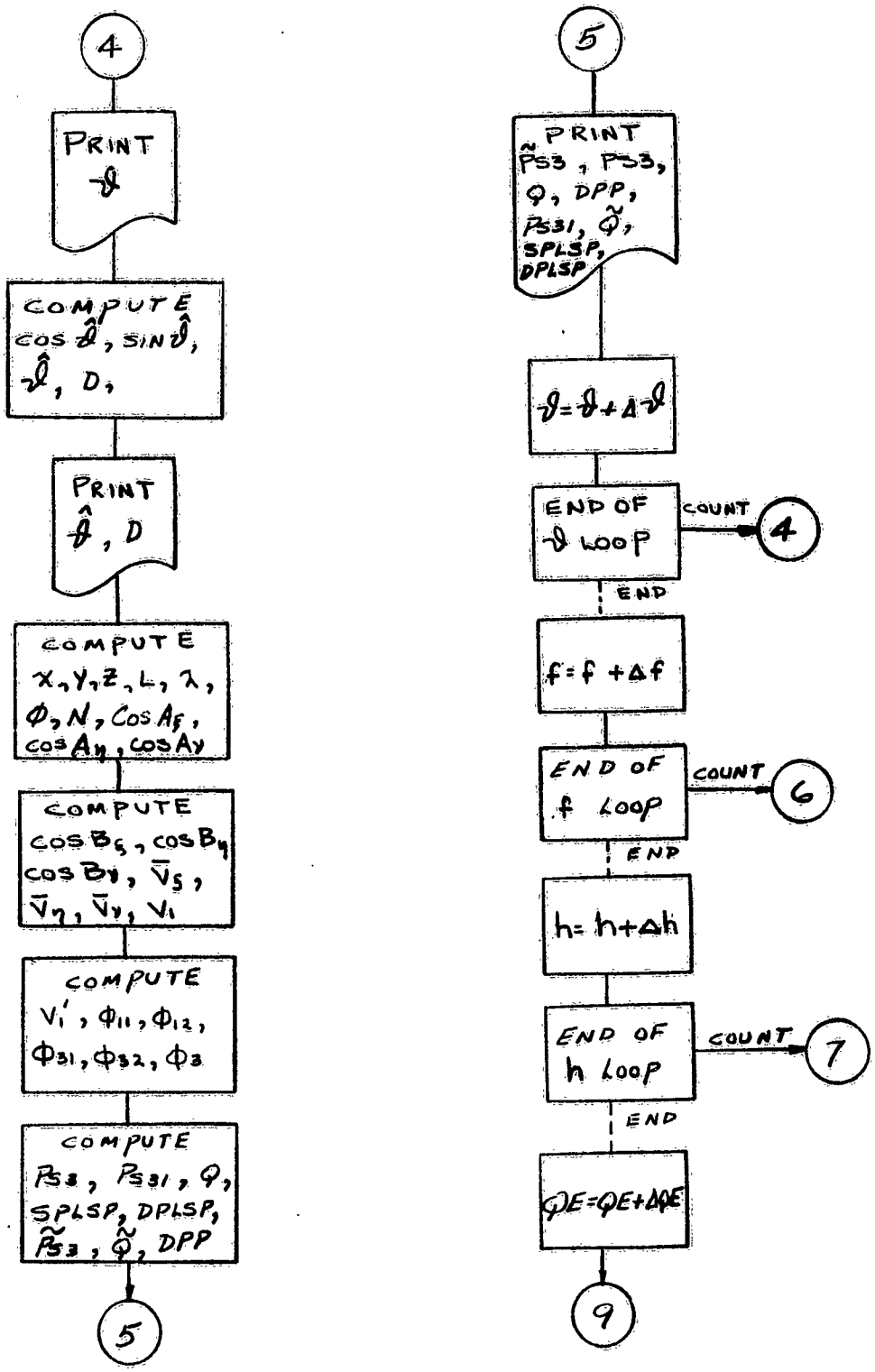
4
PRINT ϑ
COMPUTE $\cos\hat{\vartheta}$, $\sin\vartheta$, $\hat{\vartheta}$, D,
PRINT $\hat{\vartheta}$, D
COMPUTE x, y, z, L, λ, Φ, N, $\cos A_\xi$, $\cos A_\eta$, $\cos A_\gamma$
COMPUTE $\cos B_\xi$, $\cos B_\eta$, $\cos B_\gamma$, $\bar{V}_\xi$, $\bar{V}_\eta$, $\bar{V}_\gamma$, V_1
COMPUTE V_1', Φ_{11}, Φ_{12}, Φ_{31}, Φ_{32}, Φ_3
COMPUTE P_{33}, P_{331}, Q, SPLSP, DPLSP, $\tilde{P}_{33}$, $\tilde{Q}$, DPP
5
5
PRINT $\tilde{P}_{33}$, P_{33}, Q, DPP, P_{331}, $\tilde{Q}$, SPLSP, DPLSP
$\vartheta = \vartheta + \Delta\vartheta$
END OF ϑ LOOP
COUNT
4
END
$f = f + \Delta f$
END OF f LOOP
COUNT
6
END
$h = h + \Delta h$
END OF h LOOP
COUNT
7
END
$QE = QE + \Delta QE$
9

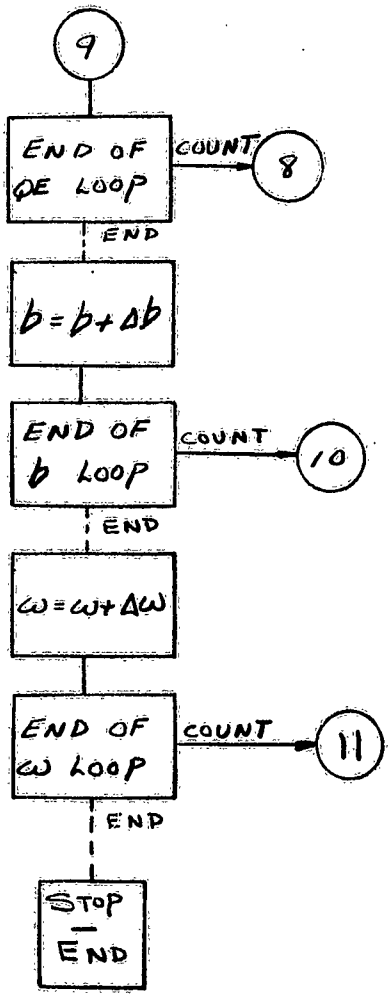
9
END OF QE LOOP
COUNT
8
END
b = b + Δb
END OF b LOOP
COUNT
10
END
ω = ω + Δω
END OF ω LOOP
COUNT
11
END
STOP
END

```
C  NUMBER  STATEMENT
C           PEAK OVERPRESSURE  SCHLENKER-OLSON  RIA R+D OCTOBER 1962
            READ INPUT TAPE 1,819, KENDAL,KEN,NORMA,MAGE,LAURA,IVAN
      819   FORMAT (6i5)
            WRITE OUTPUT TAPE 7,1
        1   FORMAT (39H    PEAK OVERPRESSURE-II SCHLENKER-OLSON, 8H RIA R+D ////)
            READ INPUT TAPE 1,2,ZETA,H,F,THETA,QE,BFLAT,DH,DF,DTHETA,DQE,
            DBFLAT,A,G,XO,YO,ZO,OMEGA,PINE,PWR,DOMEGA,PF,EFF
        2   FORMAT (F7.3)
            DIMENSION T(28),CY(28),VY(28),TK(16),PS(16)
            READ INPUT TAPE 1,3,(TK(J),J=1,16),(PS(J),J=1,16),(T(J),J=1,28),
            (CY(J),J=1,28),(VY(J),J=1,28)
        3   FORMAT (E12.8)
            READ INPUT TAPE 1,4,GAMMA,R,EC,EIG,AREA,ACNCT,VT,EMC,EMIG,EMP,EMR,VO
        4   FORMAT  (F12.6)
            HTOT=EIG*EMIG+EC*EMC
            EKEP=EMP*VO*VO/(2.0*32.17*777.5)
            TOTM=EMIG+EMC
            VRVO=(TOTM/2.0+EMP)/(TOTM/2.0+EMR
            CONST=(1.0+VRVO)**2/3.0+VRVO**2-VRVO*(1.0+VRVO)
```

```
EKEG=TOTM*VO**2*CONST/(2.*32.17*777.5)
EKER=EMR*(VRVO*VO)**2/(2.0*32.17*777.5)
EKEB=.18*ACNCT*EKEP/AREA
EGAS=HTOT-EKEB-EKER-EKEG-EKEP
TGAS=EGAS*(GAMMA-1.0)*777.5/(R*TOTM)
PGAS=12.0*EGAS*(GAMMA-1.0)*777.5/VT
AAVIN=SQRTF(GAMMA*32.17*R*TGAS)
BETA1=VO/AAVIN
PHIAV=1.04952-.25021815*BETA1.-06108024*BETA1**2
CAPPA=.97960297+.10274869*BETA1+.19109947*BETA1**2
THT=CAPPA*PHIAV
PBINT=PGAS/PHIAV
ABINT=AAVIN/SQRTF(THT)
ALPHT=AREA*32.17*PBINT/(ABINT*TOTM)
EM=.50688*TOTM
P=.44775*ABINT*TOTM/32.17
EJAYH=.58948*EGAS*777.5
A1=BFLAT
A2=OMEGA
```

```
      B1=QE
      B2=H
      B3=F
      B4=THETA
      COEF1=EM*1.309*R/(144.*((GAMMA+1.)/2.)**((GAMMA/(GAMMA-1.))))
      COEF2=GAMMA*R*EM/(GAMMA-1.)
      IA=1
      IB=1
      DELT=50
      TO=1000.
330   DO 333 J=2,28
      IF (TO-T(J)335,335,333
333   CONTINUE
335   CYE1=CY(J-1)+(CY(J)-CY(J-1))*(TO-T(J-1))/(T(J)-T(J-1))
      VYVX=VY(J-1)+(VY(J)-VY(J-1))*(TO-T(J-1)))/(T(J)-T(J-1))
      VINE=192./PINE
      EMSTR=EM+COEF1*CYE1/VINE
      V1BAR=1.46881*32.17*P/EMSTR
      FH2=EMSTR*V1BAR**2/(2.*32.17)+COEF2*TO+144.*PINE*COEF1*CYE1*(1.+VYVX)
```

```
      FTO=FH2-EJAYH
      IF (FTO)18,19,19
   18 ABFTO=(-FTO)
      GO TO 1711
   19 ABFTO=FTO
 1711 IF (ABFTO-10.)100,100,20
   20 GO TO (21,22,23), IB
   21 TOO=TO
      FTOO=FTO
      ABF=ABFTO
      TO = TO + DELT
      IB=3
      GO TO 330
   23 IF  (FTOO*FTO)25,1260,1260
   25 IB=2
   22 TOOT=TO
      TO=TO-FTO/(((FTO-FTOO)/(TO-TOO)))
      FTOO=FTO
      TOO=TOOT
      ABF=ABFTO
      GO TO 330
```

```
1260    GO TO (1261,1264),IA
1261    IA=2
        IF (ABF-ABFTO)1267,1264,1264
1264    TOO=TO
        FTOO=FTO
        ABF=ABFTO
        TO=TO+DELT
        GO TO 330
1267    DELT=(-DELT)
        GO TO 1264
 100    TOK=TO
        DO 101 J=2,16
        IF (TOK-TK(J))102,102,101
 101    CONTINUE
 102    PS2=PS(J-1)+(PS(J)-PS(J-1))*(TOK-TK(J-1))/(TK(J)-TK(J-1))
        EK=PF/1.46881
        ALPHA=(EFF*EGAS*777.5/(144.*PINE))**(1./3.)
        WRITE OUTPUT TAPE 7,800,PS2,TO
 800    FORMAT  (3HPS2,4X,F7.2,5H PSIG,11X,2HTO,F8.2,2H R///)
        R2TIL=3.*COEF1*CYE1/(4.*3.1415927)*(1.+VYVX)
        R1=(R2TIL/2.)**(1./3.)
```

```
      R2TIL=R2TIL**(1./3.)
      V2=A*SQRTF(6.*PS2/(7.*PINE)+1.)
      OMEGA=A2
      DO 10 KATE=1,KENDAL
      WRITE OUTPUT TAPE 7,820,OMEGA
820   FORMAT (////105X,5HOMEGA/105X,F6.3/)
      D1=(ABINT/ALPHT)*.523-ZETA
      BFLAT=A1
      DO 7 KAY=1,KEN
      ALMDA=1.46881*(1.-BFLAT)
      Z1=D1*ALMDA/1.46881
      Y1=D1*OMEGA/1.46881
      X1=D1*D1-Z1*Z1-Y1*Y1
      WRITE OUTPUT TAPE 7,799,BFLAT
799   FORMAT  (////105X,6HB-FLAT/105X,F6.3/)
      IF  (X1)801,802,802
801   STOP 11111
802   X1=SQRTF(X1)
      VZ1=ALMDA*V1BAR/1.46881
      VY1=OMEGA*V1BAR/1.46881
      VX1=V1BAR**2-VY1**2-VZ1**2
```

```
      IF  (VX1)803,804,804
803   STOP 22222
804   VX1=SQRTF(VX1)
      IF (VZ1)805,806,807
805   ALHAT=3.1415927+ATANF(VX1/VZ1)
      GO TO 808
806   ALHAT=3.1415927/2.
      GO TO 808
807   ALHAT=ATANF(VX1/VZ1)
808   IF  (VY1)809,810,809
809   BHAT=ATANF(VX1/VY1)
      GO TO 811
810   BHAT=3.1415927/2.
811   ALHAT=ALHAT*57.29578
      BHAT=BHAT*57.29578
      WRITE OUTPUT TAPE 7,812,ALHAT,BHAT,D1
812   FORMAT (60X,9HALPHA-HAT,6X,8HBETA-HAT,7X,2HD1/60X,F7.2,4H DEG,4X,
      F6.2,4H DEG,5X,F6.2,3H FT////)
      QE=B1
      DO 6 NIEL=1,NORMA
```

```
      WRITE OUTPUT TAPE 7,813,QE
813   FORMAT (/90X,2HQE,/90X,F6.2,4H DEG)
      H=B2
      DO 5 MAC=1,MAGE
      WRITE OUTPUT TAPE 7,814,H
814   FORMAT (/79X,1HH/75X,F6.2,3H FT)
      F=B3
      DO 8 LENNY=1,LAURA
      WRITE OUTPUT TAPE 7,815,F
815   FORMAT (/64X,1HF/60X,F6.2,3H FT)
      THETA=B4
      DO 9 IRENE=1,IVAN
      WRITE OUTPUT TAPE 7,816,THETA
816   FORMAT (/45X,5HTHETA/45X,F6.2,4H DEG)
      COSTH=COSF(THETA/57.29578)*COSF(QE/57.29578)/SQRTF(SINF(THETA/57.29578)**2
      +COSF(THETA/57.29578)**2*COSF(QE/57.29578)**2)
      SINTH=SQRTF(1.-COSTH**2)
      THTHAT=ATANF(SINTH/COSTH)*57.29578
      D=(G*COSF(QE/57.29578)+F)/COSTH
      WRITE OUTPUT TAPE 7,817,THTHAT,D
```

```
817   FORMAT (45X,9HTHETA-HAT,10X,1HD/45X,F6.2,4H DEG,5X,F6.2,3H FT)
      X=X0+X1
      Y=Y0+Y1
      Z=Z0+Z1
      EL=SQRTF(D*D+(G*SINF(QE/57.29578)-H)**2)
      WAVE=EL/ALPHA
      COM=((G+Z)*SINF(QE/57.29578)+Y*COSF(QE/57.29578)-H)**2+(D*COSTH+Z*
      COSF(QE/57.29578)-Y*SINF(QE/57.29578))**2
      O=SQRTF((D*SINTH+X)**2+COM)
      EN=SQRTF((D*SINTH-X)**2+COM)
      COSAXI=(D*SINTH-X)/EN
      COSETA=((G+Z)*SINF(QE/57.29578)+Y*COSF(QE/57.29578)-H)/EN
      COSANU=(D*COSTH+Z*COSF(QE/57.29578)-Y*SINF(QE/57.29578))/EN
      COSBXI=(D*SINTH+X)/O
      COSBTA=((G+Z)*SINF(QE/57.29578)+Y*COSF(QE/57.29578)-H)/O
      COSBNU=(D*COSTH+Z*COSF(QE/57.29578)-Y*SINF(QE/57.29578))/O
      VBARXI=VXI
      VBARET=VY1*COSF(QE/57.29578)+VZ1*SINF(QE/57.29578)
      VBARNU=VZ1*COSF(QE/57.29578)-VY1*SINF(QE/57.29578)
      V1=V2+EK*(VBARXI*COSAXI-VBARET*COSETA-VBARNU*COSANU)
```

```
      V1PR=V2-EK*(VBARXI*COSBXI+VBARET*COSBTA+VBARNU*COSBNU)
      PHI11=7./6.*((V1/A)**2-1.)
      PS1=PINE*PHI11
      PHI12=7./6.*((V1PR/A**2-1.)
      PHI31=PHI11*(R1/EN)**PWR
      PHI32=PHI12*(R1/O)**PWR
      PHI3=SQRTF((PHI31)**2+(PHI32)**2)
      PS3=PHI3*PINE
      PS31=PHI31*PINE
      Q=5.*PINE*PHI3**2/(2.*(7.+PHI3))
      SPLSP=32.2*PINE*ALPHA/(A*WAVE)
      DPLSP=1000.*PINE*ALPHA/A*(0.004/(SQRTF(WAVE)*(0.089+WAVE*WAVE))+0.0000314*
     WAVE/(0.00231+(WAVE)**5.))
      PS3TIL=PINE*EXPF(-.77394019-1.8989116*LOGF(WAVE)+.3085928*LOGF(WAVE)**2)
      P3TL=PS3TIL/PINE
      DPP=1000.*ALPHA/A*EXPF(-1.7935746-0.32274651*LOGF(P3TL)-0.021788577*
     LOGF(P3TL)**2)
      QTILDA=PINE*EXPF(-2.7828354-3.2585905*LOGF(WAVE)+.30799213*LOGF(WAVE)**2)
      WRITE OUTPUT TAPE 7,818,PS31,PS3,Q,DPP,PS3TIL,QTILDA,SPLSP,DPLSP
  818 FORMAT  (3HPS31,12X,3HPS3,12X,1HQ,14X,10HDUR POS PH,5X,9HPS3 TILDA,6X,
```

```
      7HQ TILDA,8X,10HPOS ST IMP,5X,11HPOS DYN IMP/4HPSIG,11X,4HPSIG,11X,4HPSIG,
     11X,9HMILLISECS,6X,4HPSIG,11X,4HPSIG,11X,8HPSI-MSEC,7X,8HPSI-MSEC/F7.2,
     8X,F6.2,9X,F6.2,9X,F6.2,9X,F6.2,9X,F6.2,9X,F6.2,9X,F6.2)
    9 THETA=THETA+DTHETA
    8 F=F+DF
    5 H=H+DH
    6 QE=QE+DQE
    7 BFLAT=BFLAT+DBFLAT
   10 OMEGA=OMEGA+DOMEGA
      STOP 99999
      END
```

TABLES

T°	p_s
503.2529	36.83212
559.6152	39.94112
618.2186	43.13844
679.0130	46.42399
741.9546	49.79769
807.0050	53.25947
874.1304	56.80927
943.3008	60.44707
1087.6745	67.98647
1239.9484	75.87748
1482.8697	88.37288
1925.5914	110.95481
2414.6800	135.73126
2949.4100	162.70166
3773.8406	204.14546
4962.6533	263.74723

T°	x_1	V_y/V_x	V_x
503.2529	9.765811	0.43260061	1974.0000
559.6152	10.241649	0.41816526	2030.4000
618.2186	10.688713	0.40487396	2086.8000
679.0130	11.108780	0.39260977	2143.2000
741.9546	11.503584	0.38127014	2199.6000
807.0050	11.874799	0.37076485	2256.0000
874.1304	12.224014	0.36101439	2312.4000
943.3008	12.552730	0.35194839	2368.8000
1014.4900	12.862355	0.34350447	2425.2000
1087.6745	13.154202	0.33562715	2481.6000
1162.8336	13.429495	0.32826697	2538.0000
1239.9484	13.689368	0.32137975	2594.4000
1319.0024	13.934875	0.31492590	2650.8000
1399.9806	14.166989	0.30886986	2707.2000
1482.8697	14.386613	0.30317968	2763.6000
1567.6574	14.594580	0.29782649	2820.0000
1654.3329	14.791661	0.29278425	2876.4000
1742.8862	14.978567	0.28802937	2932.8000
1833.3085	15.155963	0.28354042	2989.2000
1925.5914	15.324453	0.27929799	3045.6000
2115.7107	15.636940	0.27148336	3158.4000
2414.6800	16.051716	0.26121498	3327.6000
2730.0756	16.411611	0.25239843	3496.8000
2949.4100	16.625605	0.24719585	3609.6000
3409.7324	17.001280	0.23813229	3835.2000
3773.8406	17.244317	0.23231492	4004.4000
4284.3693	17.526006	0.22561657	4230.0000
4962.6533	17.822599	0.21861388	4512.0000

DATA FOR XM103 BLAST FIELD COMPUTATIONS

Parameter	Value	Units
γ_2	1.2402	
R_2	67.	$\frac{lb_F\ ft}{lb_m\ ^\circ R}$
e_c	1727.5	Btu/lb_m
e_{ig}	1231.	Btu/lb_m
A	13.717	in^2
A_{cnct}	10.8984	in^2
$\mathcal{V}_T$	1710.	in^3
M_c	4.46	lb_m
M_{ig}	0.042857	lb_m
M_p	28.5	lb_m
M_r	1430.	lb_m
v_o	2200.	ft/sec
ν_{eff}	1.35	
ω	0.	
x_0	0.50	ft
y_0	0.	ft
z_0	-0.416	ft
G	11.3	ft
ζ	0.933	ft

PS1G	PS2G	PS3G	MILLISECS	PS1G	PS2G	PSI-MSEC	PSI-MSEC
1.67	1.83	0.08	2.70	1.24	0.04	1.30	0.03

THETA
50.00 DEG
THETA-HAT
73.99 DEG
D
15.76 FT

PS3I PS1G	PS3 PS1G	Q PS1G	DUR POS PH MILLISECS	PS3 TILDA PS1G	Q TILDA PS1G	POS ST IMP PSI-MSEC	POS DYN IMP PSI-MSEC
1.03	1.15	0.03	2.89	0.89	0.02	1.00	0.02

SAMPLE COMPUTATIONS

In the following sample of computed results using the FORTRAN program, the results of the present theory and those of the single point-source explosion theory are printed for comparison.

G-FLAT
1.350

ALPHA-HAT
110.49 DEG
BETA-HAT
90.00 DEG
D1
4.73 FT

GE
10.00 DEG

H
0.00 FT

F
0.00 FT

THETA
0.00 DEG
THETA-HAT
-0.00 DEG
D
11.13 FT

PS3I PS1G	PS3 PS1G	Q PS1G	DUR POS PH MILLISECS	PS3 TILDA PS1G	Q TILDA PS1G	POS ST IMP PSI-MSEC	POS DYN IMP PSI-MSEC
4.70	6.65	1.01	1.95	4.75	0.49	3.26	0.29

THETA
10.00 DEG
THETA-HAT
10.15 DEG
D
11.31 FT

PS3I PS1G	PS3 PS1G	Q PS1G	DUR POS PH MILLISECS	PS3 TILDA PS1G	Q TILDA PS1G	POS ST IMP PSI-MSEC	POS DYN IMP PSI-MSEC
5.43	6.73	1.03	1.96	4.62	0.47	3.21	0.28

THETA
20.00 DEG
THETA-HAT
20.28 DEG
D
11.86 FT

PS3I PS1G	PS3 PS1G	Q PS1G	DUR POS PH MILLISECS	PS3 TILDA PS1G	Q TILDA PS1G	POS ST IMP PSI-MSEC	POS DYN IMP PSI-MSEC
6.01	6.84	1.07	2.00	4.26	0.40	3.06	0.25

THETA
30.00 DEG

			THETA-HAT	D			
			39.38 DEG	12.96 FT			
PS31	PS3	Q	DUR POS PH	PS3 TILDA	Q TILDA	POS ST IMP	POS DYN IMP
PSIG	PSIG	PSIG	MILLISECS	PSIG	PSIG	PSI-MSEC	PSI-MSEC
6.13	6.68	1.02	2.08	3.70	0.31	2.82	0.20

			THETA				
			40.00 DEG				
			THETA-HAT	D			
			40.43 DEG	14.62 FT			
PS31	PS3	Q	DUR POS PH	PS3 TILDA	Q TILDA	POS ST IMP	POS DYN IMP
PSIG	PSIG	PSIG	MILLISECS	PSIG	PSIG	PSI-MSEC	PSI-MSEC
5.58	5.88	0.79	2.19	3.02	0.22	2.50	0.15

			THETA				
			50.00 DEG				
			THETA-HAT	D			
			50.43 DEG	17.47 FT			
PS31	PS3	Q	DUR POS PH	PS3 TILDA	Q TILDA	POS ST IMP	POS DYN IMP
PSIG	PSIG	PSIG	MILLISECS	PSIG	PSIG	PSI-MSEC	PSI-MSEC
4.17	4.45	0.46	2.35	2.30	0.13	2.09	0.10

				F			
				1.56 FT			

			THETA				
			0.00 DEG				
			THETA-HAT	D			
			-0.00 DEG	12.63 FT			
PS31	PS3	Q	DUR POS PH	PS3 TILDA	Q TILDA	POS ST IMP	POS DYN IMP
PSIG	PSIG	PSIG	MILLISECS	PSIG	PSIG	PSI-MSEC	PSI-MSEC
3.97	5.61	0.73	2.06	3.83	0.33	2.88	0.21

			THETA				
			10.00 DEG				
			THETA-HAT	D			
			10.15 DEG	12.83 FT			
PS31	PS3	Q	DUR POS PH	PS3 TILDA	Q TILDA	POS ST IMP	POS DYN IMP
PSIG	PSIG	PSIG	MILLISECS	PSIG	PSIG	PSI-MSEC	PSI-MSEC
4.51	5.64	0.73	2.07	3.74	0.32	2.84	0.21

			THETA				
			20.00 DEG				
			THETA-HAT	D			
			20.23 DEG	13.46 FT			
PS31	PS3	Q	DUR POS PH	PS3 TILDA	Q TILDA	POS ST IMP	POS DYN IMP
PSIG	PSIG	PSIG	MILLISECS	PSIG	PSIG	PSI-MSEC	PSI-MSEC
4.88	5.63	0.73	2.12	3.45	0.28	2.71	0.18

			THETA				
			30.00 DEG				
			THETA-HAT	D			
			30.38 DEG	14.64 FT			
PS31	PS3	Q	DUR POS PH	PS3 TILDA	Q TILDA	POS ST IMP	POS DYN IMP
PSIG	PSIG	PSIG	MILLISECS	PSIG	PSIG	PSI-MSEC	PSI-MSEC
4.85	5.36	0.66	2.19	3.02	0.22	2.49	0.15

			THETA				
			40.00 DEG				

THETA-HAT D
40.43 DEG 16.59 FT

PS31	PS3	Q	DUR POS PH	PS3 TILDA	Q TILDA	POS ST IMP	POS DYN IMP
PSIG	PSIG	PSIG	MILLISECS	PSIG	PSIG	PSI-MSEC	PSI-MSEC
4.28	4.64	0.50	2.30	2.48	0.15	2.20	0.11

THETA
50.00 DEG
THETA-HAT D
50.43 DEG 19.82 FT

PS31	PS3	Q	DUR POS PH	PS3 TILDA	Q TILDA	POS ST IMP	POS DYN IMP
PSIG	PSIG	PSIG	MILLISECS	PSIG	PSIG	PSI-MSEC	PSI-MSEC
3.24	3.50	0.29	2.45	1.91	0.09	1.85	0.07

F
3.00 FT

THETA
0.00 DEG
THETA-HAT D
0.00 DEG 14.13 FT

PS31	PS3	Q	DUR POS PH	PS3 TILDA	Q TILDA	POS ST IMP	POS DYN IMP
PSIG	PSIG	PSIG	MILLISECS	PSIG	PSIG	PSI-MSEC	PSI-MSEC
3.39	4.00	0.53	2.16	1.19	0.24	2.58	0.16

THETA
10.00 DEG
THETA-HAT D
10.15 DEG 14.35 FT

PS31	PS3	Q	DUR POS PH	PS3 TILDA	Q TILDA	POS ST IMP	POS DYN IMP
PSIG	PSIG	PSIG	MILLISECS	PSIG	PSIG	PSI-MSEC	PSI-MSEC
3.83	4.79	0.53	2.18	1.11	0.23	2.54	0.16

THETA
20.00 DEG
THETA-HAT D
20.28 DEG 15.06 FT

PS31	PS3	Q	DUR POS PH	PS3 TILDA	Q TILDA	POS ST IMP	POS DYN IMP
PSIG	PSIG	PSIG	MILLISECS	PSIG	PSIG	PSI-MSEC	PSI-MSEC
4.04	4.72	0.52	2.22	2.88	0.20	2.42	0.14

THETA
30.00 DEG
THETA-HAT D
30.30 DEG 16.38 FT

PS31	PS3	Q	DUR POS PH	PS3 TILDA	Q TILDA	POS ST IMP	POS DYN IMP
PSIG	PSIG	PSIG	MILLISECS	PSIG	PSIG	PSI-MSEC	PSI-MSEC
3.95	4.42	0.46	2.29	2.53	0.16	2.23	0.11

THETA
40.00 DEG
THETA-HAT D
40.43 DEG 18.56 FT

PS31	PS3	Q	DUR POS PH	PS3 TILDA	Q TILDA	POS ST IMP	POS DYN IMP
PSIG	PSIG	PSIG	MILLISECS	PSIG	PSIG	PSI-MSEC	PSI-MSEC
3.45	3.78	0.34	2.40	2.10	0.11	1.97	0.08

THETA
50.00 DEG

PS31	PS3	Q	THETA-HAT	D	Q TILDA	POS ST IMP	POS DYN IMP
			50.43 DEG	22.18 FT			
PSIG	PSIG	PSIG	DUR POS PH	PS3 TILDA			
			MILLISECS	PSIG	PSIG	PSI-MSEC	PSI-MSEC
2.61	2.85	0.19	2.54	1.64	0.07	1.65	0.05

F
4.50 FT

THETA
0.00 DEG

PS31	PS3	Q	THETA-HAT	D	Q TILDA	POS ST IMP	POS DYN IMP
			0.00 DEG	15.63 FT			
PSIG	PSIG	PSIG	DUR POS PH	PS3 TILDA			
			MILLISECS	PSIG	PSIG	PSI-MSEC	PSI-MSEC
2.94	4.15	0.40	2.25	2.72	0.18	2.34	0.13

THETA
10.00 DEG

PS31	PS3	Q	THETA-HAT	D	Q TILDA	POS ST IMP	POS DYN IMP
			10.15 DEG	15.88 FT			
PSIG	PSIG	PSIG	DUR POS PH	PS3 TILDA			
			MILLISECS	PSIG	PSIG	PSI-MSEC	PSI-MSEC
3.25	4.13	0.46	2.26	2.66	0.17	2.30	0.12

THETA
20.00 DEG

PS31	PS3	Q	THETA-HAT	D	Q TILDA	POS ST IMP	POS DYN IMP
			20.28 DEG	16.66 FT			
PSIG	PSIG	PSIG	DUR POS PH	PS3 TILDA			
			MILLISECS	PSIG	PSIG	PSI-MSEC	PSI-MSEC
3.41	4.02	0.38	2.31	2.47	0.15	2.19	0.11

THETA
30.00 DEG

PS31	PS3	Q	THETA-HAT	D	Q TILDA	POS ST IMP	POS DYN IMP
			30.38 DEG	18.12 FT			
PSIG	PSIG	PSIG	DUR POS PH	PS3 TILDA			
			MILLISECS	PSIG	PSIG	PSI-MSEC	PSI-MSEC
3.29	3.72	0.33	2.38	2.18	0.12	2.02	0.09

THETA
40.00 DEG

PS31	PS3	Q	THETA-HAT	D	Q TILDA	POS ST IMP	POS DYN IMP
			40.43 DEG	20.53 FT			
PSIG	PSIG	PSIG	DUR POS PH	PS3 TILDA			
			MILLISECS	PSIG	PSIG	PSI-MSEC	PSI-MSEC
2.05	3.16	0.24	2.48	1.82	0.08	1.78	0.07

THETA
50.00 DEG

PS31	PS3	Q	THETA-HAT	D	Q TILDA	POS ST IMP	POS DYN IMP
			50.43 DEG	24.53 FT			
PSIG	PSIG	PSIG	DUR POS PH	PS3 TILDA			
			MILLISECS	PSIG	PSIG	PSI-MSEC	PSI-MSEC
2.16	2.38	0.13	2.62	1.43	0.05	1.50	0.04

F
6.00 FT

THETA
0.00 DEG
THETA-HAT
-0.00 DEG
D
17.13 FT

PS31 PSIG	PS3 PSIG	Q PSIG	DUR POS PH MILLISECS	PS3 TILDA PSIG	Q TILDA PSIG	POS ST IMP PSI-MSEC	POS DYN IMP PSI-MSEC
2.57	3.63	0.31	2.33	2.37	0.14	2.13	0.10

THETA
10.00 DEG
THETA-HAT
10.15 DEG
D
17.40 FT

PS31 PSIG	PS3 PSIG	Q PSIG	DUR POS PH MILLISECS	PS3 TILDA PSIG	Q TILDA PSIG	POS ST IMP PSI-MSEC	POS DYN IMP PSI-MSEC
2.82	3.60	0.30	2.34	2.31	0.13	2.10	0.10

THETA
20.00 DEG
THETA-HAT
20.28 DEG
D
18.26 FT

PS31 PSIG	PS3 PSIG	Q PSIG	DUR POS PH MILLISECS	PS3 TILDA PSIG	Q TILDA PSIG	POS ST IMP PSI-MSEC	POS DYN IMP PSI-MSEC
2.92	3.48	0.28	2.38	2.15	0.11	2.00	0.09

THETA
30.00 DEG
THETA-HAT
30.38 DEG
D
19.85 FT

PS31 PSIG	PS3 PSIG	Q PSIG	DUR POS PH MILLISECS	PS3 TILDA PSIG	Q TILDA PSIG	POS ST IMP PSI-MSEC	POS DYN IMP PSI-MSEC
2.79	3.19	0.24	2.45	1.93	0.09	1.84	0.07

THETA
40.00 DEG
THETA-HAT
40.43 DEG
D
22.50 FT

PS31 PSIG	PS3 PSIG	Q PSIG	DUR POS PH MILLISECS	PS3 TILDA PSIG	Q TILDA PSIG	POS ST IMP PSI-MSEC	POS DYN IMP PSI-MSEC
2.40	2.69	0.17	2.55	1.61	0.06	1.63	0.05

THETA
50.00 DEG
THETA-HAT
50.43 DEG
D
26.89 FT

PS31 PSIG	PS3 PSIG	Q PSIG	DUR POS PH MILLISECS	PS3 TILDA PSIG	Q TILDA PSIG	POS ST IMP PSI-MSEC	POS DYN IMP PSI-MSEC
1.82	2.03	0.10	2.68	1.28	0.04	1.37	0.03

H
1.00 FT

F
0.00 FT

THETA
0.00 DEG
THETA-HAT
-0.00 DEG
D
11.13 FT

			40.00 DEG THETA-HAT 67.82 DEG	D 26.14 FT
PS31 PSIG	PS3 PSIG	Q PSIG		
1.57	1.77	0.07		
			THETA 50.00 DEG THETA-HAT 73.99 DEG	D 35.76 FT
PS31 PSIG	PS3 PSIG	Q PSIG		
0.96	1.11	0.03		

B-FLAT
1.350

The printed results on this page and following pages illustrate the answers obtained from an abbreviated program. In this case only the two-shock sphere theory is evaluated with PF = 0.0625.

ALPHA-HAT
110.49 DEG

BETA-HAT
90.00 DEG

D1
4.73 FT

CE
10.00 DEG

H
0.00 FT

F
0.00 FT

			THETA 0.00 DEG THETA-HAT -0.00 DEG	D 11.12 FT
PS31 PSIG	PS3 PSIG	Q PSIG		
4.74	6.71	1.03		
			THETA 10.00 DEG THETA-HAT 10.15 DEG	D 11.31 FT
PS31 PSIG	PS3 PSIG	Q PSIG		
5.40	6.75	1.04		
			THETA 20.00 DEG	

PS31 PSIG	PS3 PSIG	Q PSIG
5.87	6.77	1.05

THETA-HAT 20.28 DEG

D 11.86 FT

PS31 PSIG	PS3 PSIG	Q PSIG
5.88	6.50	0.97

THETA 30.00 DEG

THETA-HAT 30.38 DEG

D 12.90 FT

PS31 PSIG	PS3 PSIG	Q PSIG
5.20	5.64	0.73

THETA 40.00 DEG

THETA-HAT 40.43 DEG

D 14.62 FT

PS31 PSIG	PS3 PSIG	Q PSIG
3.90	4.23	0.42

THETA 50.00 DEG

THETA-HAT 50.43 DEG

D 17.47 FT

F 1.50 FT

PS31 PSIG	PS3 PSIG	Q PSIG
3.98	5.63	0.73

THETA 0.00 DEG

THETA-HAT -0.00 DEG

D 12.63 FT

PS31 PSIG	PS3 PSIG	Q PSIG
4.46	5.63	0.73

THETA 10.00 DEG

THETA-HAT 10.15 DEG

D 12.83 FT

THETA 20.00 DEG

THETA-HAT 20.28 DEG

D 13.46 FT

PS31 PSIG	PS3 PSIG	Q PSIG
4.74	5.55	0.71

THETA 30.00 DEG
THETA-HAT 30.38 DEG
D 14.64 FT

PS31 PSIG	PS3 PSIG	Q PSIG
4.64	5.21	0.63

THETA 40.00 DEG
THETA-HAT 40.43 DEG
D 16.59 FT

PS31 PSIG	PS3 PSIG	Q PSIG
4.04	4.45	0.46

THETA 50.00 DEG
THETA-HAT 50.43 DEG
D 19.82 FT

PS31 PSIG	PS3 PSIG	Q PSIG
3.02	3.33	0.26

F 3.00 FT

THETA 0.00 DEG
THETA-HAT -0.00 DEG
D 14.13 FT

PS31 PSIG	PS3 PSIG	Q PSIG
3.39	4.80	0.53

THETA 10.00 DEG
THETA-HAT 10.15 DEG
D 14.35 FT

PS31 PSIG	PS3 PSIG	Q PSIG
3.75	4.77	0.53

THETA 20.00 DEG
THETA-HAT 20.28 DEG
D 15.06 FT

PS31 PSIG	PS3 PSIG	Q PSIG

3.92	4.65	0.50

THETA
30.00 DEG
THETA-HAT
30.38 DEG
D
16.38 FT

PS31 PSIG	PS3 PSIG	Q PSIG
3.77	4.29	0.43

THETA
40.00 DEG
THETA-HAT
40.43 DEG
D
18.56 FT

PS31 PSIG	PS3 PSIG	Q PSIG
3.25	3.63	0.31

THETA
50.00 DEG
THETA-HAT
50.43 DEG
D
22.18 FT

PS31 PSIG	PS3 PSIG	Q PSIG
2.43	2.72	0.18

F
4.50 FT

THETA
0.00 DEG
THETA-HAT
-0.00 DEG
D
15.63 FT

PS31 PSIG	PS3 PSIG	Q PSIG
2.93	4.14	0.40

THETA
10.00 DEG
THETA-HAT
10.15 DEG
D
15.88 FT

PS31 PSIG	PS3 PSIG	Q PSIG
3.20	4.10	0.39

THETA
20.00 DEG
THETA-HAT
20.28 DEG
D
16.66 FT

PS31 PSIG	PS3 PSIG	Q PSIG
3.30	3.96	0.37

THETA
30.00 DEG
THETA-HAT
30.38 DEG
D
18.12 FT

PS31	PS3	Q
PSIG	PSIG	PSIG
3.14	3.62	0.31

THETA
40.00 DEG
THETA-HAT
40.43 DEG
D
20.53 FT

PS31	PS3	Q
PSIG	PSIG	PSIG
2.68	3.04	0.22

THETA
50.00 DEG
THETA-HAT
50.43 DEG
D
24.53 FT

PS31	PS3	Q
PSIG	PSIG	PSIG
2.01	2.28	0.12

F
6.00 FT

THETA
0.00 DEG
THETA-HAT
-0.00 DEG
D
17.13 FT

PS31	PS3	Q
PSIG	PSIG	PSIG
2.55	3.61	0.31

THETA
10.00 DEG
THETA-HAT
10.15 DEG
D
17.40 FT

PS31	PS3	Q
PSIG	PSIG	PSIG
2.76	3.57	0.30

THETA
20.00 DEG
THETA-HAT
20.28 DEG
D
18.26 FT

PS31	PS3	Q
PSIG	PSIG	PSIG
2.82	3.42	0.27

THETA

			30.00 DEG		
			THETA-HAT	D	
			30.38 DEG	19.85 FT	
PS31	PS3	Q			
PSIG	PSIG	PSIG			
2.66	3.10	0.23			
			THETA		
			40.00 DEG		
			THETA-HAT	D	
			40.43 DEG	22.50 FT	
PS31	PS3	Q			
PSIG	PSIG	PSIG			
2.26	2.59	0.16			
			THETA		
			50.00 DEG		
			THETA-HAT	D	
			50.43 DEG	26.89 FT	
PS31	PS3	Q			
PSIG	PSIG	PSIG			
1.70	1.94	0.09			
					H
					1.00 FT
				F	
				0.00 FT	
			THETA		
			0.00 DEG		
			THETA-HAT	D	
			-0.00 DEG	11.13 FT	
PS31	PS3	Q			
PSIG	PSIG	PSIG			
4.81	6.80	1.06			
			THETA		
			10.00 DEG		
			THETA-HAT	D	
			10.15 DEG	11.31 FT	
PS31	PS3	Q			
PSIG	PSIG	PSIG			
5.50	6.85	1.07			
			THETA		
			20.00 DEG		
			THETA-HAT	D	
			20.28 DEG	11.86 FT	
PS31	PS3	Q			
PSIG	PSIG	PSIG			
5.98	6.89	1.08			

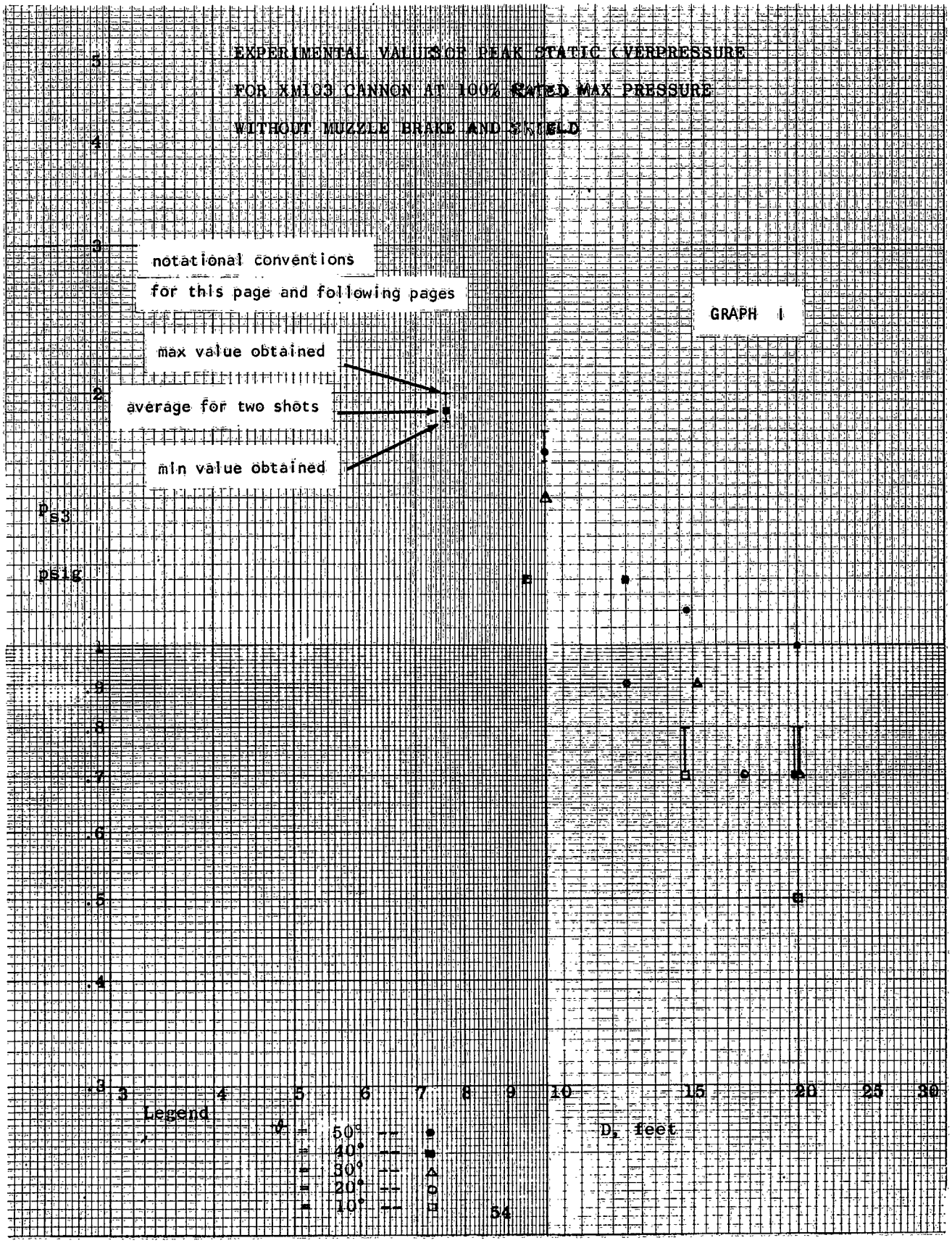
EXPERIMENTAL VALUES OF PEAK STATIC OVERPRESSURE
FOR XM103 CANNON AT 100% RATED MAX PRESSURE
WITHOUT MUZZLE BRAKE AND SHIELD
notational conventions
for this page and following pages
max value obtained
average for two shots
min value obtained
GRAPH I
p_{s3}
psig
D, feet
Legend
θ = 50° 40° 30° 20° 10°
54

PEAK STATIC SHOCK OVERPRESSURE FOR XM103

CANNON AT 100% RATED MAX PRESSURE W/O BLAST SHIELD

(Computed by assuming a point explosion at the muzzle with 50% energy utilization.) QE = 10°, h = 0

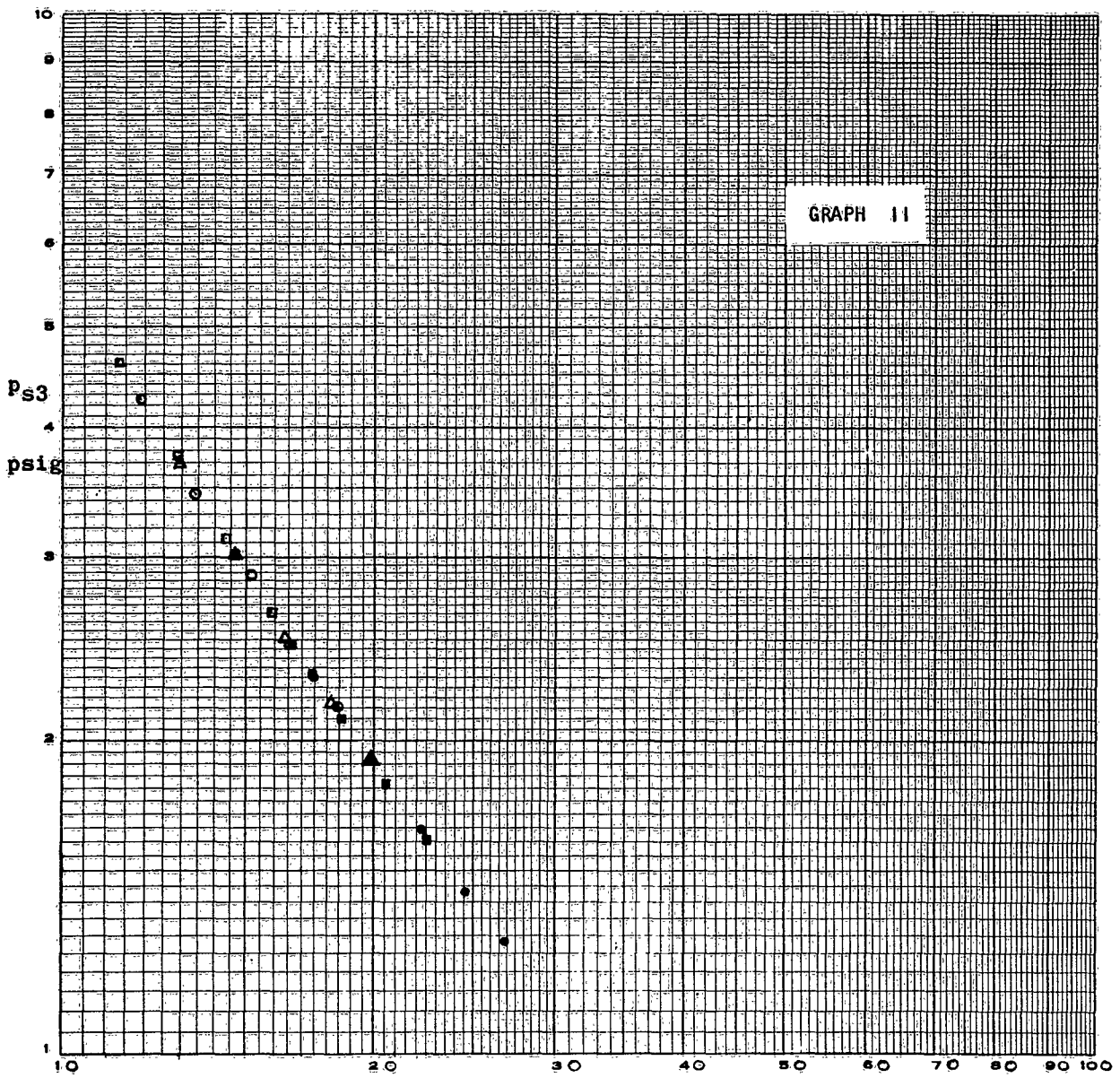

EXPERIMENTAL VALUES OF PEAK STATIC OVERPRESSURE
FOR XM103 CANNON AT 100% RMP W/MUZZLE BRAKE WTV-D8259
AND W/O BLAST SHIELD (REFERENCE 12) QE = 0°

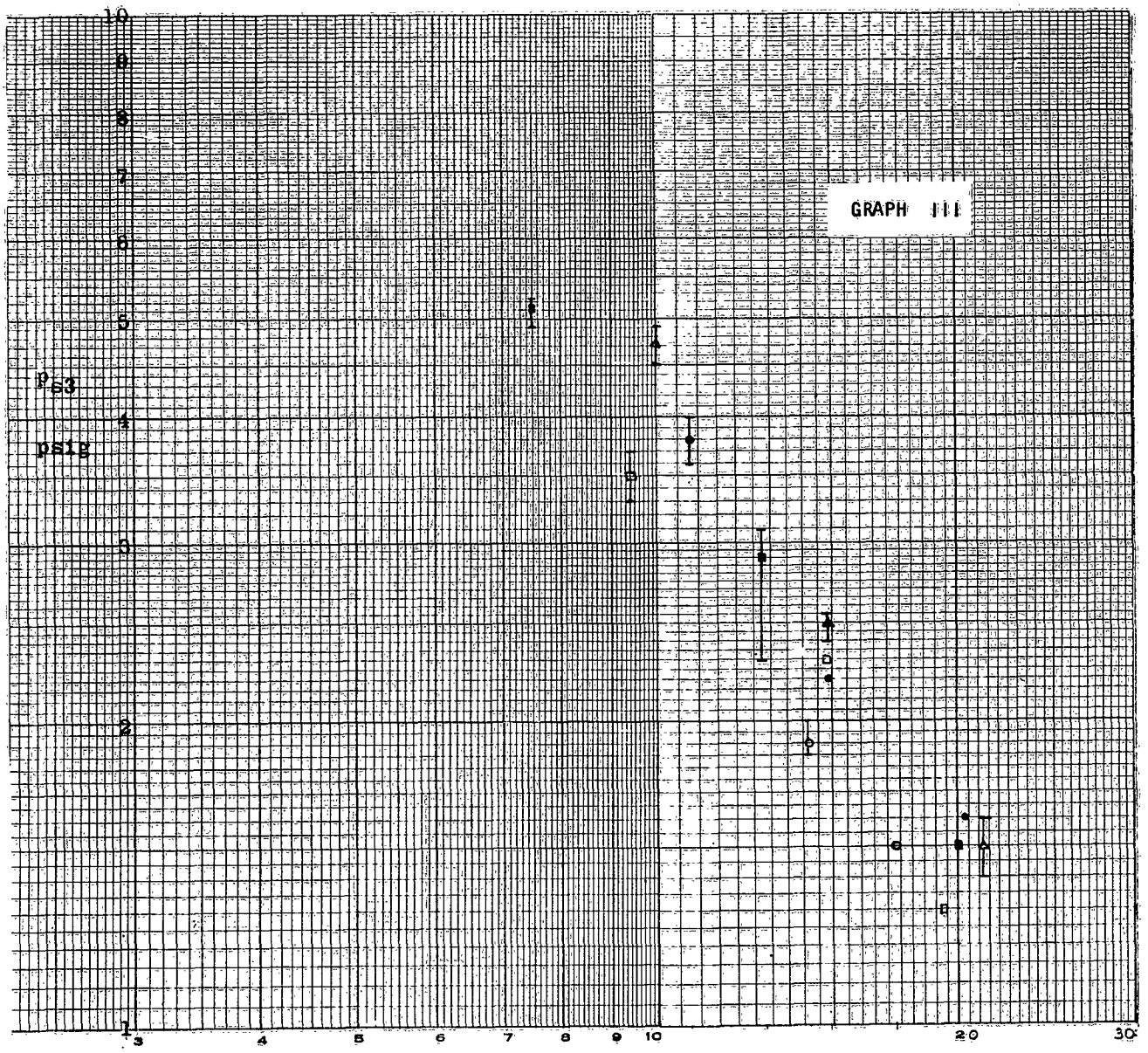

COMPUTED VALUES OF

PEAK STATIC OVERPRESSURE FOR XM103 AT 100%

RATED MAX PRESSURE W/ M2A2E2 BRAKE (WTV-D8259) AND

W/O BLAST SHIELD $\phi = 0.95$, $\omega = 0$, QE = 10°, h = 0

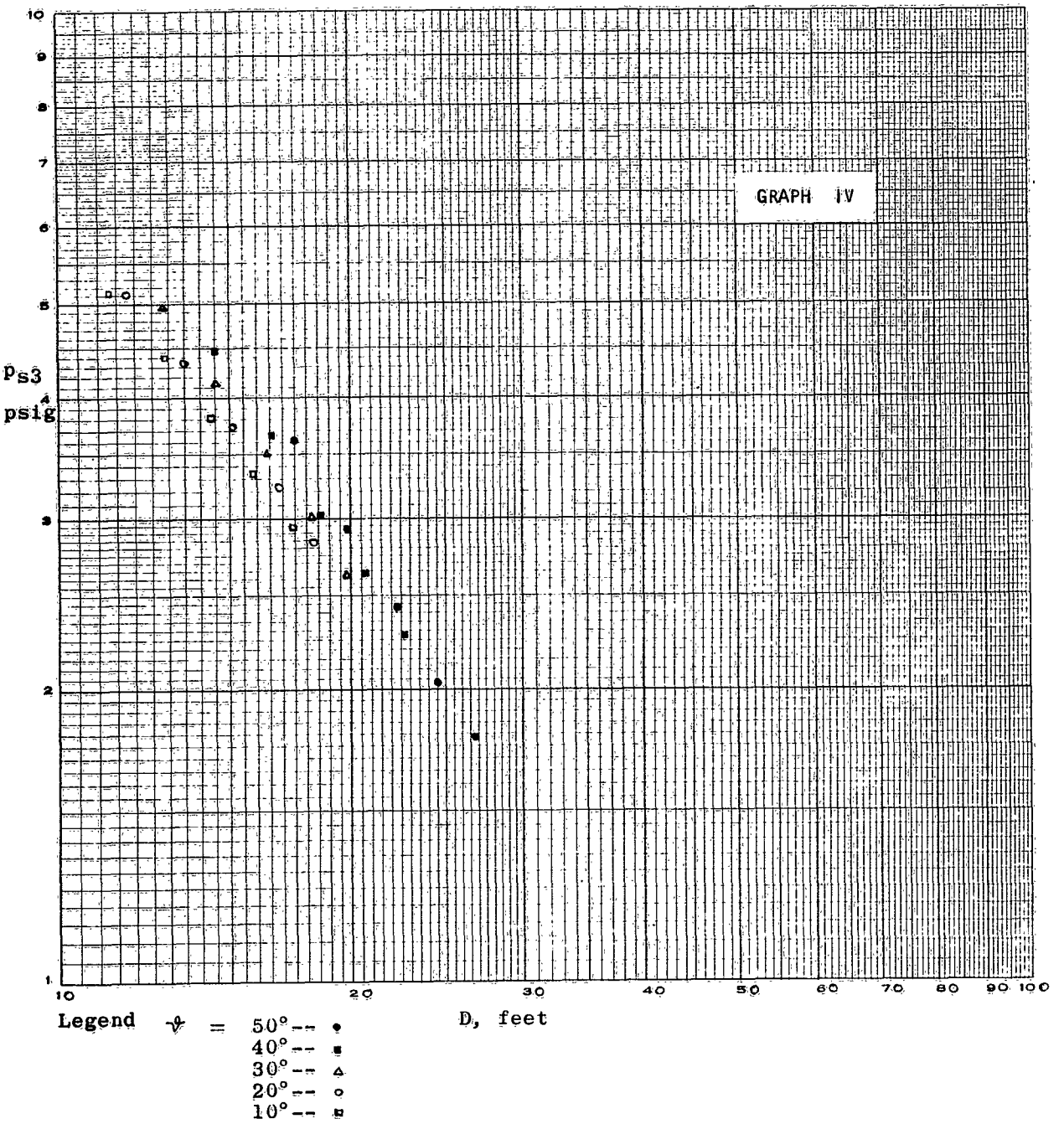

EXPERIMENTAL VALUES OF PEAK STATIC OVERPRESSURE

FOR XM103 CANNON AT 100% RMP. W/ MUZZLE BRAKE

WTV-F8241 AND W/O BLAST SHIELD (REFERENCE 12) QE = 0°

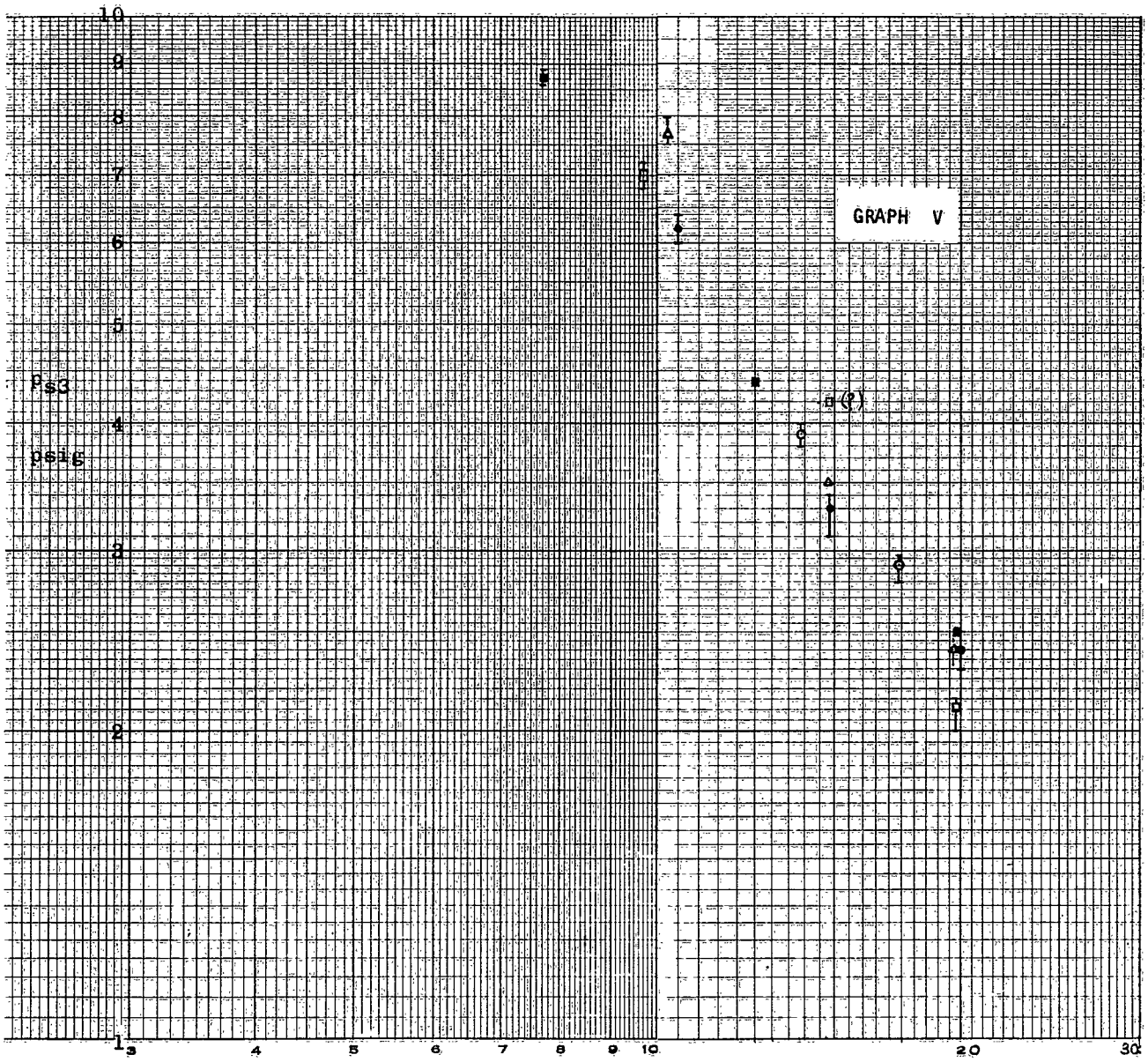

COMPUTED VALUES OF

PEAK STATIC OVERPRESSURE FOR XM103 AT 100%

RATED MAX PRESSURE W/ XM103 BRAKE (WTV-F8241) AND

W/O BLAST SHIELD $\gamma = 1.35$, $\omega = 0$, QE = 10°, h = 0

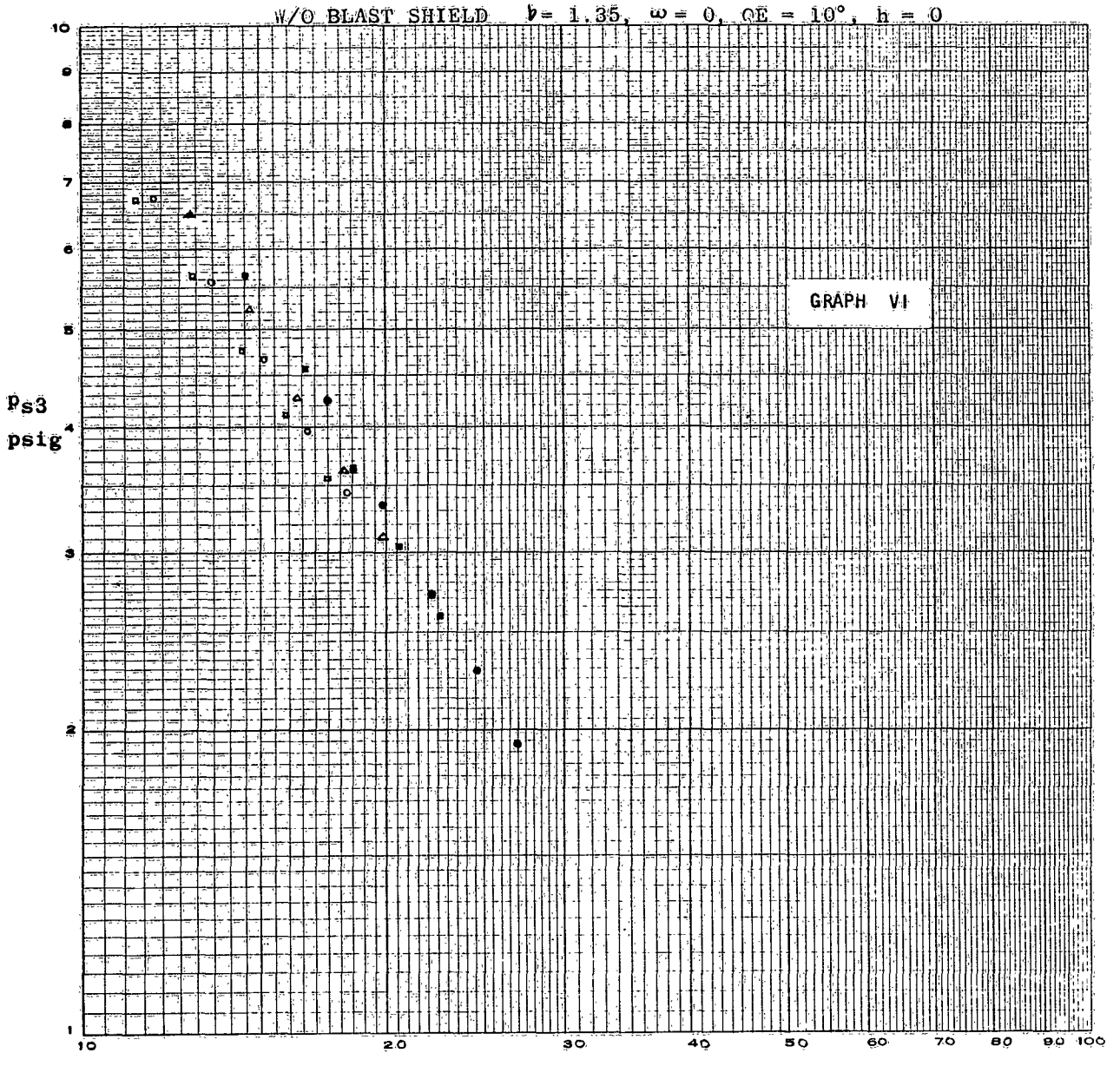

COMPUTED VALUES* OF PEAK STATIC OVERPRESSURE FOR XM103 AT 100% RATED MAX PRESSURE W/ XM103 BRAKE (WTV-F8241) AND W/O BLAST SHIELD (* assuming point-source decay from two sources) $\gamma = 1.35$, $\omega = 0$, Q.E. = 0, h = 0 .

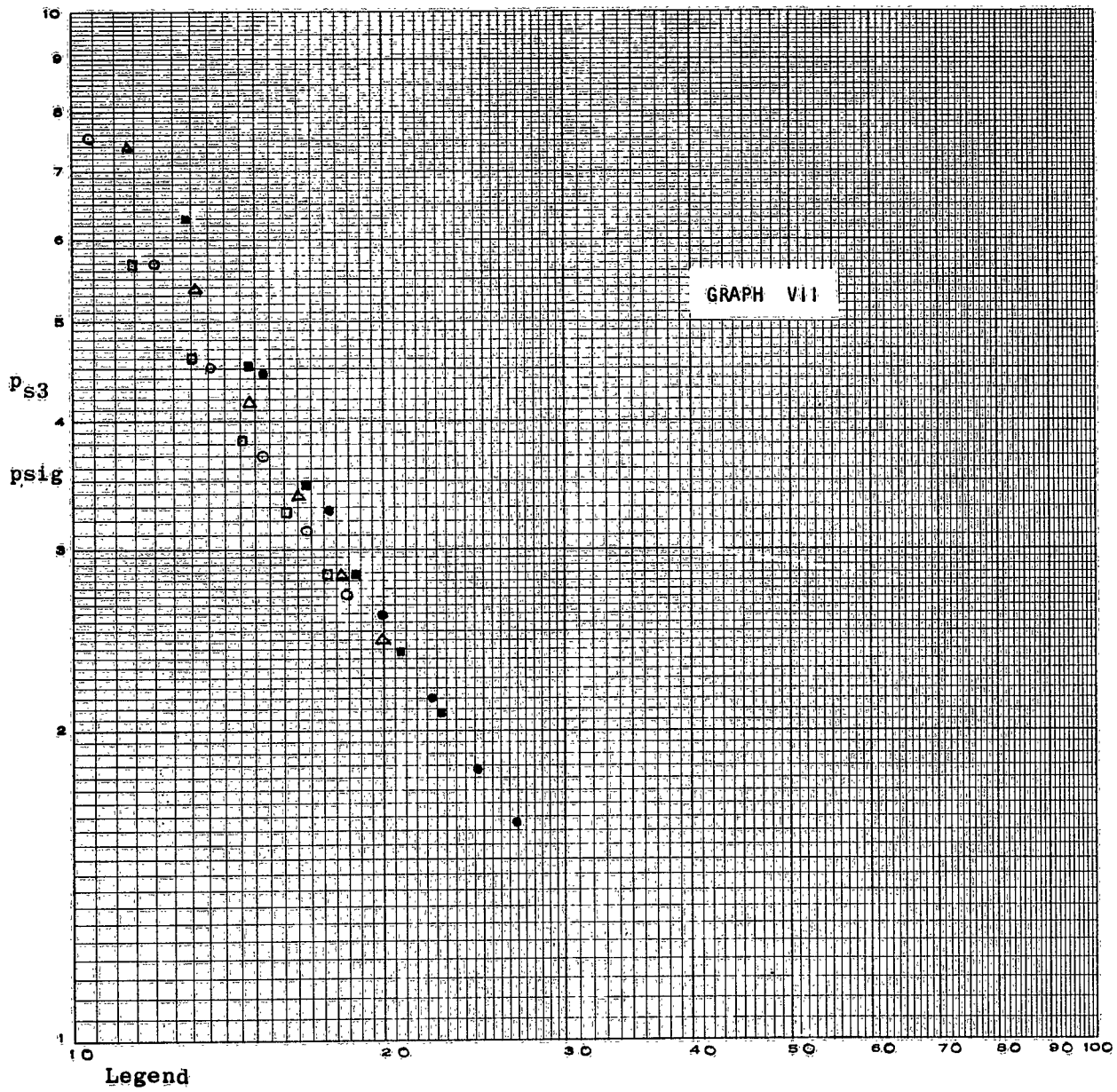

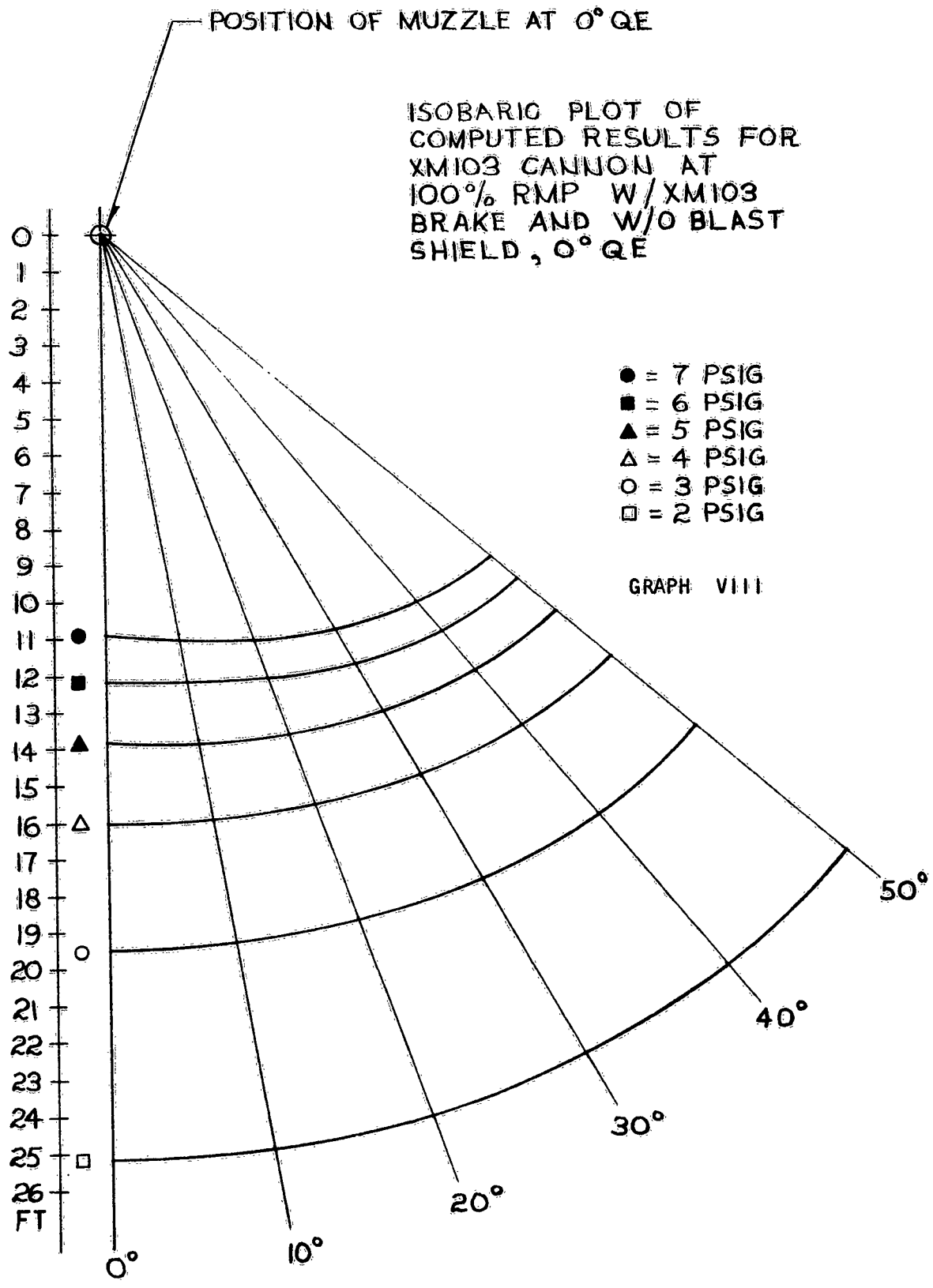
POSITION OF MUZZLE AT 0° QE
ISOBARIC PLOT OF COMPUTED RESULTS FOR XM103 CANNON AT 100% RMP W/XM103 BRAKE AND W/O BLAST SHIELD, 0° QE
● = 7 PSIG
■ = 6 PSIG
▲ = 5 PSIG
△ = 4 PSIG
○ = 3 PSIG
□ = 2 PSIG
GRAPH VIII
0
1
2
3
4
5
6
7
8
9
10
11
12
13
14
15
16
17
18
19
20
21
22
23
24
25
26
FT
0°
10°
20°
30°
40°
50°

EXPERIMENTAL VALUES OF PEAK STATIC OVERPRESSURE

FOR XM103 CANNON AT 100% RMP W/MUZZLE BRAKE

WTV-F8241 AND W/O BLAST SHIELD (REFERENCE 12), QE = 45°

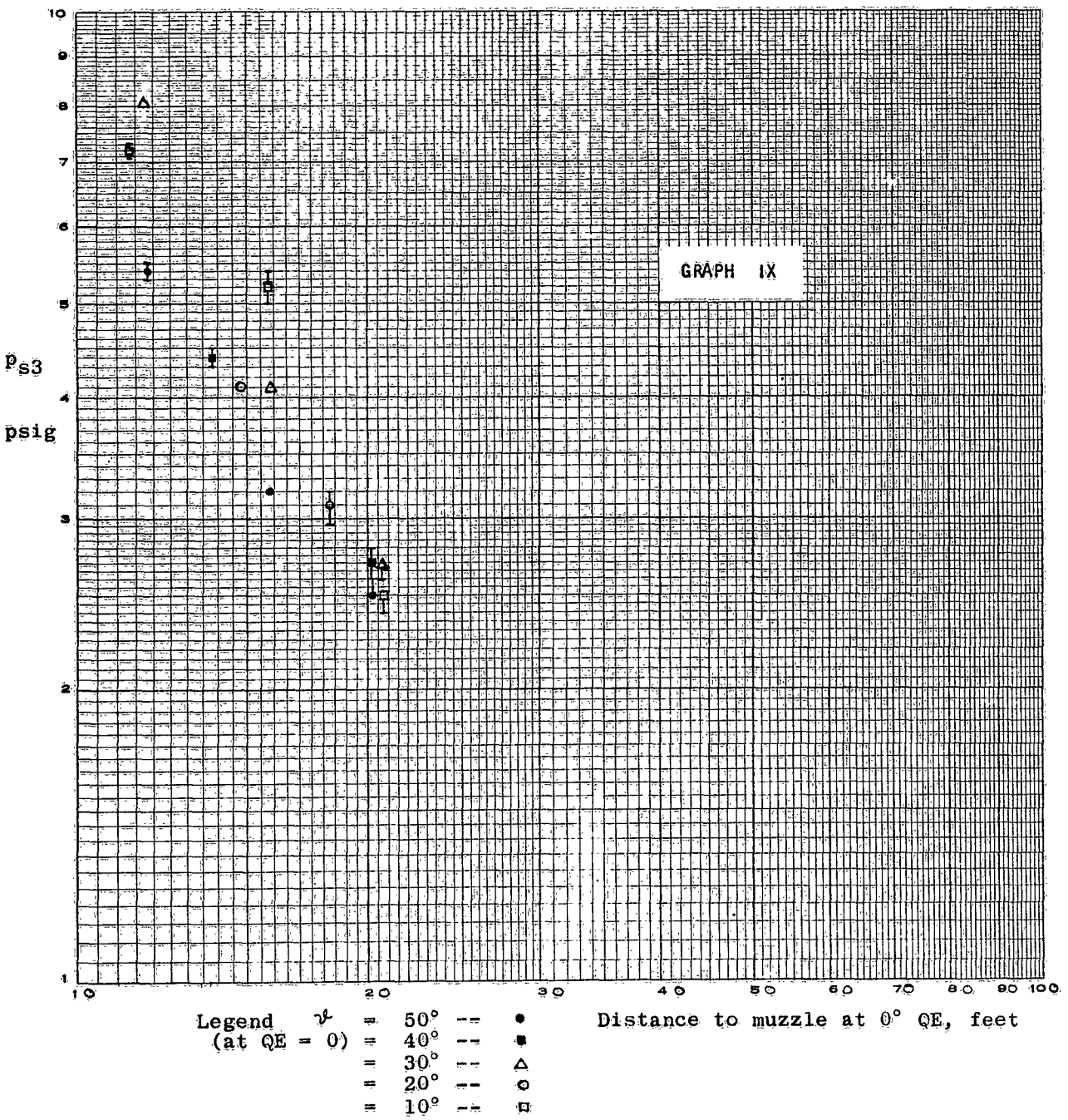

COMPUTED VALUES OF

PEAK STATIC OVERPRESSURE FOR XM103 AT 100%

RATED MAX PRESSURE W/XM103 BRAKE (WTV-F8241)

AND W/O BLAST SHIELD $\gamma = 1.35$, $\omega = 0$, QE = 45°, h = 0

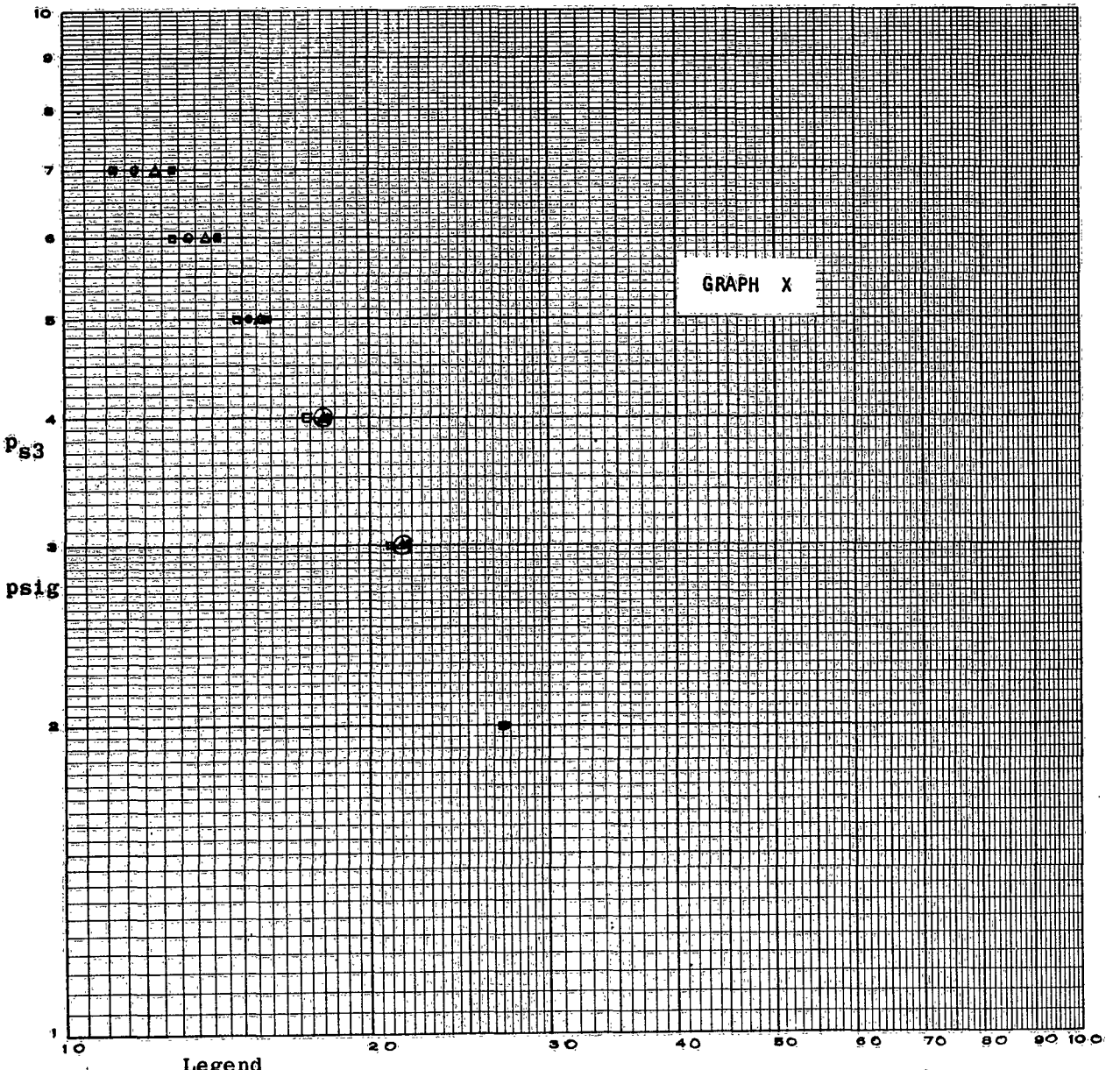

COMPUTED VALUES* OF PEAK STATIC OVERPRESSURE FOR XM103 AT 100% RATED MAX PRESSURE W/ XM103 BRAKE (WTV-F8241) AND W/O BLAST SHIELD (* assuming point-source decay from two sources) $\gamma = 1.35$, $\omega = 0$, QE = 45°, h = 0

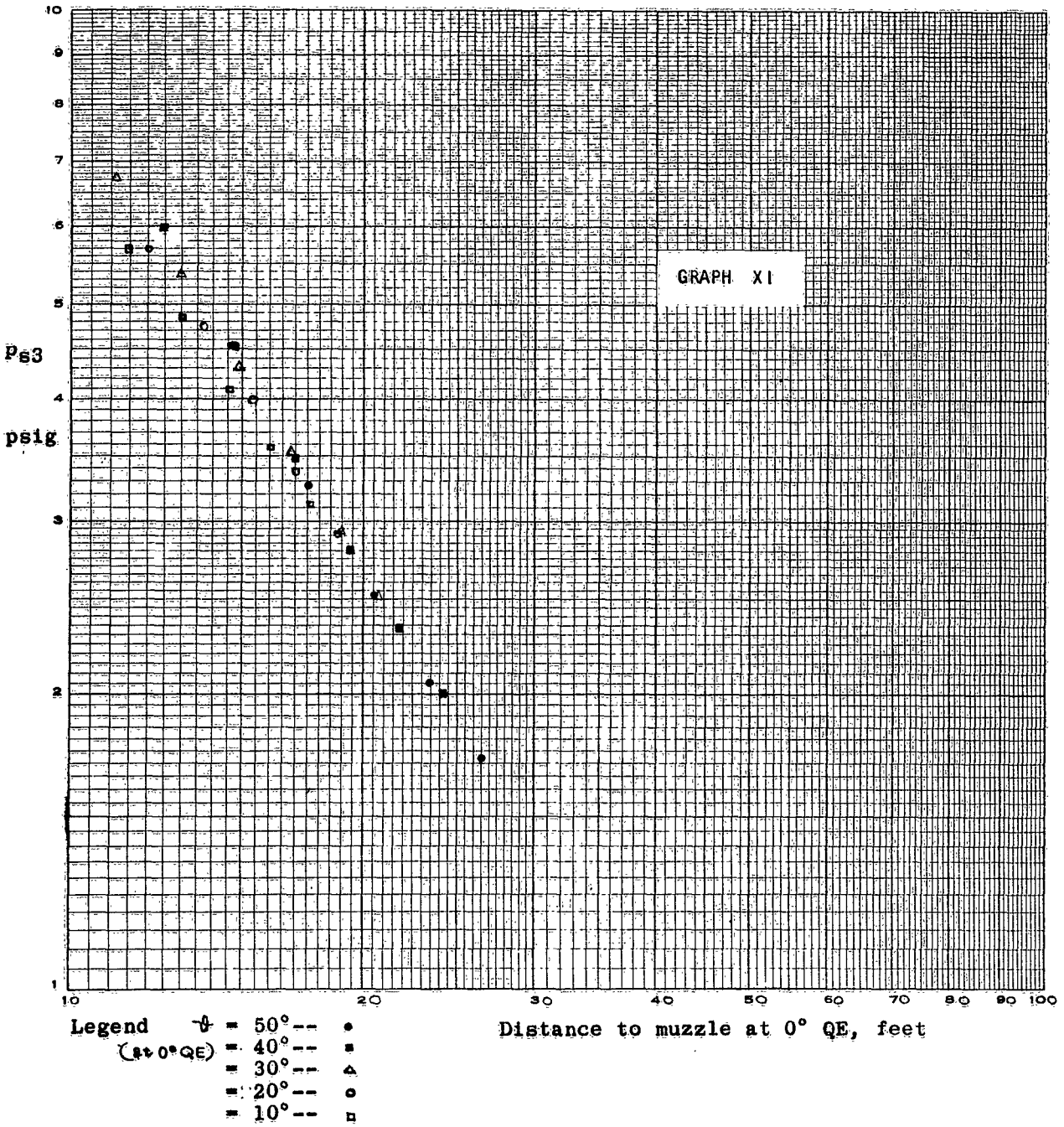

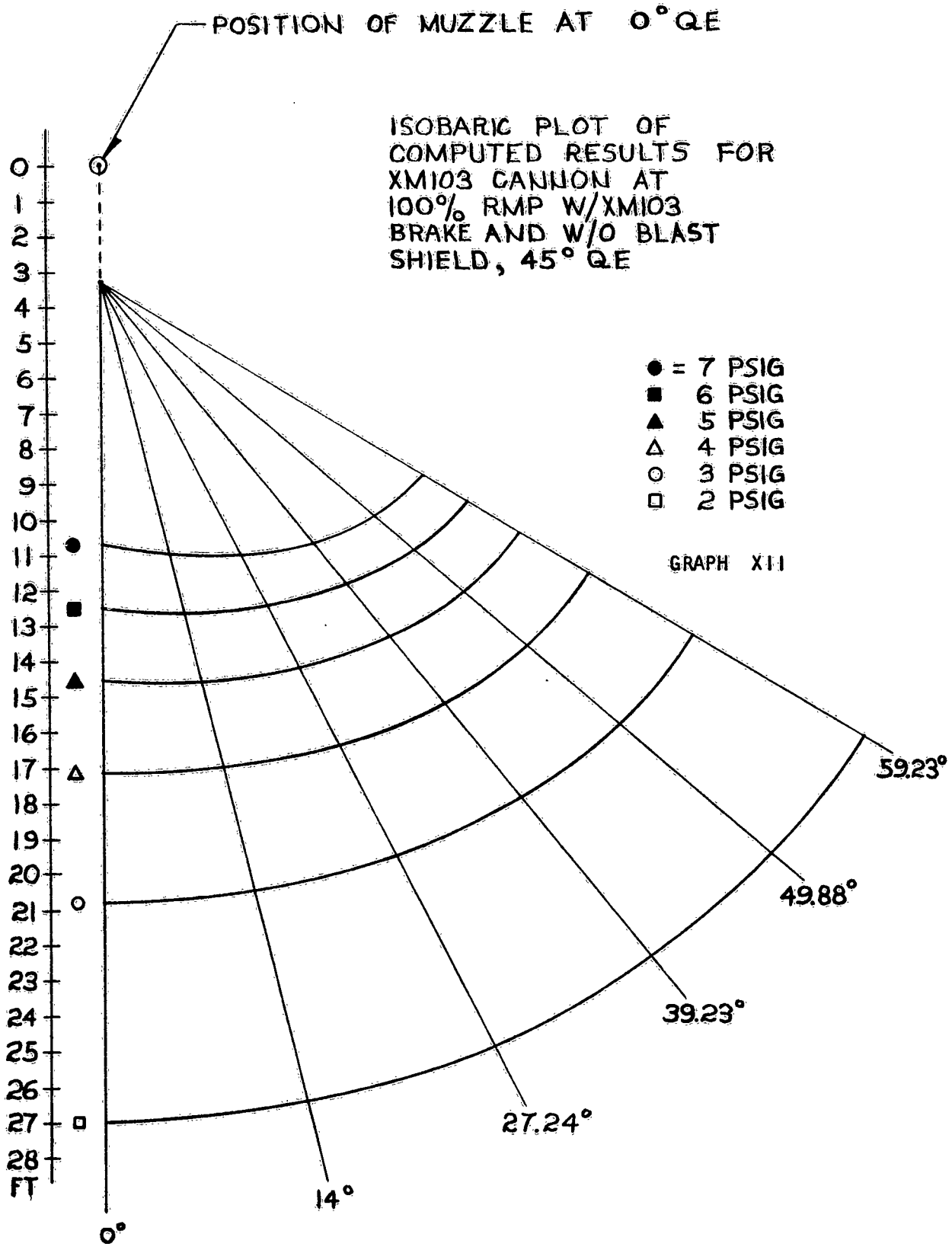
POSITION OF MUZZLE AT 0° QE
ISOBARIC PLOT OF COMPUTED RESULTS FOR XM103 CANNON AT 100% RMP W/XM103 BRAKE AND W/O BLAST SHIELD, 45° QE
● = 7 PSIG
■ 6 PSIG
▲ 5 PSIG
△ 4 PSIG
○ 3 PSIG
□ 2 PSIG
GRAPH XII
0 1 2 3 4 5 6 7 8 9 10 11 12 13 14 15 16 17 18 19 20 21 22 23 24 25 26 27 28 FT
59.23°
49.88°
39.23°
27.24°
14°
0°

DISCUSSION OF RESULTS

Comparison of the computed results with the experimental results, presented in reference 12, shows that the computed values, while displaying the proper directional and decay characteristics, remain consistently higher than the experimental values. The discrepancy in the peak static overpressure is nearly constant in magnitude. This fact allows one to use the theory to predict the "worst-case" or most pessimistic overpressure that would be encountered in using a particular muzzle brake. The differences between theory and experiment may be attributed to several simplifications in the model. Some of these are:

(1) The assumption was that maximum peak static overpressure is developed at $\mathcal{T} = 1$ after discharge begins. This obviously depends to a certain extent upon the ability of the brake to act as a reservoir. It was assumed that conventional brakes would not appreciably affect flow rates into the atmosphere relative to those from the bare muzzle. If this were not so, one could expect considerable departure from theoretical predictions.

(2) Combustion was assumed complete at the muzzle with gases passing thru the brake in a thermodynamically "frozen" state. If this assumption were not valid, departures therefrom would result in lower overpressures than predicted.

(3) The Rankine-Hugoniot relations used were strictly one-dimensional, whereas the spherical shock was quasi one-dimensional and essentially three dimensional in character. Here again the assumption resulted in too large a predicted value.

(4) Initial decay of the shock wave, i.e., at very great strength, is somewhat more rapid than the $r^{-3/2}$ rate assumed. Altho decay at very low overpressures (below about 3 psig) is not as great as the predicted rate, the total effect of the latter assumption is to predict a somewhat large value.

(5) Constructive interference in the waves emanating from the two point centers of shock expansion was assumed for all positions within the shock field. This assumption becomes progressively less tenable as ϑ increases from zero. In general, the theory predicts the correct directional effects with PF=0; however, it is noted that the theoretical overpressure values for $\vartheta = 50°$ remain somewhat greater than those at $\vartheta = 30°$ and $40°$ at all corresponding distances, D, from the muzzle, whereas the reverse situation is true for the experimental values.

This discrepancy can no doubt be explained by noting that -- contrary to assumption -- complete constructive interference is not likely for large angular deviations from the tube axis.

In general, however, a 15% agreement between theory and experiment was achieved. Considering the complications, this was all that was expected and probably all that is required for engineering purposes.

Since in general best agreement with experiment is achieved for PF=0, this is the value used in the computations for the isobaric plots. The fact that gaseous discharge is transonic rather than supersonic may account for the negligible effect of PF. As previously mentioned, this fact was suggested by the results of reference 3. With PF=0, this theory contains no empirical constants. Therefore the predictive ability of this work is no better than the assumptions, good agreement being obtained when the assumptions are valid.

As can be seen by inspection of the graphs, the experimental results from the XM103 with M2A2E2 brake and with XM103 brake bracket the computed results obtained from the point source explosion theory. This is a fortuitous result of the choice of brakes. Since the computed overpressures predicted by this theory do not depend upon angular deviation from the Z-axis or upon the momentum index, ν , of the brake, quite severe inaccuracies could result from its use as a predictive tool.

However, despite the differences in magnitude between experiment and the results of the point source theory, the latter more accurately displays the general shape (functional form) of the decay of static overpressure with distance than does the theory previously described in this report. The reason that this is the case is to be found in the assumption of a simple $r^{-3/2}$ decay rate. Therefore, a modification of the theory was made to account for a variable decay exponent. Each shock center at maximum shock strength was considered to be a point source with explosive energy equal to one-half the energy available in the gas discharged at $\mathcal{T} = 1$. Then, using the pressure decay theory developed in reference 1, the pressure components at the reference position from the near and far shock spheres were computed. These were combined as indicated in equations 0.70 and 0.72 to obtain the measurable peak static overpressure. Comparison of the computed results of this modified theory (graphs 7 and 11) with corresponding experimental results (graphs 5 and 9) indicate

an extremely favorable agreement and suggest the use of the modified theory as a predictor in place of the original theory.

It appears that the single point source explosion theory, badly underestimates the positive impulse and duration of the positive phase and is, therefore, not recommended as a predictor for these variables.

APPENDIX I

The Rankine-Hugoniot relations for stationary, normal shock are given by Shapiro in reference 18. Slight modifications and algebraic rearrangement of the equations found in Volume I on pages 137 and following may be written here as follows. Notational conventions listed there are preserved in what follows.

By requiring that $T_y^o = T_x^o$, one obtains

$$1.1 \qquad \frac{T_y}{T_x} = \frac{1 + \frac{\gamma_x - 1}{2} M_x^2}{1 + \frac{\gamma_y - 1}{2} M_y^2}$$

Also,

$$1.2 \qquad \frac{T_y}{T_x} = \left(\frac{p_y}{p_x}\right)^2 \left(\frac{M_y}{M_x}\right)^2$$

From 1.1 and 1.2, we have

$$1.3 \qquad \frac{p_y}{p_x} = \frac{M_x}{M_y} \left[\frac{1 + \frac{\gamma_x - 1}{2} M_x^2}{1 + \frac{\gamma_y - 1}{2} M_y^2} \right]^{1/2} .$$

From the combined momentum and continuity relations, one can obtain

$$1.4 \qquad p_x(1 + \gamma_x M_x^2) = p_y(1 + \gamma_y M_y^2) .$$

Elimination of p_y/p_x between 1.3 and 1.4 yields

$$1.5 \qquad \frac{M_x^2(1 + \frac{\gamma_x - 1}{2} M_x^2)}{(1 + \gamma_x M_x^2)^2} = \frac{M_y^2(1 + \frac{\gamma_y - 1}{2} M_y^2)}{(1 + \gamma_y M_y^2)^2}$$

Calling the left hand side of equation 1.5 $F = F(M_x)$, we have

$$1.6 \qquad M_y^2 = \frac{1 - 2\gamma_y F - (1 - 2\gamma_y F - 2F)^{1/2}}{1 - \gamma_y (1 - 2\gamma_y F)}$$

Following Shapiro, we let primed quantities refer to conditions observed by a stationary observer in region x toward whom the shock is propagating. Then, the transformation conditions relative to a stationary-shock frame of reference are:

1.7 $$p'_x = p_x$$

1.8 $$p'_y = p_y$$

1.9 $$T'_x = T_x$$

1.10 $$T'_y = T_y$$

1.11 $$M_x = \frac{v_x}{a_x}$$

1.12 $$M_y = \frac{v_y}{a_y}$$

1.13 $$M'_x = 0$$

1.14 $$M'_y = \frac{v'_y}{a_y} = \frac{v_x - v_y}{a_y} = \frac{a_x}{a_y} M_x - M_y$$

By assuming that the flow is isentropic in the y'-region, one has additionally

1.15 $$\frac{T_y^{o'}}{T_y'} = 1 + \left(\frac{\gamma_y - 1}{2}\right) M_y'^2 \quad \text{and}$$

1.16 $$\frac{p_y^{o'}}{p_y'} = \left[1 + \left(\frac{\gamma_y - 1}{2}\right) M_y'^2\right]^{\frac{\gamma_y}{\gamma_y - 1}}$$

Since

1.17 $$a_x = (g\, \gamma_x\, R_x\, T_x)^{1/2}$$

and

1.18 $$a_y = (g\, \gamma_y\, R_y\, T_y)^{1/2}$$, one can rewrite equation 1.2 as

1.19a $$a_y^2 = \sigma^2 a_x^2 \left(\frac{p_y}{p_x}\right)^2 \left(\frac{M_y}{M_x}\right)^2 , \text{ where}$$

b $$\sigma^2 = \frac{\gamma_x R_x}{\gamma_y R_y} .$$

Using equations 1.4 and 1.14, one can write

1.20a $$M_y' = \frac{v_x}{a_y} - \left[\frac{1 + \gamma_x M_x^2 - \left(\frac{p_y}{p_x}\right)}{\gamma_y \left(\frac{p_y}{p_x}\right)}\right]^{1/2} ,$$

and

1.20b $$v_y' = a_y M_y' .$$

By definition $M_x = \frac{v_x}{a_x}$, or by equation 1.17,

1.21 $$M_x = \frac{v_x}{(g \gamma_x R_x T_x)^{1/2}} .$$

Considering v_x, the shock velocity, to be the independent variable, one can successively compute M_x, M_y, $\frac{p_y}{p_x}$, T_y, a_y, M_y', and v_y' by sequential application of formulas 1.21, 1.6, 1.3, 1.2, 1.19, 1.20a, and 1.20b. Thus, tables can be constructed, functionally relating the above variables.

Utilizing the characteristics of the mathematical model of the shock phenomenon, previously described, one can additionally relate the stagnation temperature at the center of the shock sphere, T^o, to the above parameters. By assuming that the combustion products expand nearly adiabatically, one can write

1.22 $$\frac{T^o}{T_2} = 1 + \frac{\gamma_2 - 1}{2} M_2^2 .$$

However, it was assumed in the model that $M_2^2 = 1$ and, therefore, that $v_2 = a_2 = (g\ \gamma_2\ R_2\ T_2)^{1/2}$.

Thus,

$$1.23a \quad T^{\circ} = \left(\frac{\gamma_2 + 1}{2}\right)\left(\frac{v_2^2}{\gamma_2\ g\ R_2}\right) .$$

Further, at the interface $v_y' = v_2$.

Finally, therefore,

$$1.23b \quad T^{\circ} = \frac{(\gamma_2 + 1)\ v_y'^2}{2\ \gamma_2\ g\ R_2} .$$

Three additional relations that were found to be useful to tabulate were

$$1.24 \quad \frac{V_y}{V_x} = \frac{1}{V_\infty}\left(\frac{R_y\ T_y}{144\ p_y}\right)$$

$$1.25 \quad X_1 = \frac{T^{\circ}}{p_y} \quad \text{and}$$

$$1.26 \quad p_s = p_y - p_\infty .$$

The above tables were computed using the following constants.

$$g = 32.17$$

$$\gamma_x = 1.4036$$

$$\gamma_y = 1.3900$$

$$\gamma_2 = 1.2593$$

$$R_x = 53.280$$

$$R_y = 53.290$$

$$R_2 = 70.036$$

$$T_\infty \equiv T_x = 518.7\ ^{\circ}R$$

$$p_\infty \equiv p_x = 14.7\ \text{psia}$$

$$a_\infty \equiv a_x = (\gamma_x \, g \, R_x \, T_x)^{1/2}$$

$$V_\infty \equiv V_x = \frac{R_x \, T_x}{144 \, p_x} \quad .$$

The variables χ_1, V_y/V_x, and p_s are listed as functions of T^o on pages 40-41 of this report.

For $\gamma_y = \gamma_x = 1.4$, Shapiro has derived the relationship between the shock velocity and the peak static overpressure shown below.

1.27a $$\varphi = \frac{7}{6}\left[\left(\frac{v_x}{a}\right)^2 - 1\right], \text{ where}$$

b $$\varphi = p_s/p_\infty \quad .$$

Also, for the above conditions, reference 1. gives the following relationship for the dynamic pressure.

1.28 $$q = \frac{5 \, p_\infty \, \varphi^2}{2(7 + \varphi)} \quad .$$

The expressions for $\tilde{\varphi}$, $\tilde{q}$, DPP, SPLSP, and DPLSP, listed in the EQUATIONS, were obtained by fitting data given in reference 1.

APPENDIX II.

Derivation of Shock Model Equations

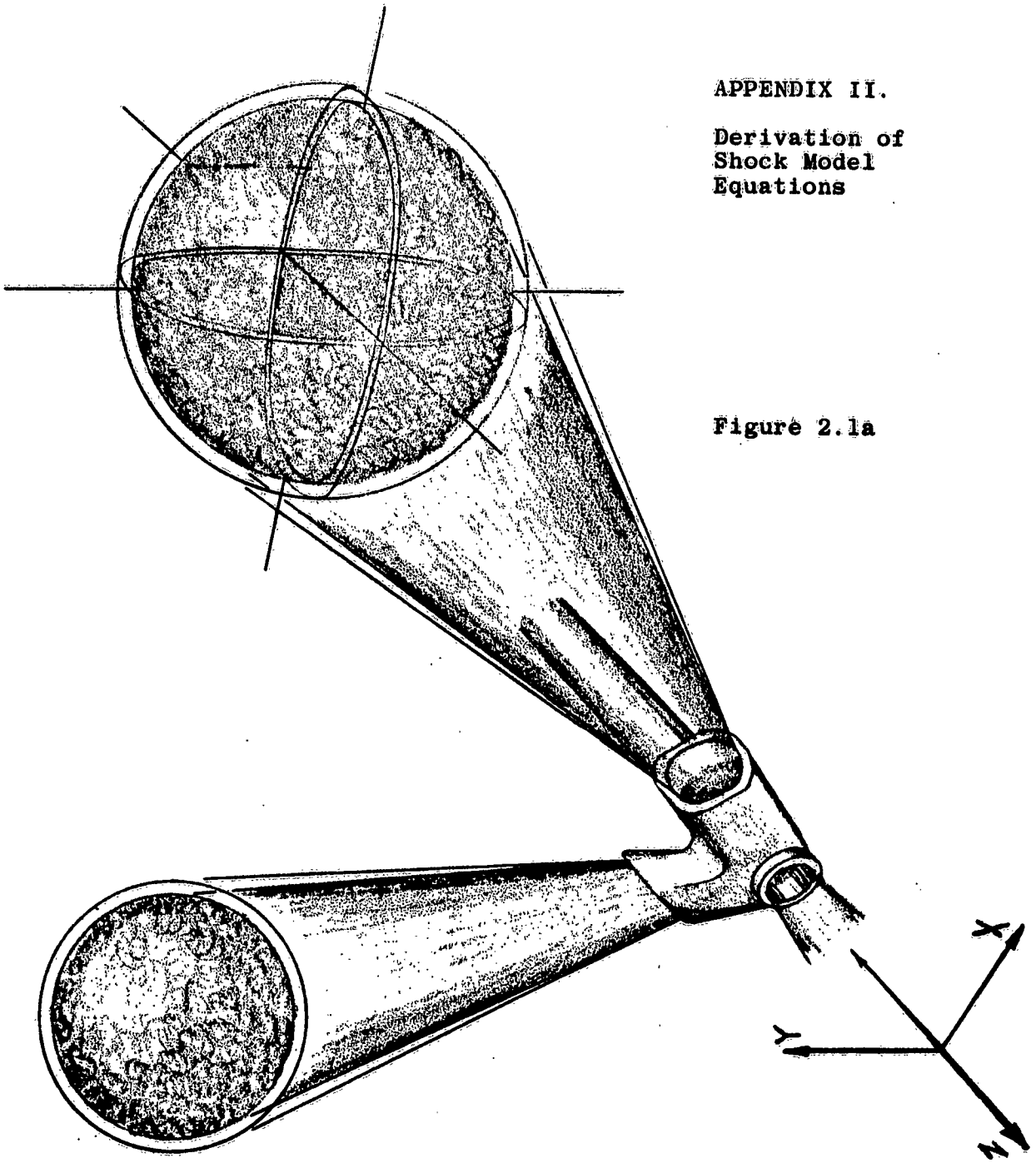

Figure 2.1a

FIGURE 2.1 B

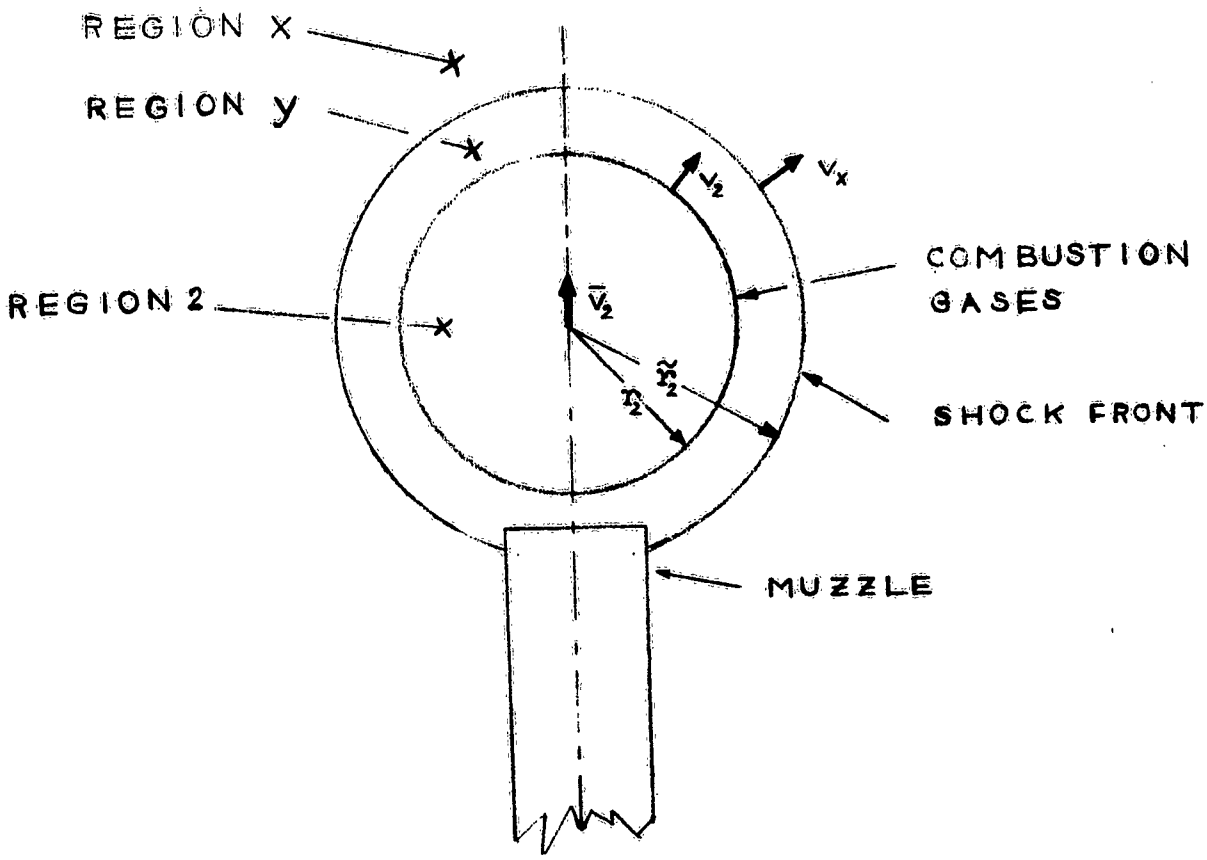

SINGLE SHOCK (SPHERE) MODEL

As shown in figure 2.1a, flow of combustion gases from a muzzle brake is conceived as issuing principally from two ports of equal area. The air which these gases replace is compressed as shells in front of the rapidly expanding spheres of combustion gases. The spheres are shown here fully developed. We shall return shortly to a description of the two-shock model.

In figure 2.1b is seen the single-shock model. The sphere of combustion gases is labeled region 2; the shell of compressed air is labeled region y; and the surrounding undisturbed air is labeled ∞. At maximum shock strength, the speed of the center of mass of the shock sphere in the Z-direction is given by $\bar{v}_2$. For momentum conservation in this direction,

2.1
$$\int_0^{\tau=1} B d\tau = B_T(1) = \frac{M^*(1)\ \bar{v}_2}{g} ,$$

where M^* is the total mass set in motion in the Z-direction. It should be recognized that $\bar{v}_2$ is an effective speed chosen for momentum conservation. Considering only the momentum discharged from the muzzle, one can obtain the actual average gas speed from

2.2
$$\frac{g\ P(1)}{M^*(1)} = \frac{P}{B_T}\ \bar{v}_2 = \frac{\bar{v}_2}{1.46881} .$$

Since the compressed air in region y formerly occupied the volume $4/3\ \pi r_2^3$ at ambient conditions, one can write

2.3a
$$\frac{4/3\ \pi r_2^3}{V_x} = \frac{4/3\ \pi(\tilde{r}_2^3 - r_2^3)}{V_y} \quad \text{or}$$

b
$$\tilde{r}_2 = r_2(1 + V_y/V_x)^{1/3} . \quad \text{Also}$$

2.4
$$M^*(1) = M(1) + \frac{4\pi r_2^3}{3\ V_\infty} .$$

Now, the gas discharged to $\mathcal{T} = 1$, is considered to occupy the volume $4/3\ \pi r_2^3$. Thus,

2.5 $$\frac{4/3\ \pi r_2^3}{V_{2\ av}} = M(1) \text{ and}$$

2.6a $$4/3\ \pi r_2^3 = \frac{V_{2\ av}\ M(1)\ V^o}{V^o} \quad \text{or}$$

b $$4/3\ \pi r_2^3 = \kappa_{2\ av}\ M(1) V^o, \text{ where}$$

c $$\kappa_{2\ av} = \frac{V_{2\ av}}{V^o} \quad .$$

But, assuming ideal gas behavior,

2.7 $$V^o = \frac{R_2\ T^o}{144 p^o} \quad .$$

With the additional assumptions of nearly adiabatic flow within region 2 and sonic flow at the interface,

2.8 $$\frac{p^o}{p_2} = \frac{p^o}{p'_y} = \left(\frac{\gamma_2 + 1}{2} \right)^{(\gamma_2/(\gamma_2 - 1))}$$

Equations 2.7 and 2.8 yield

2.9a $$V^o = \frac{R_2\ T^o}{144\ p'_y \left[(\gamma_2 + 1)/2 \right]^{(\gamma_2/(\gamma_2 - 1))}}$$

or

b $$V^o = \frac{R_2\ \kappa_1}{144 \left[(\gamma_2 + 1)/2 \right]^{(\gamma_2/(\gamma_2 - 1))}}$$

where

c $$\kappa_1 = \frac{T^o}{p'_y}$$

Finally, substitution of V^o in 2.9b into 2.6b gives

2.10 $$\frac{4\pi r_2^3}{3} = \frac{\gamma_{2\ av}\ M(1)\ R_2\ X_1}{144\ \left[(\gamma_2 + 1)/2 \right]^{(\gamma_2/(\gamma_2 - 1))}}$$

To obtain an expression for $\gamma_{2\ av}$, we make the additional assumption that the radial velocity within region 2 can be written approximately as

2.11 $\frac{v}{v_2} = \frac{r}{r_2}$ in the center of mass frame of reference.

Thus

2.12 $v = v_2 \rho$, where $0 \leq \rho \leq 1$.

Within region 2(adiabatic flow),

2.13 $$\gamma_2 = \frac{V}{V^o} = \left[1 + \left(\frac{\gamma_2 - 1}{2} \right) \left(\frac{v^2}{\gamma_2\ g\ R_2\ T} \right) \right]^{(1/(\gamma_2 - 1))}$$

Also,

2.14a $$\gamma_2\ g\ R_2\ T = \gamma_2\ g\ R_2\ T^o - \left(\frac{\gamma_2 - 1}{2} \right) v^2$$

b $$\gamma_2\ g\ R_2\ T_2 = \gamma_2\ g\ R_2\ T^o - \left(\frac{\gamma_2 - 1}{2} \right) v_2^2$$

Subtracting 2.14b from 2.14a and using 2.12, we have

2.15 $$\gamma_2\ g\ R_2\ T = \gamma_2\ g\ R_2\ T_2 + \left(\frac{\gamma_2 - 1}{2} \right) v_2^2 \ (1 - \rho^2)$$.

By assumption, the mach number at the interface is unity; so that

2.16 $v_2^2 = \gamma_2\ g\ R_2\ T_2$. Thus,

2.17 $$\gamma_2\ g\ R_2\ T = v_2^2 \left[1 + ((\gamma_2 - 1)/2)(1 - \rho^2) \right]$$.

By 2.13 and 2.17,

2.18 $$\frac{V}{V^o} = \gamma_2 = \left[1 + \left(\frac{\gamma_2 - 1}{2} \right) \frac{\rho^2}{1 + ((\gamma_2 - 1)/2)(1 - \rho^2)} \right]^{(1/(\gamma_2 - 1))}$$.

By definition,

$$2.19a \quad V_{av} = \frac{\frac{4\pi}{3}(1)^3}{4\pi \int_0^1 (\rho^2/V(\rho))\,d\rho}$$

$$b \quad \kappa_{2\,av} = \frac{V_{av}}{V^o} = \left(3\int_0^1 \left(\rho^2/\kappa_2\right) d\rho\right)^{-1} .$$

Equation 2.19b was evaluated numerically using a value of 1.26 for γ_2. The resulting value $\kappa_{2\,av} = 1.309$ was used thruout the rest of the computations.

In the preceeding derivations in this appendix, we have made use of mass and momentum conservation. Now we shall appeal to the principle of energy conservation to derive a most important relationship.

The total energy available for distribution is that discharged up to $\tilde{\sigma} = 1$, $J\,H(1)$. Part of this is involved as translational kinetic energy of the gas relative to the ground: $M^*(1)\bar{v}_2^2/2g$.

Another part is involved as stagnation enthalpy in the center of mass system: $\frac{\gamma_2 R_2}{\gamma_2 - 1} M(1)T^o$. The final major portion of the energy is invested in doing work against the atmosphere. This work is just the work done in displacing the volume $4/3\,\pi\tilde{r}_2^3$ against atmospheric pressure. This portion is thus $144\,p_\infty \left(\frac{4\pi r_2^3}{3}\right)\left(1 + \frac{V_y}{V_\infty}\right)$.

After striking an energy balance, we have

$$2.20 \quad J\,H(1) = \frac{M^*(1)\,\bar{v}_2^2}{2g} + \frac{\gamma_2 R_2}{\gamma_2 - 1} M(1)T^o$$

$$+ 144\,p_\infty \left(\frac{4\pi r_2^3}{3}\right)\left(1 + \frac{V_y}{V_\infty}\right) .$$

Having written these equations for the single shock model, we shall now examine what modifications must be made for a two shock model, i.e., what must be done to account for the presence of the muzzle brake.

The first alteration in the above equations that must be made for a model with two shock spheres concerns the mass contained in each of the identical spheres. Ignoring discharge from the front port, this is one half the mass contained in the single sphere model. Thus, mass contained in each sphere is $M^*(1)/2$. Similarly, the momentum transported by each sphere is just $P(1)/2$. Thus the average speed of the mass in each sphere is

$$g\,\frac{P(1)/2}{M^*(1)/2} = \frac{g\,P(1)}{M^*(1)}, \text{ as}$$

before for the single-shock model. Thus, $\bar{v}_1 = \bar{v}_2$.

It must be noted that the total energy available to each sphere is now $H(1)/2$. Now, by examining equations 2.10 and 2.20, it can be seen that substitution of $M(1)/2$, $H(1)/2$, and $\bar{v}_1$ for $M(1)$, $H(1)$, and $\bar{v}_2$, respectively, produces the conditions:

2.21 T° (two-shock model) = T° (single-shock model)

2.22 radius of each gas sphere $= \left(\frac{r_2^3}{2}\right)^{1/3}$.

By equation 2.3b and 2.22,

2.23 $r_1 = \left(\frac{\tilde{r}_2^3}{2}\right)^{1/3}$, where r_1 is the shock radius

for each sphere.

To predict the position of each of the fully developed shock spheres with respect to the muzzle brake, we must first apply momentum conservation to the system of spheres and muzzle brake. Regard figure 2.2 .

In figure 2.2a a cross sectional view of a conventional two-baffle brake is pictured. To simplify the theoretical treatment, we find the effective center of the side ports and imagine the equivalent* brake to be pictured as in figure 2.2b .

* A brake with two side ports having the same axial and vertical momentum indices.

FIGURE 2.2 A

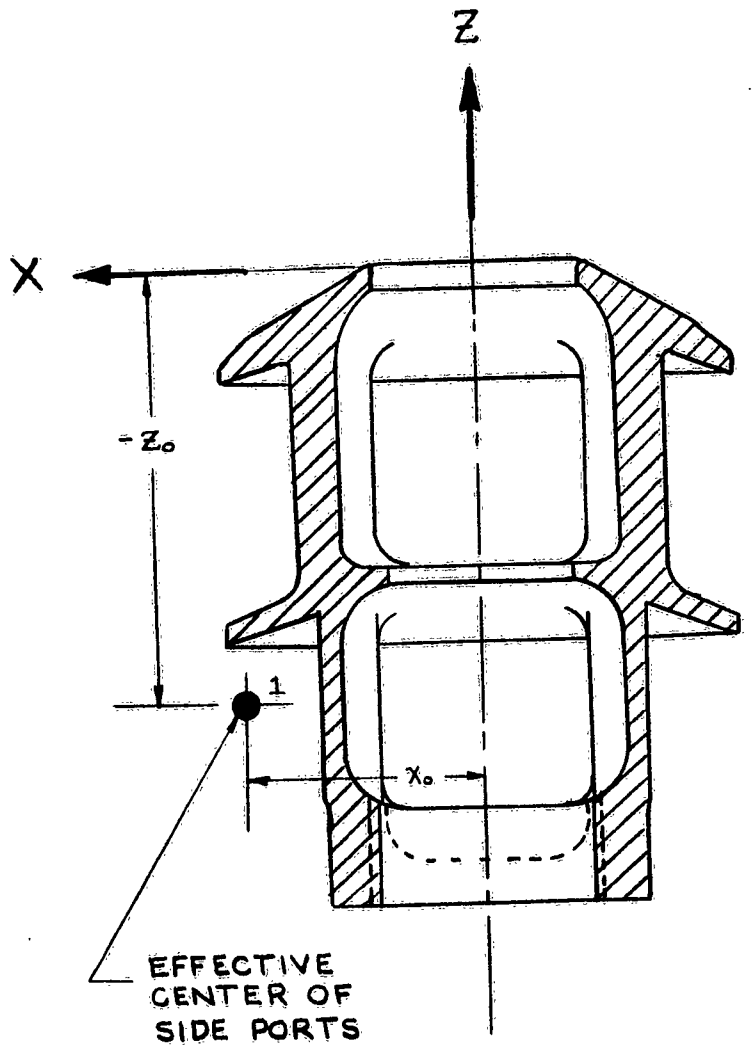

FIGURE 2.2B

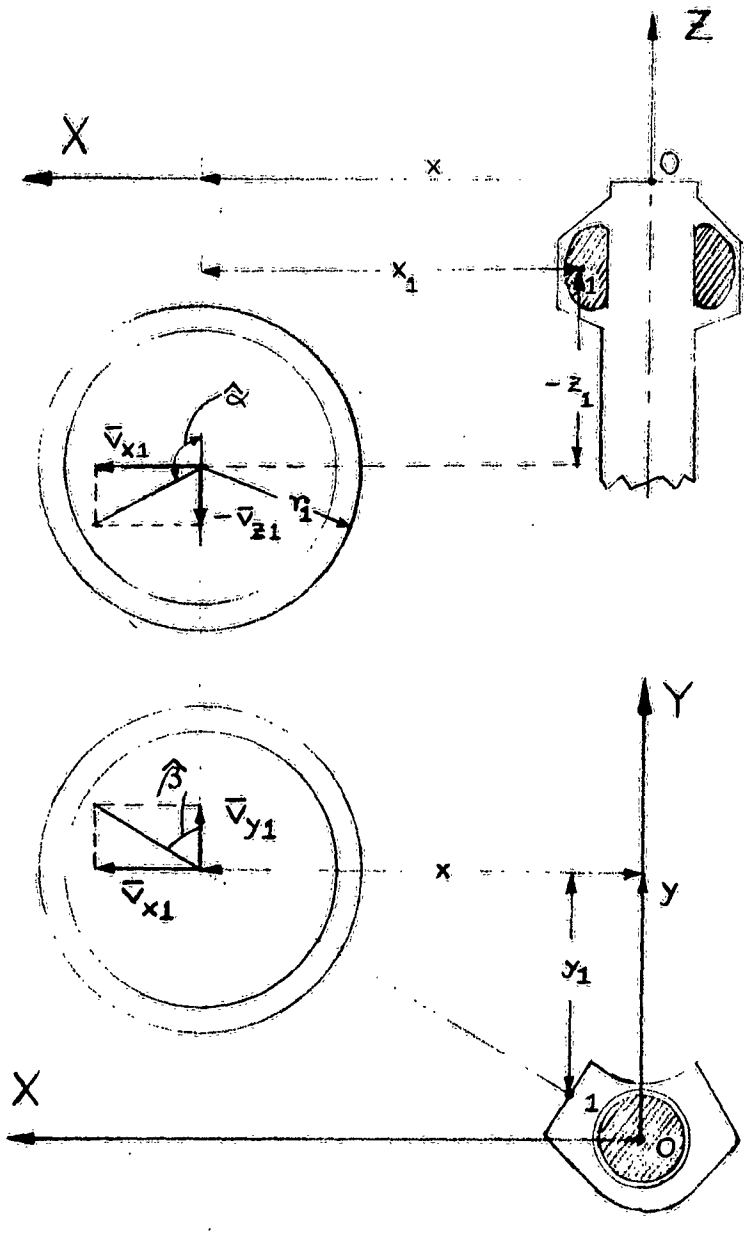
Z
X
x
O
x_1
1
$-z_1$
$\hat{\alpha}$
$\bar{v}_{x1}$
$-\bar{v}_{z1}$
η_1
Y
$\hat{\beta}$
$\bar{v}_{y1}$
$\bar{v}_{x1}$
x
y
y_1
X
1
O

For momentum conservation in the Z-direction at $\mathcal{T} = 1$,

2.24 $M^*(1)\bar{v}_{z1}/g$ + Z-impulse on brake at $\mathcal{T} = 1 = B_T(1)$.

However,

2.25 Z-impulse on brake (at $\mathcal{T} = 1$) $\cong$ $\flat_{eff}\ B_T(1)$.

Therefore,

2.26 $$\bar{v}_{z1} = \frac{g\ B_T(1)}{M^*(1)}\ (1 - \flat_{eff})\ ;$$

and from 2.1 and 2.26,

2.27a $\bar{v}_{z1} = \bar{v}_2(1 - \flat_{eff})$ or

b $\bar{v}_{z1} = \bar{v}_1(1 - \flat_{eff})$.

Defining

2.28 $$\lambda_r = \frac{\text{net Z-axis impulse}}{P}\ ,$$

2.29a $$\lambda_r = \frac{B_T}{P}(1 - \flat_{eff}) \text{ or , for } \gamma = 1.26\ ,$$

b $\lambda_r = 1.46881(1 - \flat_{eff})$.

Thus,

2.30 $$\bar{v}_{z1} = \frac{\bar{v}_1\ \lambda_r}{1.46881}$$

We have defined,

2.31 $$\omega = \frac{\text{net Y-axis impulse}}{P}$$.

But,

2.32 $$\text{net Y-axis impulse} = \frac{M^*(1)\ \bar{v}_{y1}}{g} \quad .$$

From 2.2, 2.31, and 2.32, one has

2.33 $$\bar{v}_{y1} = \frac{\bar{v}_1\ \omega}{1.46881} \quad .$$

Since $\bar{v}_1$ is a vector with components $\bar{v}_{x1}$, $\bar{v}_{y1}$, and $\bar{v}_{z1}$,

2.34 $$\bar{v}_{x1} = (\bar{v}_1^2 - \bar{v}_{y1}^2 - \bar{v}_{z1}^2)^{1/2}$$

From figure 2.2b, it can be seen that

2.35a $$\hat{\alpha} = \tan^{-1}\left(\frac{\bar{v}_{x1}}{\bar{v}_{z1}}\right), \text{ for } \bar{v}_{z1} > 0 \ ;$$

b $$\hat{\alpha} = \frac{\pi}{2}, \text{ for } \bar{v}_{z1} = 0 \ ;$$

c $$\hat{\alpha} = \pi + \tan^{-1}\left(\frac{\bar{v}_{x1}}{\bar{v}_{z1}}\right), \text{ for } \bar{v}_{z1} < 0 \ .$$

Similarly,

2.36a $$\hat{\beta} = \tan^{-1}\left(\frac{\bar{v}_{x1}}{\bar{v}_{y1}}\right), \text{ for } \bar{v}_{y1} \neq 0 \ ;$$

b $$\hat{\beta} = \frac{\pi}{2}, \text{ for } \bar{v}_{y1} = 0 \ .$$

Calling the distance from the center of the side port of the brake to the center of one of the shock spheres d_1, one can write

2.37 $$\frac{d_1}{B_T} = \frac{z_1}{\text{net Z-axis impulse}} \quad \text{and}$$

$$2.38 \qquad \frac{d_1}{B_T} = \frac{y_1}{\text{net Y-axis impulse}} \quad ,$$

by similarity of the displacement and velocity vectors. Then, from 2.28 and 2.37,

$$2.39 \qquad z_1 = \frac{d_1 \lambda_r}{1.46881} \quad .$$

Also, from 2.31 and 2.38,

$$2.40 \qquad y_1 = \frac{d_1 \omega}{1.46881} \quad .$$

Since d_1 is a vector with components x_1 , y_1 , z_1 ,

$$2.41 \qquad x_1 = (d_1^2 - y_1^2 - z_1^2)^{1/2} \quad .$$

We shall now find an expression for d_1 . Gas discharge starts at the muzzle. Therefore, the center of mass of the gas discharged travels a distance ζ thru the brake itself before reaching a side port. This gas is expanding and starting to shock the surrounding air even while in the brake. Let us call d the distance the center of mass of the gas discharged travels to time of maximum shock strength, i.e., to $\bar{\zeta} = 1$. Then, d_1 can be written as

$$2.42 \qquad d_1 = d - \zeta \quad .$$

The infinitesimal mass discharged during the interval dt is $\dot{M}\, dt$. The distance traveled by this mass from the time of its ejection, t , to the time t^* is given by $v_{av}\,(t^* - t)$, where v_{av} is the average velocity of the mass during this interval. Thus, the distance from the muzzle to the center of mass of all the gas discharged to t^* is

$$2.43 \qquad d = \frac{\int_0^{t^*} v_{av}\, \dot{M}\, dt\, (t^* - t)}{M(t^*)} \quad .$$

Specifically, we are interested in t^* such that $\tau = 1$. Remembering that $t = \frac{\tau}{\alpha_T}$ or $dt = \frac{d\tau}{\alpha_T}$, 2.43 can be written as

$$2.44 \qquad d = \frac{\int_0^1 v_{av} \dot{M}\, d\tau\ (1 - \tau)}{M(1)\, \alpha_T^2}$$

From reference 10 we have

$$2.45a \qquad \frac{\dot{M}}{\alpha_T} = M_T\, C_4\, (C_1 \tau + 1)^{-C_5} \quad \text{where}$$

$$b \qquad C_1 = \frac{\gamma - 1}{2}\ C_4$$

$$c \qquad C_4 = \gamma\left(\frac{2}{\gamma + 1}\right)^{((\gamma + 1)/2(\gamma - 1))}$$

$$d \qquad C_5 = \frac{\gamma + 1}{\gamma - 1} \quad \text{and}$$

$$2.46 \qquad M(1) = 0.50688\, M_T\ .$$

In our case $\gamma = \gamma_2 = 1.26$, and

$$2.47 \qquad d = \frac{C_4\, a_{b\ init}}{0.50688\, \alpha_T} \int_0^1 (v_{av}/a_{b\ init})(C_1 \tau + 1)^{-C_5}(1-\tau)\, d\tau\ .$$

To complete our evaluation of d, we need an expression for v_{av} for the interval $(1 - \tau)$. Let us proceed by developing an expression for the velocity of the gas, $v_g = v_g(\tau)$. We note that the velocity with which the gas leaves the muzzle can be expressed as

$$2.48 \qquad v_{go} = \frac{g\, \dot{P}(\tau)}{\dot{M}(\tau)} \quad . \quad \text{From reference 10 we have}$$

$$2.49a \qquad \dot{P}(\tau) = C_3\, A p_{b\ init}\, \Phi \quad , \quad \text{where}$$

b $$C_3 = \frac{\gamma\left[2/(\gamma+1)\right]^{\frac{\gamma+1}{2(\gamma-1)}}}{(\gamma+1)^{(\gamma-1)/2\gamma}}$$

c $$\Phi = (C_1\tau + 1)^{\frac{2\gamma}{(1-\gamma)}}$$

Also,

2.50 $$\dot{M}(\tau) = \frac{A\, g\, p_{b\ init}}{a_{b\ init}} C_4 \Phi^{(\gamma+1)/2\gamma} .$$

From 2.48 , 2.49 , and 2.50 ,

2.51 $$\frac{v_{go}}{a_{b\ init}} = \frac{C_3}{C_4(C_1\tau + 1)} .$$

Due to atmospheric entrainment, the gas discharged slows down as it proceeds away from the muzzle. After traveling for a time $\tau \cong 1$, we shall assume that the gas is traveling at $\bar{v}_1$; and that for $\tau \gg 1$, the gas velocity asymptotically approaches a_∞ . Actually, of course, for τ approaching ∞ , v_g approaches zero. It is regarded as more realistic to assume that v_g approaches a_∞ , for the purpose of establishing a function $v_g(\tau)$ for the interval $0 \leq \tau \leq 1$.

Let

2.52a $$u = v_g - a_\infty$$

b $$u_0 = \bar{v}_{go} - a_\infty$$

c $$u_1 = \bar{v}_1 - a_\infty .$$

Selecting a simple function which passes thru the points $(v_{go}, 0)$, $(\bar{v}_1, 1)$; and approaches a_∞ as τ' approaches ∞ , indicates the following form:

2.53a $$u = u_0 - \frac{a\ \tau'}{1 + b\ \tau'} ,$$

b $a = u_0\, b$

c $b = u_0/u_1 - 1$ or

2.54 $$u = \frac{u_0}{1 + \frac{(u_0 - u_1)}{u_1}\,\mathcal{T}'}$$

Letting

2.55a $$s = \frac{u}{a_\infty}$$

b $$s_0 = \frac{u_0}{a_\infty}$$

c $$s_1 = \frac{u_1}{a_\infty}$$

d $r = s_0 - s_1$, equation 2.54 becomes

2.56 $$s = \frac{s_0\, s_1}{s_1 + r\,\mathcal{T}'}$$

By definition,

2.57 $$s_{av} = \frac{1}{\mathcal{T}'} \int_0^{\mathcal{T}'} s\, d\mathcal{T}'$$

From 2.56 and 2.57,

2.58 $$s_{av} = \frac{s_0\, s_1}{r\,\mathcal{T}'}\, \ell n\left(1 + \frac{r}{s_1}\,\mathcal{T}'\right)$$

Replacement of s, etc. in 2.58 with their equivalents (2.52 and 2.55) produces

2.59 $$\frac{v_{av} - a_\infty}{v_{go} - a_\infty} = \frac{\ell n\left[1 + \left(\frac{v_{go} - \bar{v}_1}{\bar{v}_1 - a_\infty}\right)\mathcal{T}'\right]}{\left(\frac{v_{go} - \bar{v}_1}{\bar{v}_1 - a_\infty}\right)\mathcal{T}'}$$

Sample computations with typical weapons have shown that

2.60 $$\bar{v}_1 \cong a_{b\ init}$$.

Substituting the latter expression into 2.59, and letting $\mathcal{F}' = 1 - \mathcal{F}$, the time interval of interest, we obtain

2.61 $$v_{av}/a_{b\ init} - a_\infty/a_{b\ init} =$$

$$\frac{v_{go}/a_{b\ init} - a_\infty/a_{b\ init}}{\frac{(v_{go}/a_{b\ init} - 1)(1-\mathcal{F})}{(1 - a_\infty/a_{b\ init})}} \ell n \left[1 + \frac{(v_{go}/a_{b\ init} - 1)(1-\mathcal{F})}{(1 - a_\infty/a_{b\ init})} \right].$$

Equations 2.47, 2.51, and 2.61 suffice to determine $\alpha_T\ d/a_{b\ init}$ numerically as a function of $a_{b\ init}/a_\infty$. This evaluation has been performed for $a_{b\ init}/a_\infty$ between 1.5 and 3.5, a realistic range for the examples we have treated. The resulting values for $\alpha_T\ d/a_{b\ init}$ lie between 0.521 and 0.523 . To three significant figures a value of 0.523 was chosen. Therefore, equation 2.42 gives

2.62 $$d_1 = \frac{0.523\ a_{b\ init}}{\alpha_T} - \zeta .$$

APPENDIX III

Derivation of Shock Model Equations: Shock Decay

As shown schematically in figure 3.1a, the plane thru the axis of the rear trunnion and center of the front port of the muzzle brake has been labled I. The I-plane is, in general, inclined at some angle QE to the H-plane, a horizontal plane thru the trunnion axis. If the rear trunnion axis passes thru the tube centerline, the angle QE is exactly the quadrant elevation; if not, there is some small, constant difference between QE and the quadrant elevation.

Using the X-Y-Z coordinate axes at the center of the front port of the muzzle brake, the position of the center of the near shock sphere is at (x,y,z). As seen from figure 3.1, these components can be written as

3.1a $\quad x = x_0 + x_1$

b $\quad y = y_0 + y_1$

c $\quad z = z_0 + z_1$.

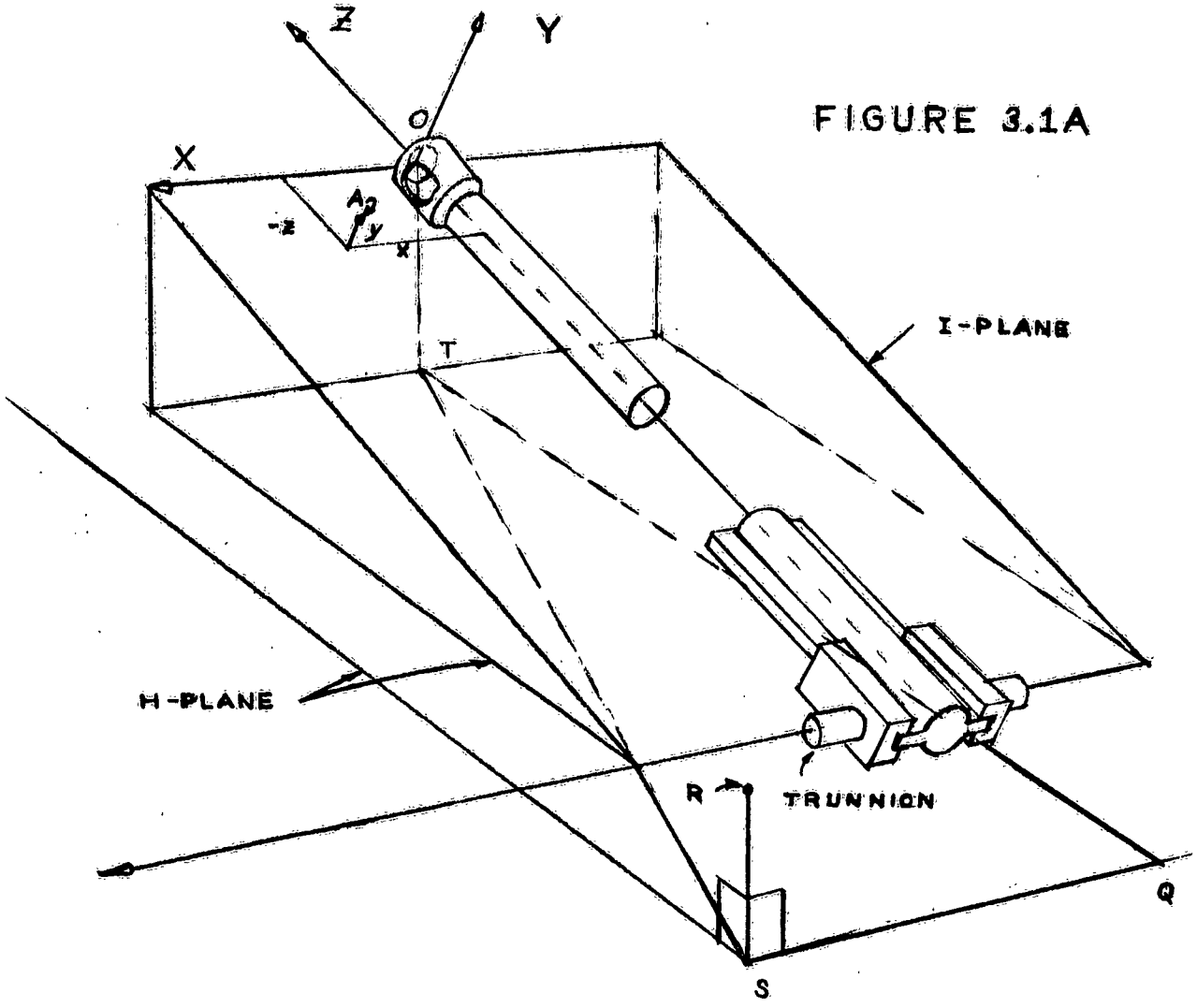

FIGURE 3.1A

3.1 B

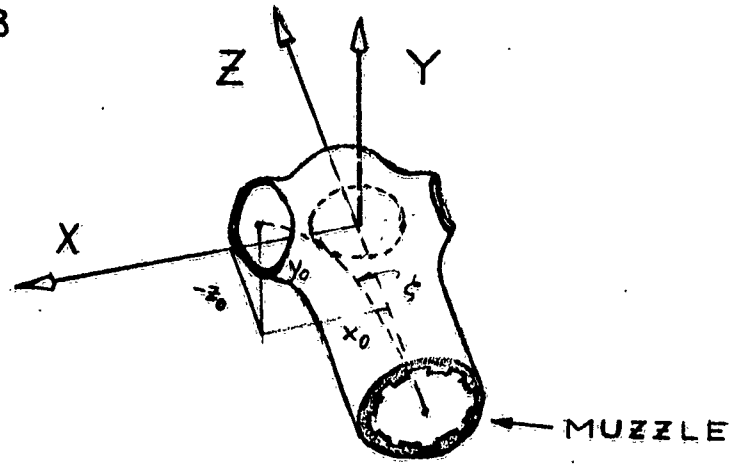

FIGURE 3.2

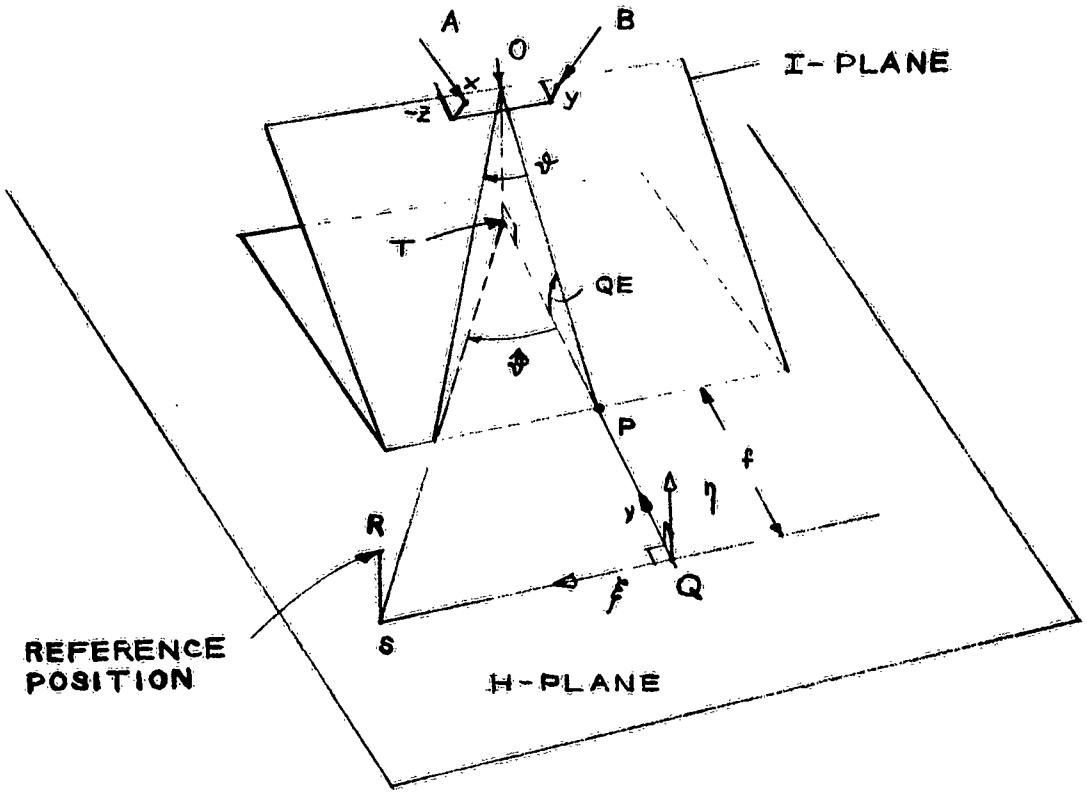

GIVEN DIMENSIONS

$\overline{OP} = G$

$\overline{PQ} = f$

$\overline{RS} = h$

ϑ

QE

DERIVED DIMENSIONS

$\overline{TS} = D$

$\overline{SQ} = D \sin \Phi$

$\overline{TQ} = G \cos(QE) + f$

$\overline{AR} = N$

$\overline{BR} = \emptyset$

Φ

In figure 3.2 we have defined a reference position, R. R is in a plane normal to H thru an axis parallel to the trunnion axis at a distance f behind it. Within this plane, R is at a height h above the H-plane and is in another plane normal to H, passing thru O, the angle of intersection of this plane with I making an angle φ with respect to the tube axis. Note that we have defined an orthogonal frame (ξ, η , ν) at Q along $\overline{TPQ}$. The centers of the near and far shock spheres are labeled A and B, respectively. The distance $\overline{AR}$ is called N and the distance $\overline{BR}$ is called $\emptyset$.

The other given dimensions have been assigned literals as shown in figure 3.2 . Also, from the geometry of the figure, we have given some derived dimensions. In figure 3.3a other derived dimensions are given in the ξ, η , ν -- coordinate system which serve to specify the reference position with respect to the centers of the near and far shock spheres.

FIGURE 3.3A

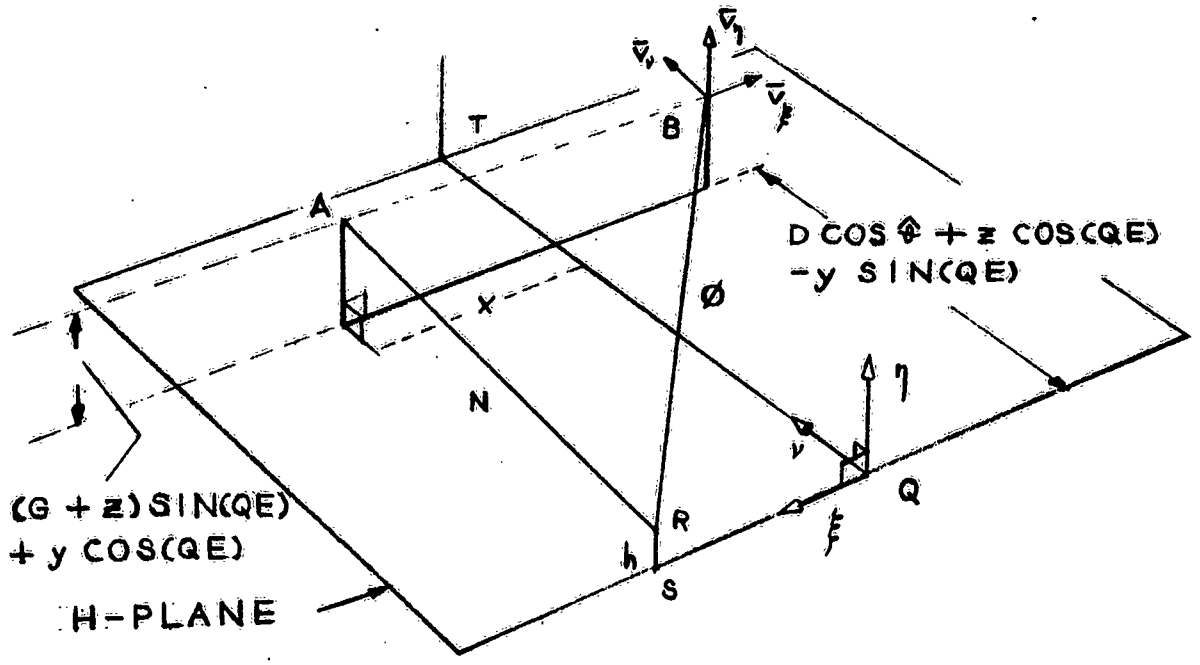

3.3B

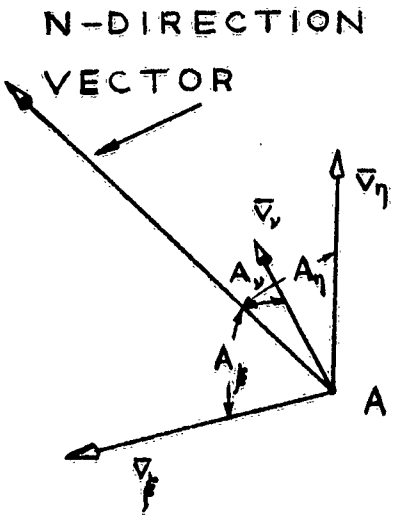

3.3C

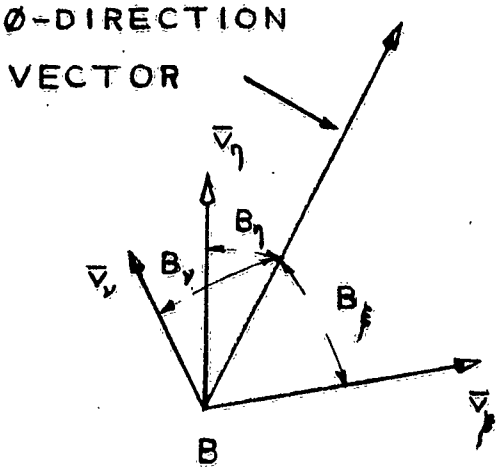

With respect to R the ξ- , η- , and ν- components of the distance to A are: $\left[D \sin\hat{\vartheta} - x\right]$, $\left[(G + z) \sin(QE) + y \cos(QE) - h\right]$, and $\left[D \cos\hat{\vartheta} + z \cos(QE) - y \sin(QE)\right]$. With respect to R the ξ- , η- , and ν- components of the distance to B are: $\left[D \sin\hat{\vartheta} + x\right]$, $\left[(G + z)\sin(QE) + y \cos(QE) - h\right]$, and $\left[D \cos\hat{\vartheta} + z \cos(QE) - y \sin(QE)\right]$. Therefore, one can write N and Ø as follows.

3.2 $$N = \left[(D \sin\hat{\vartheta} - x)^2 + ((G + z) \sin(QE) + y \cos(QE) - h)^2 + (D \cos\hat{\vartheta} + z \cos(QE) - y \sin(QE))^2\right]^{1/2}$$

3.3 $$\text{Ø} = \left[(D \sin\hat{\vartheta} + x)^2 + ((G + z) \sin(QE) + y \cos(QE) - h)^2 + (D \cos\hat{\vartheta} + z \cos(QE) - y \sin(QE))^2\right]^{1/2} .$$

From figure 3.2, the distance, L, from the center of the muzzle to the reference position can be found from

3.4 $$L^2 = D^2 + (G \sin(QE) - h)^2 .$$

Figures 3.3b and c show the center-of-mass velocity components at A and B, respectively. The direction cosines of the angles A_ξ , A_η , and A_ν and their counterparts at B are obtained by noting that for the velocity component projections along N and Ø, the ξ- , η- , and ν- velocity components are proportional to the corresponding distance components. Thus, we have

3.5a $$\cos A_\xi = (D \sin\hat{\vartheta} - x)/N$$

b $$\cos A_\eta = ((G + z) \sin(QE) + y \cos(QE) - h)/N$$

c $$\cos A_\nu = (D \cos\hat{\vartheta} + z \cos(QE) - y \sin(QE))/N ,$$

and

3.6a $\cos B_\xi = (D \sin\Phi + x)/\emptyset$

b $\cos B_\eta = ((G + z)\sin(QE) + y\cos(QE) - h)/\emptyset$

c $\cos B_\nu = (D\cos\ + z\cos(QE) - y\sin(QE)/\emptyset$.

To find the center-of-mass velocity components along the ξ- , η- , and ν- axes, given the components $\bar{v}_{x1}$, $\bar{v}_{y1}$, and $\bar{v}_{z1}$, we note that the X, Y, Z axes are rotated thru the angle (QE) about the X-axis to obtain the ξ, η, ν axes. Thus, one can write

3.7
$$\begin{bmatrix} \bar{v}_\xi \\ \bar{v}_\eta \\ \bar{v}_\nu \end{bmatrix} = \begin{bmatrix} 1 & 0 & 0 \\ 0 & \cos(QE) & \sin(QE) \\ 0 & -\sin(QE) & \cos(QE) \end{bmatrix} \begin{bmatrix} \bar{v}_{x1} \\ \bar{v}_{y1} \\ \bar{v}_{z1} \end{bmatrix} .$$

Using the direction cosines, defined in 3.5 and 3.6, and the velocity components, defined in 3.7, we find the projections of $\bar{v}_1$ in the direction of the reference position from A and B to be, respectively,

$$\bar{v}_\xi \cos A_\xi - \bar{v}_\eta \cos A_\eta - \bar{v}_\nu \cos A_\nu \quad \text{and}$$
$$-\bar{v}_\xi \cos B_\xi - \bar{v}_\eta \cos B_\eta - \bar{v}_\nu \cos B_\nu \quad .$$

The fraction of these velocity projections which is effective in raising the shock velocity above v_2 in the ground fixed frame we have called K, where K is related to the empirical propagation factor, PF, by the equation.

3.8 $K = PF/1.46881$.

Therefore, one can write the shock front velocities at max shock strength for the near and far shock spheres in the direction of the reference position as

3.9 $v_1 = v_2 + K(\bar{v}_\xi \cos A_\xi - \bar{v}_\eta \cos A_\eta - \bar{v}_\nu \cos A_\nu)$ and

3.10 $v_1' = v_2 - K(\bar{v}_\xi \cos B_\xi + \bar{v}_\eta \cos B_\eta + \bar{v}_\nu \cos B_\nu)$.

Using equation 1.27 with 3.9 and 3.10, yields

3.11 $$\varphi_{11} = \frac{7}{6}\left[(v_1/a)^2 - 1\right] \quad \text{and}$$

3.12 $$\varphi_{12} = \frac{7}{6}\left[(v_1'/a)^2 - 1\right] .$$

As mentioned in the discussion of the shock model, it is assumed that the overpressure for each shock sphere decays independently of the other with an $r^{-3/2}$ dependence on distance. The dimensionless overpressure components at the reference position due to the waves from the near and far spheres are

3.13 $$\varphi_{31} = \varphi_{11}\left(\frac{r_1}{N}\right)^{3/2} \quad \text{and}$$

3.14 $$\varphi_{32} = \varphi_{12}\left(\frac{r_1}{\emptyset}\right)^{3/2} .$$

From the definition of φ,

3.15 $$p_{s31} = \varphi_{31}\, p_\infty \quad \text{and}$$

3.16 $$p_{s32} = \varphi_{32}\, p_\infty .$$

The question that is now suggested is: "How should the above overpressure components be combined so as to reflect the measurable static overpressure at the reference position?" The immediate answer for waves of infinitesimal amplitude would be the sum of the two components. For waves of finite amplitude, however, such is not the case. Our determination of the correct functional relationship is as follows.

FIGURE 3.4A

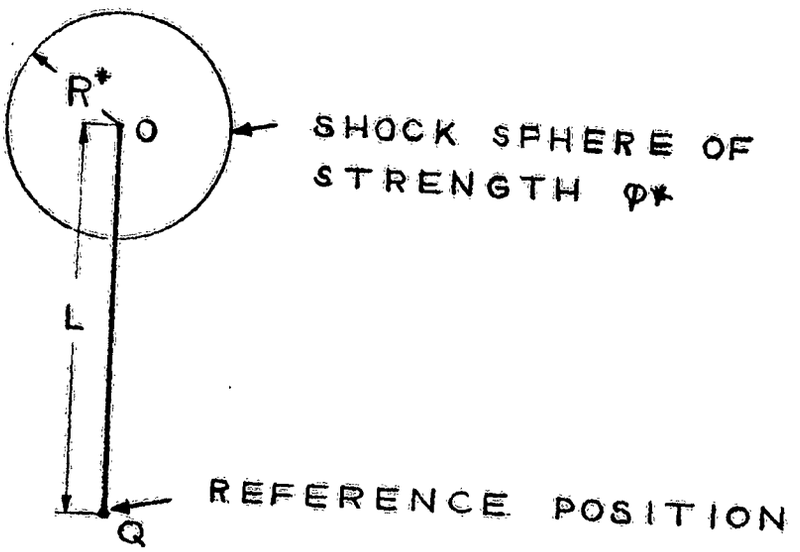

3.4 B

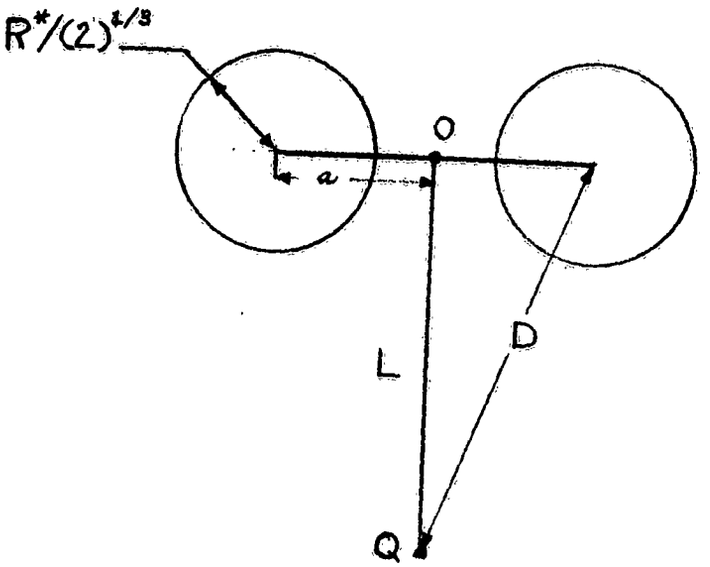

Consider two cases. In the first (figure 3.4a), a single shock sphere, at maximum shock strength, is located at O, a distance L from a reference position Q. The radius of the shock at maximum strength is R^*, where $R^* << L$. We consider a shock of such strength, φ^*, that the $r^{-3/2}$ decay rate is tenable. Then, the dimensionless overpressure at the reference position would be

3.17 $$\varphi = \varphi^* (R^*/L)^{3/2} \quad .$$

In the second instance (figure 3.4b), we divide the shock energy and volume at max strength, available in the first instance, into two parts, the shock centers being located symmetrically at a distance a from the line OQ. We choose $a << L$. Under these assumptions, we would not expect the resulting pressure at Q in the second instance to differ greatly from that in the first. Calling the equal overpressure components from the two spheres at Q φ_1 and φ_2, one can write

3.18 $$\varphi^* (R/L)^{3/2} = f(\varphi_1, \varphi_2) \text{ , where}$$

$f(\varphi_1, \varphi_2)$ is a function involving the components φ_1 and φ_2. To preserve geometric symmetry, we require

3.19 $$f(\varphi_1, \varphi_2) \equiv f(\varphi_2, \varphi_1) \quad ,$$

that is, the function chosen shall be symmetric with respect to φ_1 and φ_2. Further, the function shall

be non-dimensional. One function satisfying these requirements is

$$3.20 \qquad f(\varphi_1, \varphi_2) = (\varphi_1^p + \varphi_2^p)^{1/p} \quad .$$

One might remark that, by assuming equal shock energy and volume in the first and second instance, the maximum peak overpressure in the latter is identical to that in the former, as proven in Appendix II. Further, the radii of the spheres at max strength are given by $R^*/(2)^{1/3}$. Thus,

$$3.21 \qquad \varphi_1 = \varphi_2 = \frac{\varphi^*(R^*/D)^{3/2}}{\sqrt{2}} \quad .$$

Substitution of the latter values of φ_1 and φ_2 into 3.18 and 3.20 gives

$$3.22a \qquad \varphi^*(R/L)^{3/2} = \left[2\left(\frac{\varphi^*(R^*/D)^{3/2}}{\sqrt{2}}\right)^p\right]^{1/p} \quad , \text{ or}$$

$$b \qquad (R^*/L)^{3/2} = \frac{2^{1/p}}{\sqrt{2}}(R^*/D)^{3/2} \quad .$$

By assumption, $R/L \cong R/D$; hence

$$3.23a \qquad \sqrt{2} = 2^{1/p} \text{ and}$$

$$b \qquad p = 2 \quad .$$

It must be stated that this line of reasoning has certain arbitrary features which from any position other than an operational engineering viewpoint would be inadmissable. However, the case treated in this report certainly satisfies the assumption well enough. Therefore, from 3.20 and 3.23b, one can write

$$3.24a \qquad \varphi_3 = (\varphi_{31}^2 + \varphi_{32}^2)^{1/2} \quad \text{and}$$

$$b \qquad p_{s3} = \varphi_3 p_\infty \quad .$$

Finally, from equation 1.28,

$$3.25 \qquad q_3 = \frac{5p_\infty \varphi_3^2}{2(7 + \varphi_3)} \quad .$$

BIBLIOGRAPHY

1. Brode, Harold L. "Point Source Explosion in Air," RM-1824-AEC, ASTIA Document No. AD 133030, Rand Corp., Santa Monica, Calif., Dec. 1956.

2. Brode, Harold L. "Space Plots of Pressure, Density, and Particle Velocity for the Blast Wave from a Point Source in Air," RM-1913-AEC, ASTIA Document No. AD 133043, Rand Corp., Santa Monica, Calif., June 1957.

3. Cole, J. D. "Note on Directional Effects of Pressure Field of Moving Blast," RM-848, Rand Corporation, Santa Monica, Calif., June 1952.

4. Dosanjh, Darshan S. and Weeks, Thomas M. "Interaction of Traveling Shock Wave with Turbulent Flow Fields," Report No. ME 552-6204F, Mechanical Engineering Department, Syracuse Univ. Research Institute, Syracuse, New York.

5. Fitzgerald, James W. "Design Considerations for Pencil Type Air Blast Gages," Report prepared for Ballistic Research Laboratories, Aberdeen Proving Ground, Md. by Atlantic Research Corp., Alexandria, Va., Nov. 1955.

6. Groak, G. S., Jr. "An Evaluation of the Performance of Three Types of Muzzle Brakes for the 155mm Howitzer, T258," Report No. DPS/TW-103/4, Development and Proof Services, Aberdeen Proving Ground, Md., May 1960.

7. Hammer, E. W., Jr. "Muzzle Brakes, Vols. I and II," Franklin Institute Laboratories, Ordnance Department, U. S. Army, June 1949.

8. Holland, Howard, Jr. "Muzzle Blast Measurements on Howitzer 105mm, M2A2E2 with Muzzle Brake No. 8," TM 12-60, U.S.A. Ordnance Human Engineering Laboratories, Aberdeen Proving Ground, Md., August 1960.

9. Romba, J. J. and Martin, P. "The Propagation of Air Shock Waves on a Biophysical Model," U. S. Army Ordnance Human Engineering Laboratories, Aberdeen Proving Ground, Md., September 1961.

10. Schlenker, George. "Contribution to the Analysis of Muzzle Brake Design," Report No. 62-1794, Rock Island Arsenal Research and Development, Rock Island, Ill., May 1962.

11. Thornhill, C. K. "Explosions in Air," (CONFIDENTIAL) A.R.D.E. Memorandum B 57/60, Armament Research and Development Establishment, Secretary of the War Office, Whitehall, London, England, September 1960.

12. "Muzzle Blast Distribution for Howitzer, 105mm, XM103E1, No. 1, without Muzzle Brake and with Muzzle Brakes WTV-F8241, WTV-D8259 and 5/K," Analytical Laboratory Report 62-AL-81, Artillery Weapons Br., Artillery Div., Development and Proof Services, Aberdeen Proving Ground, Md., June 1962.

13. "Investigation of Muzzle Blast of Howitzer, 155mm, M1A2E3," Report No. DPS-169, Development and Proof Services, Aberdeen Proving Ground, Md., March 1961.

14. "Report on Development Test of Muzzle Brakes (Single Baffle) for 76mm Gun, T124E2," Eleventh Report on Ordnance Project No. TRI-1037, Development and Proof Services, Aberdeen Proving Ground, Md., December 1956.

15. "Blast Measurements, 155mm Howitzer T-255 w/Muzzle Brake," Report No. 2, Project No. 91H, Erie Ordnance Depot, Port Clinton, Ohio.

16. Courant, R. and Friedrichs, K. O. Supersonic Flow and Shock Waves, New York: Interscience Publishers, Inc., 1956.

17. Keenan, J. H. and Kaye, J. Gas Tables, New York: John Wiley and Sons, Inc., 1948.

18. Shapiro, A. H. The Dynamics and Thermodynamics of Compressible Fluid Flow, Vols. I and II, New York: The Ronald Press Co., 1953.

ACKNOWLEDGEMENT

The author gratefully acknowledges the assistance of Mr. Stuart Olson, who wrote the digital program for numerical evaluation of the theory.

DISTRIBUTION

1 Commanding General
U. S. Army Materiel Command
Building T-7, Gravelly Point
Washington 25, D. C.
1 ATTN: Document Section
1 ATTN: AMCRD-WE

Commanding General
U. S. Army Weapons Command
Rock Island Arsenal
Rock Island, Illinois
2 ATTN: AMSWE-RDA, Mr. G. Rendall

Commanding General
Headquarters, CONARC
Ft. Monroe, Virginia
1 ATTN: Chief, Development Section

Commanding General
U. S. Army Test and Evaluation Command
Aberdeen, Maryland
2 ATTN: STEAP-TE-APS-GH, Mr. E. Parker

Commanding Officer
Aberdeen Proving Ground, Maryland
1 ATTN: Human Engineering Laboratories

1 Commanding Officer
U. S. Army Ballistic Research Laboratory
Aberdeen, Maryland

Commanding Officer
Harry Diamond Laboratories
Connecticut Ave. & Van Ness Sts., N.W.
Washington 25, D. C.
1 ATTN: Technical Reference Section

Commanding General
U. S. Army Mobility Command
3811 Van Dyke Ave.
Centerline, Michigan
1 ATTN: AMSMO-R, Directorate of R&D

Commanding General
U. S. Army Tank-Automotive Center
Detroit Arsenal
Centerline, Michigan
1 ATTN: SMOTA-RE.1, Mr. Fred Fisher
1 ATTN: SMOTA-R/E, Mr. J. Tannenbaum

Commanding Officer
U. S. Army Combat Developments
Experimentation Center
Fort Ord, California
1 ATTN: Ordnance Liaison Officer (USAOCDA)
Bldg. #2870

Ordnance Engineering Associates, Inc.
3032 N. Oakley Ave.
Chicago 18, Illinois
1 ATTN: Mr. A. D. Kafadar, President

Commander
Armed Services Technical Information Agency
Arlington Hall Station
Arlington 12, Virginia
30 ATTN: TIPDR

Commanding Officer
Picatinny Arsenal
Dover, N. J.
1 ATTN: ORDBB-DR3, Mr. S. Bernstein

Commanding Officer
Watervliet Arsenal
Watervliet, New York
2 ATTN: R&D Division

Commanding Officer
Springfield Armory
Springfield, Massachusetts
2 ATTN: R&D Division

Commandant
U. S. Military Academy
West Point, New York
1 ATTN: Department of Ordnance
and Gunnery

Director
U. S. Army Artillery Board
Ft. Bliss, Texas
1 ATTN: Missile Division

1 President
U. S. Army Artillery Board
Ft. Sill, Oklahoma

Commandant
U. S. Army, A. & M. School
Ft. Sill, Oklahoma
1 ATTN: AKPSI-GCR
1 ATTN: AKPSIDA-MA, Maj. Ylinen

AD ______________ Accession No. ______

Research and Development, Rock Island Arsenal, Rock Island, Illinois.
THEORETICAL STUDY OF THE BLAST FIELD OF ARTILLERY WITH MUZZLE BRAKES (U)
by George Schlenker

RIA R&D Rept. 62-4257, Dec 62, 105 p.
D.A. Project No. 5W01-01-034.
Unclassified Report.

A means is described for computing the peak static and peak dynamic overpressures of the shock wave generated by an artillery piece with muzzle brake as a function of position within the crew area. Computed results are compared with recent experimental results and indicate a favorable agreement.

UNCLASSIFIED

1. Artillery Blast
2. Shock Waves
3. Muzzle Brakes
4. Computer Applications

I. George Schlenker
II. Rock Island Arsenal, Design Engineering
III. D.A. Project No. 5W01-01-034

DISTRIBUTION:
Copies obtainable from ASTIA-TIPDR

UNCLASSIFIED

AD ______________ Accession No. ______

Research and Development, Rock Island Arsenal, Rock Island, Illinois.
THEORETICAL STUDY OF THE BLAST FIELD OF ARTILLERY WITH MUZZLE BRAKES (U)
by George Schlenker

RIA R&D Rept. 62-4257, Dec 62, 105 p.
D.A. Project No. 5W01-01-034.
Unclassified Report.

A means is described for computing the peak static and peak dynamic overpressures of the shock wave generated by an artillery piece with muzzle brake as a function of position within the crew area. Computed results are compared with recent experimental results and indicate a favorable agreement.

UNCLASSIFIED

1. Artillery Blast
2. Shock Waves
3. Muzzle Brakes
4. Computer Applications

I. George Schlenker
II. Rock Island Arsenal, Design Engineering
III. D.A. Project No. 5W01-01-034

DISTRIBUTION:
Copies obtainable from ASTIA-TIPDR

UNCLASSIFIED

AD ______________ Accession No. ______

Research and Development, Rock Island Arsenal, Rock Island, Illinois.
THEORETICAL STUDY OF THE BLAST FIELD OF ARTILLERY WITH MUZZLE BRAKES (U)
by George Schlenker

RIA R&D Rept. 62-4257, Dec 62, 105 p.
D.A. Project No. 5W01-01-034.
Unclassified Report.

A means is described for computing the peak static and peak dynamic overpressures of the shock wave generated by an artillery piece with muzzle brake as a function of position within the crew area. Computed results are compared with recent experimental results and indicate a favorable agreement.

UNCLASSIFIED

1. Artillery Blast
2. Shock Waves
3. Muzzle Brakes
4. Computer Applications

I. George Schlenker
II. Rock Island Arsenal, Design Engineering
III. D.A. Project No. 5W01-01-034

DISTRIBUTION:
Copies obtainable from ASTIA-TIPDR

UNCLASSIFIED

AD ______________ Accession No. ______

Research and Development, Rock Island Arsenal, Rock Island, Illinois.
THEORETICAL STUDY OF THE BLAST FIELD OF ARTILLERY WITH MUZZLE BRAKES (U)
by George Schlenker

RIA R&D Rept. 62-4257, Dec 62, 105 p.
D.A. Project No. 5W01-01-034.
Unclassified Report.

A means is described for computing the peak static and peak dynamic overpressures of the shock wave generated by an artillery piece with muzzle brake as a function of position within the crew area. Computed results are compared with recent experimental results and indicate a favorable agreement.

UNCLASSIFIED

1. Artillery Blast
2. Shock Waves
3. Muzzle Brakes
4. Computer Applications

I. George Schlenker
II. Rock Island Arsenal, Design Engineering
III. D.A. Project No. 5W01-01-034

DISTRIBUTION:
Copies obtainable from ASTIA-TIPDR

UNCLASSIFIED

AD ______________ Accession No. ______

Research and Development, Rock Island Arsenal, Rock Island, Illinois.
THEORETICAL STUDY OF THE BLAST FIELD OF ARTILLERY WITH MUZZLE BRAKES (U)
by George Schlenker

RIA R&D Rept. 62-4257, Dec 62, 105 p.
D.A. Project No. 5W01-01-034.
Unclassified Report.

A means is described for computing the peak static and peak dynamic over-pressures of the shock wave generated by an artillery piece with muzzle brake as a function of position within the crew area. Computed results are compared with recent experimental results and indicate a favorable agreement.

UNCLASSIFIED

1. Artillery Blast
2. Shock Waves
3. Muzzle Brakes
4. Computer Applications

I. George Schlenker
II. Rock Island Arsenal, Design Engineering
III. D.A. Project No. 5W01-01-034

DISTRIBUTION:
Copies obtainable from ASTIA-TIPDR

UNCLASSIFIED

AD ______________ Accession No. ______

Research and Development, Rock Island Arsenal, Rock Island, Illinois.
THEORETICAL STUDY OF THE BLAST FIELD OF ARTILLERY WITH MUZZLE BRAKES (U)
by George Schlenker

RIA R&D Rept. 62-4257, Dec 62, 105 p.
D.A. Project No. 5W01-01-034.
Unclassified Report.

A means is described for computing the peak static and peak dynamic over-pressures of the shock wave generated by an artillery piece with muzzle brake as a function of position within the crew area. Computed results are compared with recent experimental results and indicate a favorable agreement.

UNCLASSIFIED

1. Artillery Blast
2. Shock Waves
3. Muzzle Brakes
4. Computer Applications

I. George Schlenker
II. Rock Island Arsenal, Design Engineering
III. D.A. Project No. 5W01-01-034

DISTRIBUTION:
Copies obtainable from ASTIA-TIPDR

UNCLASSIFIED

AD ______________ Accession No. ______

Research and Development, Rock Island Arsenal, Rock Island, Illinois.
THEORETICAL STUDY OF THE BLAST FIELD OF ARTILLERY WITH MUZZLE BRAKES (U)
by George Schlenker

RIA R&D Rept. 62-4257, Dec 62, 105 p.
D.A. Project No. 5W01-01-034.
Unclassified Report.

A means is described for computing the peak static and peak dynamic over-pressures of the shock wave generated by an artillery piece with muzzle brake as a function of position within the crew area. Computed results are compared with recent experimental results and indicate a favorable agreement.

UNCLASSIFIED

1. Artillery Blast
2. Shock Waves
3. Muzzle Brakes
4. Computer Applications

I. George Schlenker
II. Rock Island Arsenal, Design Engineering
III. D.A. Project No. 5W01-01-034

DISTRIBUTION:
Copies obtainable from ASTIA-TIPDR

UNCLASSIFIED

AD ______________ Accession No. ______

Research and Development, Rock Island Arsenal, Rock Island, Illinois.
THEORETICAL STUDY OF THE BLAST FIELD OF ARTILLERY WITH MUZZLE BRAKES (U)
by George Schlenker

RIA R&D Rept. 62-4257, Dec 62, 105 p.
D.A. Project No. 5W01-01-034.
Unclassified Report.

A means is described for computing the peak static and peak dynamic over-pressures of the shock wave generated by an artillery piece with muzzle brake as a function of position within the crew area. Computed results are compared with recent experimental results and indicate a favorable agreement.

UNCLASSIFIED

1. Artillery Blast
2. Shock Waves
3. Muzzle Brakes
4. Computer Applications

I. George Schlenker
II. Rock Island Arsenal, Design Engineering
III. D.A. Project No. 5W01-01-034

DISTRIBUTION:
Copies obtainable from ASTIA-TIPDR

UNCLASSIFIED